Investigation into the Catalytic Role of Threonine 712 in VP4 Protease from the Blotched Snakehead Virus

by

Michael Ungerer

B.Sc., Simon Fraser University, 2012

Thesis Submitted in Partial Fulfillment of the
Requirements for the Degree of
Master of Science

in the
Department of Molecular Biology and Biochemistry
Faculty of Science

SIMON FRASER UNIVERSITY

Summer 2014

Approval

Name: **Michael Ungerer**

Degree: **Master of Science**

Title of Thesis: ***Investigation into the Catalytic Role of Threonine 712 in VP4 Protease from the Blotched Snakehead Virus***

Examining Committee: **Chair:** Dr. Jonathan C. Choy
Assistant Professor

Dr. Mark Paetzel
Senior Supervisor
Professor

Dr. Peter J. Unrau
Supervisor
Associate Professor

Dr. David J. Vocadlo
Supervisor
Professor

Dr. Frederic F. Pio
Internal Examiner
Professor
MBB

Date Defended/Approved: July 24, 2014

Partial Copyright Licence

Abstract

The blotched snakehead virus (BSNV) is a member of the *Birnaviridae* family; it is characterized by a single-shelled capsid and a bisegmented, double-stranded RNA genome. One segment of its genome, segment A, encodes the BSNV polyprotein, NH_3^+-pVP2-X-VP4-VP3-COO^-, which includes VP4 - a peptidase that uses a 'nonclassical', Ser-Lys catalytic dyad mechanism. VP4 cleaves the polyprotein at specific recognition sites to release four peptides and four polypeptides. The polypeptides include the capsid protein, VP2, protein X (whose function is unknown), the multifunctional protein VP3, and also VP4.

Previous site-directed mutagenesis and crystallographic studies of BSNV VP4 have identified the serine nucleophile and lysine general base, however the potential roles played by other residues within the active site have yet to be experimentally investigated. One conserved active site residue of interest is Thr712, which is appropriately positioned, according to the BSNV VP4 crystal structure (PDB ID 2GEF), to form a hydrogen bond with the active site's general base, Lys729. Herein, we present data supporting Thr712's significance to VP4-mediated catalysis from experiments using site-directed mutagenesis and time-course cleavage assays. We also describe the crystallization of a truncated, active site mutant construct - K729A - of BSNV VP4.

- **Keywords**: blotched snakehead virus (BSNV); VP4; Ser-Lys catalytic dyad; threonine 712; time-course cleavage assays; crystallography.

For Mom, Dad, Thomas and Vanessa

Acknowledgements

Thank you Dr. Mark Paetzel for supervising me during my graduate studies, offering guidance and encouragement, and for making this thesis possible. Thank you Deidre de Jong-Wong for your services to the lab – I am much obliged. I am also grateful for the advice and instruction offered by my fellow lab members, Suraaj Aulakh, Daniel Chiang, Minfei Fu, Dr. Apollos Kim, Dr. Kelly Kim, Chuanyun Luo, Dr. Sung-Eun Nam, Zohreh Sharafianardekani, Eugean Shin, Dr. Charles Stevens, Xiaolu Linda Zhang and especially by my mentor, Dr. Ivy Y. W. Chung.

I should also like to acknowledge my gratitude to my committee members, Dr. Peter J. Unrau and Dr. David J. Vocadlo; to Dr. Jonathan C. Choy for chairing my defence and Dr. Frederic F. Pio for serving as my internal examiner; to the MBB department's staff; and to the wonderful teachers with whom I had the pleasure to work as a teacher's assistant and from whom I received an education.

Table of Contents

List of Tables

List of Figures

List of Acronyms

aa	Amino acid
ATP	Adenosine triphosphate
BSNV	Blotched snakehead virus
CPNV	Chicken proventricular necrosis virus
dH_20	Distilled water
Da	Dalton
DPI	Dots per inch
DTT	Dithiothreitol
DXV	Drosophila X virus
EDTA	Ethylenediaminetetraacetic acid
IBDV	Infectious bursal disease virus
IPNV	Infectious pancreatic necrosis virus
IPTG	Isopropyl β-D-1-thiogalactopyranoside
LB	Luria-Bertani
M	Molarity
NMR	Nuclear magnetic resonance
O/N	Overnight
ORF	Open reading frame
PAGE	Polyacrylamide gel electrophoresis
PDB	Protein data bank
PDB ID	Protein data bank identifier
RdRP	RNA-dependent RNA polymerase
RPM	Revolutions per minute
s	Second
SDS	Sodium dodecyl sulfate
SEM	Standard error of measurement
TV-1	Tellina virus 1
w/v	Weight/volume
wt	Wild type
YAV	Yellowtail ascites virus

Glossary

Accession number	An identifier for a sequence deposited in the UniProt database consisting of letters and numbers.
Å	Ångströms (10^{-10} m).
Bicistronic	An RNA or mRNA encoding two gene products.
Bisegmented genome	A genome that is divided into two segments. Both segments are required to constitute the complete genetic information.
BL21 (DE3) cells	An *E. coli* strain for the expression of recombinant proteins. The DE3 designation denotes that the strain has a DE3 lysogen, which includes a gene for T7 RNA polymerase whose expression can be chemically induced with IPTG.
Capsid	The protein coat of a virus.
Crystal	An arrangement of atoms or molecules in three-dimensional space that regularly repeats itself.
C-terminus	The carboxyl terminus of a protein.
Dalton	A unit of mass equal to 1/12 the mass of a single carbon-12 atom.
Densitometry	The measurement of the darkness or opacity of a substance, specimen, or demarcated region of an image.
Disulfide bond	A covalent bond formed between the sulfhydryl groups of the side chains of two cysteines.
Edman degradation	A chemical method for sequencing polypeptides, one amino acid at a time, at the amino-terminus.
Enzyme	A biomolecule that binds and acts upon a substrate.
Guanylylation	The addition of phospho-guanosine to an amino acid via covalent bonding.
Homodimer	An assembly of two identical monomers to form a dimer.
In vitro	"In glass", or in a test tube.
In vivo	"In the living", or within a living organism.
k_{cat}	The turnover number, which is a first-order rate constant with units of reciprocal time (s^{-1}). This kinetic parameter is equivalent to the number of substrate molecules converted to product per unit of time by a single enzyme molecule when saturated with substrate.
k_{cat}/K_m	The specificity constant, which is a second-order rate constant with units of M^{-1} s^{-1}. It is the rate constant for the conversion of enzyme and substrate to enzyme and product.
K_m	The Michaelis constant, which has units of concentration, M.

Monocistronic	An RNA or mRNA that encodes one protein.
Moonlighting protein	A protein that has evolved at least two different functions.
N-terminus	The amino terminus of a protein.
P(n)	A position, or amino acid, of a peptide or polypeptide substrate. The integer, n, denotes a position relative to the cleavage site. It is part of the Schechter and Berger nomenclature.
Polycistronic	An RNA or mRNA that encodes two or more proteins.
Protease	An enzyme that hydrolyzes, or breaks, the peptide bonds of proteins.
R group	The side chain of an amino acid, which influences its size, shape, charge and solubility. It also serves as a unique amino acid identifier.
re-face	Designates the face, of a carbonyl carbon, that is closest to the observer when the priorities of the substituents bound to the carbon decrease in a clockwise direction. The substituents are assigned priorities in accordance with the Cahn-Ingold-Prelog system.
Ribonucleoprotein	A complex made from RNA and protein.
Root mean square deviation	In protein structural biology, the root mean square deviation is the measurement of the degree of similarity, in three dimensions, between two proteins. It is 0 Å for identical structures.
Serotype II IBDV	A type of IBDV detected in the blood serum of infected individuals. It has been characterized as non-pathogenic.
si-face	Designates the face, of a carbonyl carbon, that is closest to the observer when the priorities of the substituents bound to the carbon decrease in a counter-clockwise direction. The substituents are assigned priorities in accordance with the Cahn-Ingold-Prelog system.
S(n)	A subsite of a protease. The integer, n, denotes a subsite's position relative to the location of cleavage of a bound substrate's scissile peptide bond. It is part of the Schechter and Berger nomenclature.
Substrate	A substance, or molecule, that is bound and acted upon by an enzyme.
Virion	A complete virus particle, including a core and a capsid.
Virus	An obligate intracellular parasite.
VP4	In the *Birnaviridae* family, viral protein 4 (VP4) is the Ser-Lys catalytic dyad protease.

Chapter 1. Introduction

Birnaviruses are economically important pathogens that infect diverse arrays of eukaryotes and are of ongoing research interest. A wealth of data regarding their molecular biology and epidemiology has accumulated and many key discoveries and advancements are herein summarized.

One of the conserved birnaviral enzymes is VP4, a Ser-Lys protease that cleaves the viral polyprotein to release essential proteins such as VP2, which constitutes the capsid. The solved structure of BSNV VP4 shows that the O^{γ} of the conserved residue, Thr712, is within hydrogen bonding distance of the N^{ζ} of the general base, Lys729. We address how mutating Thr712 to alanine, cysteine, serine, or valine affect BSNV VP4's rate of catalysis as well as the crystallization of BSNV VP4 (K729A).

1.1. Birnaviruses

1.1.1. Taxonomy

The *Birnaviridae* virus family is comprised of four genera: (1) *aquabirnavirus*, (2) *avibirnavirus*, (3) *blosnavirus* and (4) *entomobirnavirus* (Delmas *et al.*, 2012) [1]. *Aquabirnaviruses* infect fish, mollusks and crustaceans; this genus includes the species infectious pancreatic necrosis virus (IPNV) and yellowtail ascites virus (YAV). *Avibirnaviruses*, such as infectious bursal disease virus (IBDV), infect chickens and turkeys. The blotched snakehead virus (BSNV) represents the *blosnaviruses*. BSNV

infects the blotched snakehead fish (*Channa lucius*). *Entomobirnaviruses* are represented by the drosophila X virus (DXV), which infects the fruit fly (*Drosophila melanogaster*).

Two virus species are candidates for defining new *Birnaviridae* genera. Nobiron *et al.* (2008) proposed that Tellina virus 1 (TV-1) represents a fifth genetic cluster of birnaviruses[2]. In 2011, chicken proventricular necrosis virus (CPNV) was recommended for assignment as a sixth genetic cluster of birnaviruses (Guy *et al.*, 2011) [3]. These recent taxonomic proposals have yet to be accepted or rejected.

1.1.2. Genomic organization: segments A and B

The birnaviral genome is bisegmented - with segments called A and B - and is replicated in a semi-conservative fashion (Bernard, 1980; Mertens *et al.*, 1982) [4, 5]. The bicistronic segment A includes two open reading frames (ORFs); one of these encodes a large polyprotein (NH_3^+-pVP2-VP4-VP3-COO^-) and the other encodes VP5 (fig. 1.1.) (Macdonald and Dobos, 1981; Petit *et al.*, 2000) [6, 7]. Segment B encodes the RNA-dependent RNA polymerase (RdRP), called VP1, in a large ORF (Macdonald and Dobos, 1981) [6]. Virus particles contain both segments of the genome (Macdonald *et al.*, 1977; Nagy and Dobos, 1984) [8, 9], which are in approximately equal concentrations relative to one another (Lange *et al.*, 1987) [10].

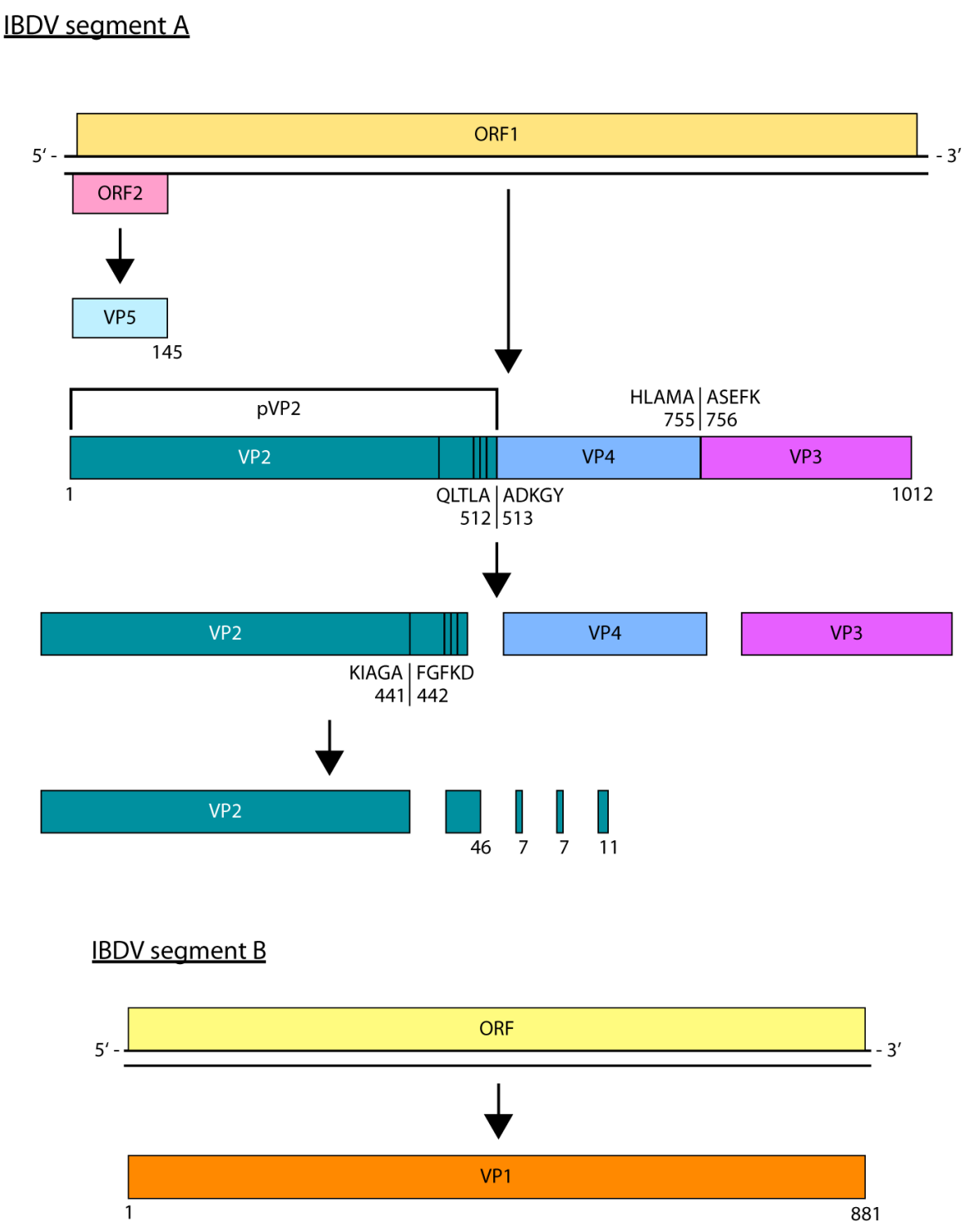

Fig. 1.1. (*Legend on the next page.*)

Figure 1.1. Cartoons of IBDV segments A and B.
The translation of IBDV segments A and B is depicted as well as polyprotein maturation. Segment A is composed of approximately 3.0 kbp. It includes ORF1 and ORF2, which are translated into the polyprotein (pVP2-VP4-VP3) and VP5, respectively. The polyprotein is co-translationally processed by the protease, VP4, to yield pVP2, VP4 and VP3. pVP2 matures into VP2 and four peptides that range in size from seven to 46 aa. The locations, and P5 - P5' residues, of major polyprotein cleavage sites are labeled in black. Segment B is composed of approximately 2.8 kbp and encodes the enzyme VP1. Black numbers indicate the terminuses of one strand of each of the dsRNA genome segments and the aa length of the peptides and polypeptides. The sequence data for the IBDV polyprotein (accession number Q9WI42), VP1 (accession number Q9Q6Q5), and VP5 (accession number P0C751) is available through UniProt. The schematics are adapted from Delmas *et al.* (2012) [1].

1.1.3. Viral proteins and peptides

Viral protein 1

The RNA-dependent RNA polymerase (RdRP), which serves to replicate the genome, is viral protein 1 (VP1). It is the largest birnaviral protein and is encoded by a monocistronic gene of segment B (von Einem *et al.*, 2004) [11]. VP1 can exist in virions either in a genome-linked (VPg) or unlinked state (Persson and Macdonald, 1982; Calvert *et al.*, 1991) [12, 13]. For instance, IPNV VP1 can become genome-linked via a covalent bond between the R group of a serine and a 5'-terminus of the viral genome (Xu and Dobos, 2004) [14]. In the genome-linked state, it serves as both primer and polymerase - this state has been described as being part of an efficient mechanism for viruses that ensures the complete replication of their genomes including terminal sequences (Salas, 1991) [15]. VP1's self-guanylylation activity forms the genome linkage; VP1 is also capable of forming covalent VP1-GMP complexes in the presence of GTP (Dobos, 1993) [16].

A noteworthy feature of VP1s is their lack of a "GDD" motif that is highly conserved in the polymerases of other viruses such as Reovirus and the Norwalk virus (Poch *et al.*, 1989; Duncan *et al.*, 1991; Shwed *et al.*, 2002) [17-19]. This motif's aspartate residues are important for metal ion cofactor binding; in IBDV VP1, this motif's sequence

is "ADN", which, of course, includes one less aspartate residue than the “GDD” motif - as a result, cofactor binding is slightly impaired (Pan *et al.*, 2007) [20]. Another feature of interest is the permuted order of VP1 sequence motifs: the canonical, viral RdRPs' sequence motifs are ordered A-B-C-D, whereas in birnaviruses they are ordered C-A-B-D (Gorbalenya *et al.*, 2002) [21].

Viral protein 2

The structural protein VP2 is encoded within a large ORF of segment A that is translated into a polyprotein. VP2 is located at the N-terminus of this polyprotein and is released from it in the VP2 precursor (pVP2) state by proteolytic cleavage. pVP2 is subsequently cleaved at its C-terminus to produce mature VP2 and three or four short peptides, depending on the *Birnaviridae* species.

During viral morphogenesis, three pVP2 monomers assemble into trimers, and 13 trimers are required to make one face of a virion (Coulibaly *et al.*, 2005) [22]. An intact capsid - which is a single, icosahedral, T = 13 lattice shell - is made from 260 pVP2 trimers (Coulibaly *et al.*, 2005) [22]. After capsid assembly, pVP2 partially matures into VP2 - pVP2 and VP2 are both found in intact capsids (Coulibaly *et al.*, 2005; Kibenge *et al.*, 1999) [22, 23]. The fully formed capsid has a diameter of approximately 70 nm (Böttcher *et al.*, 1997) [24]. pVP2 can also form structures called type I tubules with a diameter of approximately 60 nm (Martinez-Torrecuadrada *et al.*, 2000) [25].

VP2 is implicated in a variety of viral functions including binding the receptors of virus-susceptible host cells for endocytosis (Delgui *et al.*, 2009) [26]. It is also the subject of selective pressures because the exposed, outer-shell is the target of neutralizing antibodies (Azad *et al.*, 1987; Letzel *et al.*, 2007) [27, 28]. These pressures give rise to

interstrain sequence variability in VP2's outer-shell and influence pathogenicity (Bayliss *et al.*, 1990) [29]. VP2 is also an apoptotic inducer (Fernández-Arias *et al.*, 1997; Busnadiego *et al.*, 2012) [30, 31].

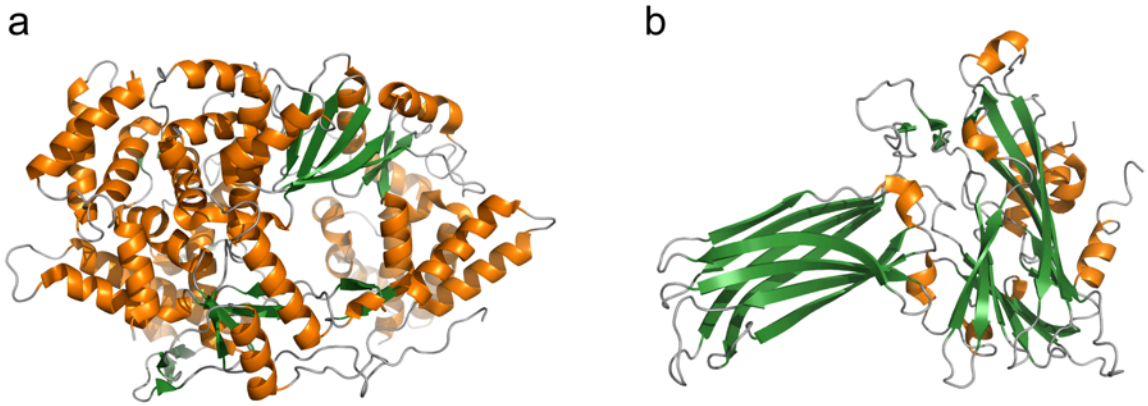

Figure 1.2. Crystal structures of IBDV VP1 and VP2.
(a) IBDV VP1 structure (PDB ID 2PGG). (b) IBDV VP2 structure (PDB ID 1WCD). α-helices are coloured orange, β-strands are green, and random coils are grey.

pVP2 peptides

Birnaviral polyproteins encode three or four peptides at the C-terminus of pVP2 (Chung *et al.*, 1996; Galloux *et al.*, 2004) [32, 33]. In IBDV, whose peptides are well characterized, four peptides constitute the C-terminus of pVP2: pep7a, pep7b, pep11 and pep46. The "pep-" prefix denotes that they are peptides and the numerical suffix gives their aa length. Reverse genetics studies of the four IBDV peptides revealed that the virus is viable without pep7a and pep7b (Da Costa *et al.*, 2002) [34]. However, virions require pep46 and pep11 for viral morphogenesis (Da Costa *et al.*, 2002) [34]. Pep46, which includes a membrane active domain, has been found to produce pores in cell membranes; this finding has exciting implications for host-entry, among other aspects of the viral life cycle (Chevalier *et al.*, 2005; Galloux *et al.*, 2007) [35, 36]. An NMR structure of pep46 has been solved (fig. 1.3.a) (Galloux *et al.*, 2007) [36].

Viral protein 3

The multifunctional protein, VP3, serves as a scaffold upon which pVP2 forms the capsid (Martinez-Torrecuadrada *et al.*, 2000) [25]. pVP2/VP2 and VP3 together constitute over 80% of the virion mass of DXV, IPNV, and IBDV (Dobos *et al.*, 1979) [37]. In a fully assembled capsid, VP3 molecules are completely enclosed by the pVP2/VP2 shell. Interestingly, when the crystal structure of the intact IBDV capsid was solved by X-ray crystallography to 7.0 Å, no electron density for VP3 was observed (Coulibaly *et al.*, 2005) [22]. This suggested that VP3, although present in the crystals at a similar concentration as VP2, was less ordered than VP2 (Coulibaly *et al.*, 2005) [22]. The structure of the central region of IBDV VP3 has however been solved to 2.3 Å by X-ray crystallography (fig. 1.3.b) (Casañas *et al.*, 2008) [38].

In addition to interacting with pVP2/VP2, VP3 is also known to bind VP1 and the dsRNA genome (Tacken *et al.*, 2002) [39]. Lombardo *et al.* (1999) demonstrated that the inclusion of VP1 in virions is dependent upon the formation of a complex with VP3[40]. This discovery was supported by the solution of the structure of IPNV VP1 bound to the 12 C-terminal residues of VP3 that are necessary for the VP1-VP3 interaction (Bahar *et al.*, 2013) [41]. This interaction is also significant because VP1 shields an acidic residue, Glu257, of VP3's C-terminus, which is essential for capsid assembly (Chevalier *et al.*, 2004) [42]. Regarding the dsRNA genome segments, VP3s support their integrity by non-specifically binding them to form ribonucleoproteins (Luque *et al.*, 2009) [43]. Due to VP3's diverse, unrelated functions it has been proposed to be a moonlighting protein (Jeffery, 2004) [44] because it adds significant complexity to birnaviruses, which encode few proteins (Luque *et al.*, 2009) [43].

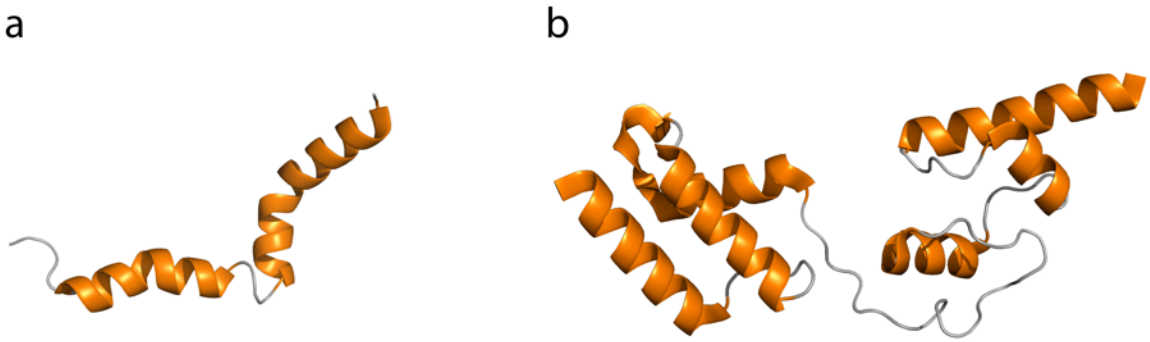

Figure 1.3. Structures of IBDV pep46 and VP3.
(a) NMR structure of IBDV pep46 (PDB ID 2IMU). (b) Crystal structure of IBDV VP3 (PDB ID 2R18). α-helices are coloured orange and random coils are grey.

Viral protein 4

In the 1980s, it was speculated that the large polyprotein encoded by segment A included a protease (Hudson *et al.*, 1986; Nagy *et al.*, 1987) [45, 46]. The presence of this internal protease, called viral protein 4 (VP4), was confirmed by *in vitro* and *in vivo* studies that demonstrated that the polyprotein could be self-processed into its constituent parts (Duncan *et al.*, 1987; Manning *et al.*, 1990) [47, 48]. This event, also known as polyprotein maturation, is efficient; very few or no polyproteins are detected within, or associated with, virions (Magyar and Dobos, 1994) [49]. It has been argued that VP4 cleaves the polyprotein strictly in *cis*, but *trans*-cleavage is possible and its contribution has not been ruled out.

The concentration of VP4 in birnaviral virions is low: Dobos *et al.* (1979) reported that VP4 constitutes 6% of IBDV, 9% of DXV, and 15% of IPNV[37]. IBDV-infected chicken embryo fibroblasts display cytoplasmic and nuclear VP4 in tubular form; these VP4 complexes are called type II tubules (Granzow *et al.*, 1997) [50]. Type II tubules are approximately 25 nm in diameter, exclusively assembled from VP4 and distinct from

birnaviral type I (pVP2) tubules[50]. Lee *et al.* (2007) and Chung and Paetzel (2013) have captured X-ray crystal structures of tubular VP4s from IPNV and YAV, respectively[51, 52].

In 2000, Birghan *et al.* observed that VP4 is a non-canonical viral protease: it contains a 'nonclassical' Ser-Lys catalytic dyad, which is an active site configuration that is infrequently observed in proteases[53]. Site-directed mutagenesis experiments confirmed this dyad-configuration: changing either one of the Ser-Lys dyad residues significantly decreased the rate of polyprotein maturation (Petit *et al.*, 2000; Lejal *et al.*, 2000) [7, 54]. Birnaviral VP4s are considered the first viral proteases in which such a configuration has been observed (Lee *et al.*, 2006a) [55]. Like other Ser-Lys proteases, they attack carbonyl carbons of protein substrates from the *si*-face rather than from the *re*-face (Feldman *et al.*, 2006) [56].

Viral protein 5

In addition to the polyprotein, segment A encodes an arginine-rich protein, VP5 (Magyar and Dobos, 1994; Mundt *et al.*, 1995) [49, 57]. This protein is considered a minor player in birnaviruses: it was found to be dispensable for viral replication (Mundt *et al.*, 1997) [58]. However, IBDV VP5 is an inhibitor of apoptosis that counteracts the apoptotic activities of VP2 (Wei *et al.*, 2011) [59]. No solved VP5 structures are currently available.

1.1.4. IBDV and IPNV diseases

IBDV and IPNV are the best-characterized birnaviruses (Coulibaly *et al.*, 2005) [22]. They cause significant losses in the poultry industry and aquaculture, respectively (Müller *et al.*, 2003; Roberts and Pearson, 2005) [60, 61]. IBDV is also called "Gumboro disease" - a name based on the geographic location where the disease was first reported (Cosgrove, 1962) [62]. It has been observed in chickens and turkeys (Barnes *et*

al., 1982) [63]. IPNV was first observed in trout, but it has since been reported to infect various salmonid species including Atlantic salmon (Wood *et al.*, 1955; Knott and Munro, 1986) [64, 65].

IBDV disease features

In the first report on infectious bursal disease, Cosgrove (1962) noted features of this disease, which are now regarded as its hallmarks[62]. They include its prevalence in juvenile chickens rather than adults, and the commonly observed symptom of an enlarged and lesioned bursa of Fabricius (Winterfield *et al.*, 1972) [66]. Cosgrove's hypothesis that the disease is virally transmitted has also been supported (Cheville, 1967) [67].

In addition to targeting the bursa of Fabricius, IBDV damages the thymus and spleen (Cheville, 1967) [67]. The destruction of lymphoid organs causes immunodeficiency in host chickens (Käufer and Weiss, 1980) [68]. Furthermore, IBDV's impact upon the immune system is exacerbated because it also mediates the apoptosis of B cells, which are an essential component of the adaptive immune system (Rodríguez-Lecompte *et al.*, 2005) [69]. These complications render infected individuals poorly responsive to vaccines and more susceptible to other infectious diseases resulting in higher mortality (Rosenberger and Gelb, 1978) [70]. "Very virulent" strains of IBDV have emerged that are linked to flock mortality rates of 60% (Chettle *et al.*, 1989; van den Berg *et al.*, 1991) [71, 72]. However, not all strains cause high mortality: serotype II IBDV strains have been reported to cause asymptomatic infections (Ismail *et al.*, 1988; Kibenge *et al.*, 1991) [73, 74].

IPNV disease features

IPNV was the first fish virus isolated and studied in cell culture (Wolf *et al.*, 1960) [75]. It is an etiological agent that causes physiological and behavioural changes in infected individuals. Changes in behaviour include an unusual corkscrew swimming motion (Wood et al., 1955) [64]; infected individuals also display darkened pigmentation, abdominal swelling, and pale gills (Wolf, 1988) [76]. These traits are more apparent in young fish, under six months of age, which are at a higher risk of mortality than adults (Frantsi and Savan, 1971) [77]. IPNV subjects the pancreas to necrosis; the liver and kidneys may also show signs of infection, but to a lesser extent than the pancreas (Swanson and Gillespie, 1981) [78].

1.2. Blotched snakehead virus (BSNV)

1.2.1. Discovery and characterization

In 1999, John and Richards reported the discovery of a virus from a cell line prepared from the blotched snakehead fish (*Channa lucius*) [79]. The virus had the characteristics of a birnavirus including a dsRNA genome and a single, non-enveloped, icosahedral shell. Purified virions were found to contain a bisegmented genome and the proteins VP1, VP2, and VP3 (fig. 1.4.). The virions were resistant to heat treatment at 56°C for 2 h and also to pH conditions ranging from 3.0 to 9.0 for 30 min. John and Richards (1999) named it the blotched snakehead virus (BSNV) and recommended its inclusion in the *Birnaviridae* family[79]. It has been accepted as the type species of the genus *Blosnavirus* (Delmas *et al.*, 2012) [1].

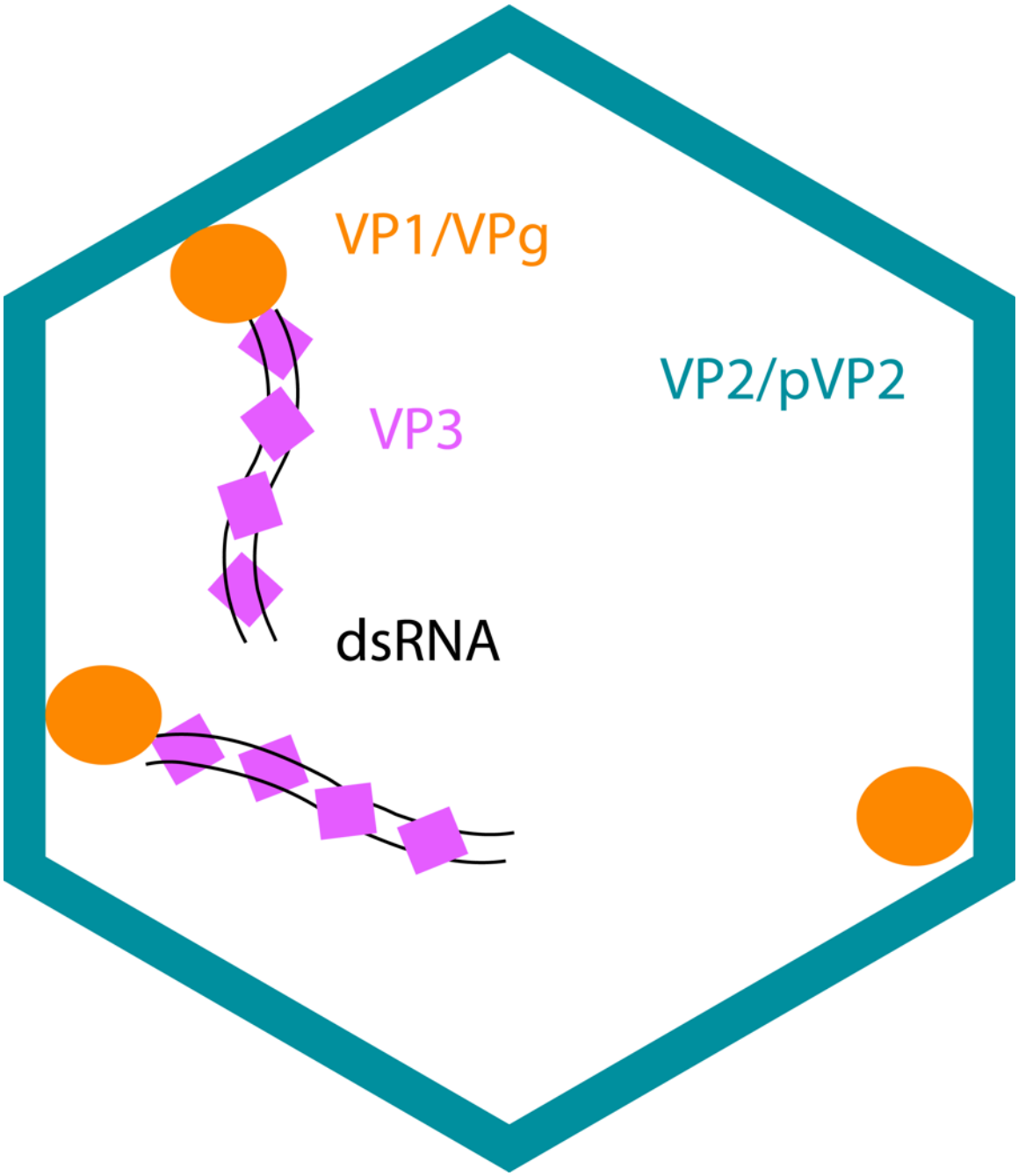

Figure 1.4. *Birnaviridae* virion cartoon.
The icosahedral shell, made from VP2 and pVP2, is depicted in green. The dsRNA genome segments are shown as black lines. VP3 (pink), binds the genome segments, forming ribonucleoproteins. The RdRP, VP1 (orange), is shown in its genome-bound state (VPg) and "free" state. This cartoon is adapted from Delmas *et al.* (2012) [1].

1.2.2. Genome and polypeptides

The BSNV genome (segments A and B) and the segment A polyprotein were characterized by Da Costa *et al.* (2003) (fig. 1.5.) [80]. They found that segment A included two overlapping ORFs - a large ORF (named ORF1) encoding the BSNV polyprotein and a small ORF (named ORF2) encoding a 139 aa polypeptide (fig. 1.5.). The 139 aa polypeptide is analogous, in sequence and gene location, to VP5 of IBDV and IPNV, but its role in BSNV has yet to be experimentally clarified. The 1069 aa polyprotein, pVP2-X-VP4-VP3, was found to be processed into its constituents by the protease VP4. Polyprotein maturation yields four polypeptides - VP2, X, VP4 and VP3. Four peptides are also released that are 43, seven, seven and 12 aa long and called p1, p2, p3 and p4, respectively. It was found that two VP4 residues - Ser692 and Lys729 - were essential for polyprotein maturation. Da Costa *et al.* (2003) sequenced genomic segment B and found that it contained the RdRP, VP1[80].

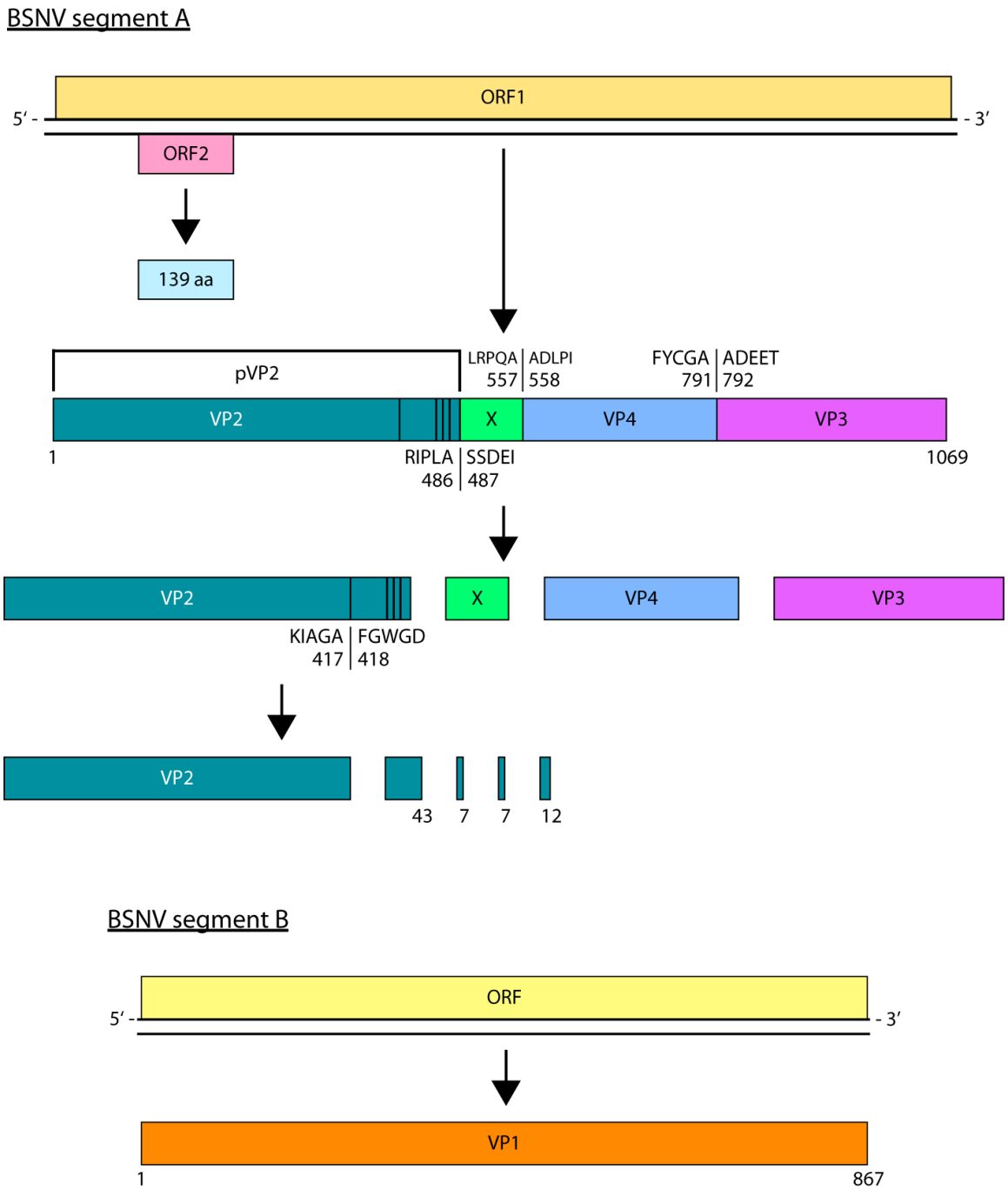

Fig. 1.5. (*Legend on the next page.*)

Figure 1.5. Cartoons of BSNV segment A and B.
The translation of segments A and B is depicted as well as polyprotein maturation. Segment A is composed of approximately 3.4 kbp. It includes ORF1 and ORF2, which are translated into the polyprotein (pVP2-X-VP4-VP3) and a 139 aa polypeptide, respectively. The polyprotein is co-translationally processed by the protease, VP4, to yield pVP2, X, VP4 and VP3. pVP2 matures into VP2 and four peptides that range in size from seven to 43 aa. The locations, and P5 - P5' residues, of major polyprotein cleavage sites are labeled in black. Segment B is composed of approximately 2.8 kbp and encodes the enzyme VP1. Black numbers indicate the terminuses of one strand of each of the dsRNA genome segments and the aa length of the peptides and polypeptides. The BSNV polypeptide (accession number Q8AZM0) and VP1 (accession number Q8AZL8) sequence data is available through UniProt. The schematics are adapted from Delmas *et al.* (2012) [1].

1.3. BSNV VP4

1.3.1. Structure and properties

BSNV VP4 is 234 amino acids in length; it has a calculated molecular mass of 25,247 Da and a theoretical isoelectric point of 5.64 - these values were computed with the ProtParam tool (http://web.expasy.org/protparam/)[81]. The residues are numbered 558 - 791 according to their location within the BSNV polyprotein. The structure, which was solved with a resolution of 2.2 Å, has an α/β protein fold: it includes 13 β-strands, three α-helices, and one 3_{10}-helix (Feldman *et al.*, 2006) [56].

1.3.2. Function and the active site

BSNV VP4 is an endopeptidase, with a Ser-Lys catalytic dyad, that engages in limited proteolysis with the BSNV polyprotein. This event releases mature peptides and polypeptides, such as p1 and VP3. The nucleophile, Ser692, and the general base, Lys729, were identified by site-directed mutagenesis (Da Costa *et al.*, 2003) [80] and X-ray crystallography (Feldman *et al.*, 2006) [56]. The X-ray crystal structure further revealed the presence of an active site water molecule that may serve as the deacylating agent during substrate cleavage. This water molecule is positioned with a 150.2° angle of

attack, as predicted by modeling studies, relative to the carbonyl carbon of the ester intermediate (Feldman *et al.*, 2006; Bürgi *et al.*, 1973) [56, 82].

Da Costa *et al.* (2003) defined the recognition sequence as Pro-X-Ala ↓ (Ala/Ser), based on the characterization of the native polyprotein cleavage sites[80]. The native cleavage sites are listed in table 1.1. Ekici *et al.* (2009) profiled BSNV VP4's substrate specificity and discovered that it is broader in range than the original recognition sequence implied: they redefined the recognition sequence as (Abu/Ala/Pro)-X-Ala ↓ X[83]. An exception to the proposed recognition sequences is that cysteine is tolerated at the P3 position, as well as L-2-aminobutyric acid (Abu), alanine and proline.

Table 1.1. BSNV polyprotein cleavage sites

BSNV Polyprotein Cleavage Sites	Residues P5 - P5'
VP2/p1	KIAGA ↓ FGWGD
p1/p2	KYPEA ↓ ASGRP
p2/p3	GRPLA ↓ ASGRP
p3/p4	GRPMA ↓ ASGTF
p4/X	RIPLA ↓ SSDEI
X/VP4	LRPQA ↓ ADLPI
VP4/VP3	FYCGA ↓ ADEET

Da Costa *et al.* (2003) identified the P5 – P5' residues, included in this table, for all BSNV polyprotein cleavage sites[80].

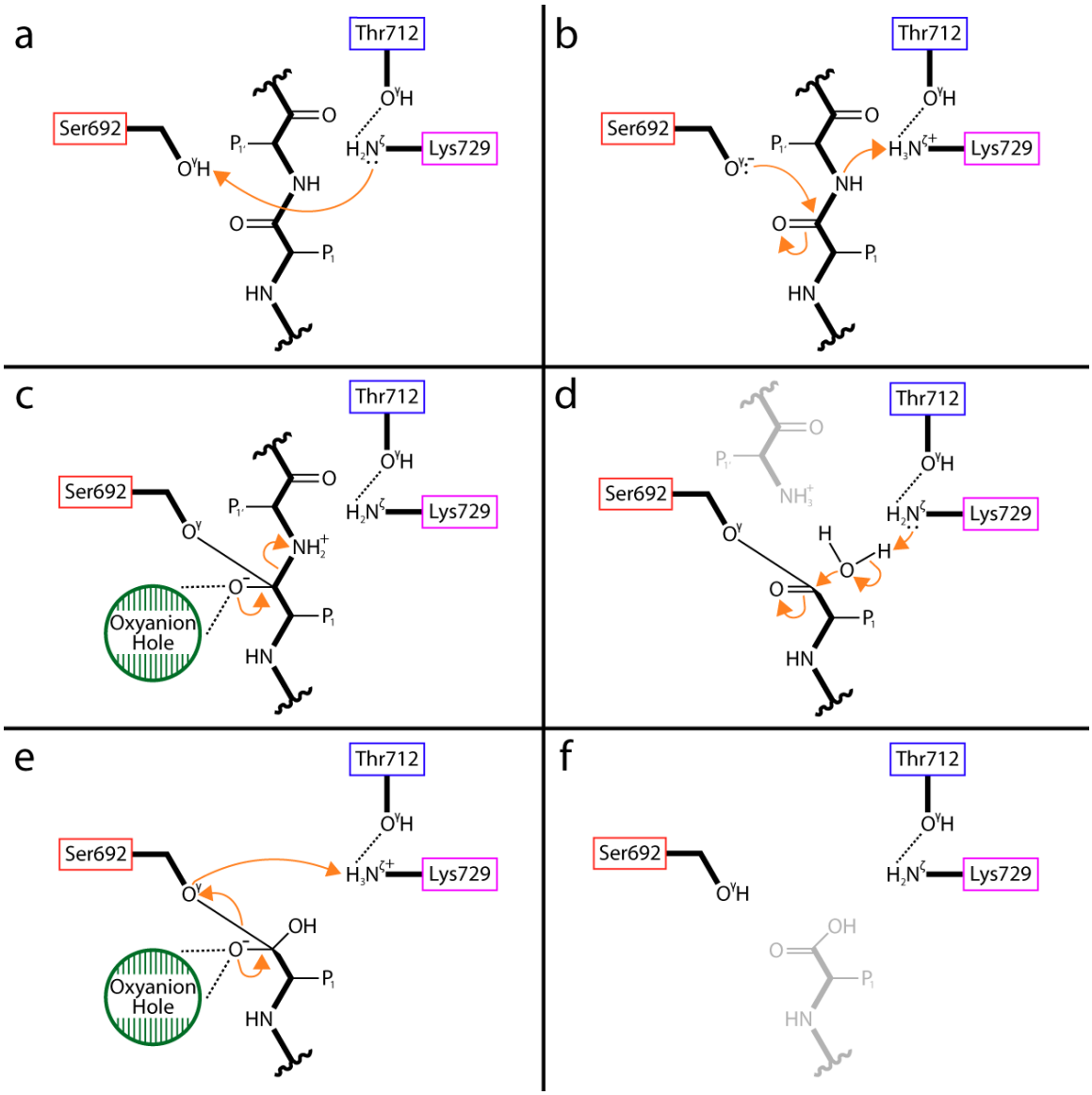

Figure 1.6. Proposed catalytic mechanism for BSNV VP4.
A description of the mechanism is provided in section 1.3.3. The nucleophile, Ser692, is indicated in red. The general base, Lys729, is shown in violet and the coordinator, Thr712, is shown in blue. A substrate, including residues P1 to P1', is shown. Solid, black lines and dotted, black lines represent covalent bonds and hydrogen bonds, respectively. Orange arrows indicate electron pushing. The oxyanion hole is shown in green. This figure is adapted from Paetzel (2014) [84].

1.3.3. Proposed serine-lysine catalytic dyad mechanism

The proposed catalytic mechanism for BSNV VP4 is adapted from the work by Paetzel (2014) [84]. When a peptide or polypeptide substrate binds BSNV VP4's active site under physiological conditions, the Lys729 general base activates the Ser692 nucleophile by abstracting a proton from Ser692's side chain's O^{γ} (fig. 1.6.a). A lone pair of electrons, of the activated nucleophile, attacks the carbonyl carbon of the substrate's scissile peptide bond (fig. 1.6.b) forming the first, transient, tetrahedral transition state. This transition state is characterized by the negative charge of the carbonyl carbon's oxygen, which is stabilized by the oxyanion hole - a substrate-bound structure of BSNV VP4 is needed to confirm which residues, or structural features, constitute its oxyanion hole. The carbonyl carbon of the scissile peptide bond re-establishes a double bond with its oxygen; the C-terminal region of the substrate serves as a leaving group and is the first mature product of catalysis (fig. 1.6.c). The complex that includes the substrate's N-terminal region, bound to VP4, is now called the acyl-enzyme intermediate; a water molecule, activated by the general base, Lys729, attacks the substrate's carbonyl carbon bound to Ser692's O^{γ} (fig. 1.6.d). The oxyanion hole stabilizes the negative charge of the resulting, second, tetrahedral transition state. Following this tetrahedral transition state's collapse (fig. 1.6.e), the N-terminal segment of the substrate exits VP4's active site - it is the second product to do so. BSNV VP4's active site is then available to bind another substrate molecule for a new cycle of catalysis (fig. 1.6.f).

1.3.4. cis- and trans-cleavage

Lejal *et al.* (2000) provide strong evidence for the *trans*-cleavage abilities of IBDV VP4, using the IBDV polyprotein as a test substrate[54]. They also describe experiments testing for heterologous *trans*-cleavage activity between IPNV and IBDV VP4; they found

that neither of these proteases could cleave their homologue's cleavage sites - just as IBDV VP4 was unable to cleave IPNV's polyprotein cleavage sites, IPNV VP4 was unable to cleave IBDV's polyprotein cleavage sites. This data supports the evolutionary divergence of IBDV and IPNV.

YAV VP4 has also been shown to be capable of *trans*-cleavage (Chung and Paetzel, 2013) [52]. A crystal structure of a YAV VP4 molecule's internal cleavage site bound to the active site of a separate YAV VP4 gave direct support for the viability of *trans*-cleavage (Chung and Paetzel, 2013) [52]. This case is comparable to that of a crystal structure of tubular IPNV VP4 displaying intermolecular binding: the structure displays the IPNV VP4 internal cleavage site bound to the active site of a separate VP4 molecule (Lee *et al.*, 2007) [51].

The crystallographic evidence for YAV VP4's *trans*-cleavage activity is supported by *in vitro* data (Chung and Paetzel, 2013) [52]. Fluorometric peptide cleavage assays were performed to demonstrate that YAV VP4 is capable of cutting short peptides carrying a recognition site mimicking residues P7 - P4' of the internal YAV VP4 cleavage site. YAV VP4 was also able to cleave a polypeptide substrate carrying the internal cleavage site sequence.

An intramolecular acyl-enzyme complex structure of TV-1 VP4 offers the strongest evidence for the putative *cis*-cleavage activities of birnaviral VP4s (Chung and Paetzel, 2011a) [85]. This complex displays the catalytic core of TV-1 VP4 forming an acyl-enzyme with its own C-terminal VP4-3 junction. It reveals the protease's ability to bind its C-terminus in *cis*, with high specificity and precision for the correct recognition site. VP4 likely cleaves this site, in this manner, during polyprotein maturation.

1.3.5. Structural comparison with homologues

Infectious pancreatic necrosis virus (IPNV) VP4

Structural studies of IPNV and BSNV VP4 have shown that they are highly similar in spite of sharing only 19% sequence identity across 225 residues (Lee *et al.*, 2007) [51]; they are currently the only members of the S50 peptidase family whose structures have been solved. Bernard Delmas' group was the first to show that they are Ser-Lys proteases through site-directed mutagenesis experiments (Petit *et al.*, 2000; Da Costa *et al.*, 2003) [7, 80]. Structural studies later confirmed the identities of the serine and lysine that serve as the nucleophile and general base, respectively, for BSNV and IPNV VP4: the key active site residues were appropriately positioned and in a suitable environment for catalysis (Lee *et al.*, 2007; Feldman *et al.*, 2006) [51, 56].

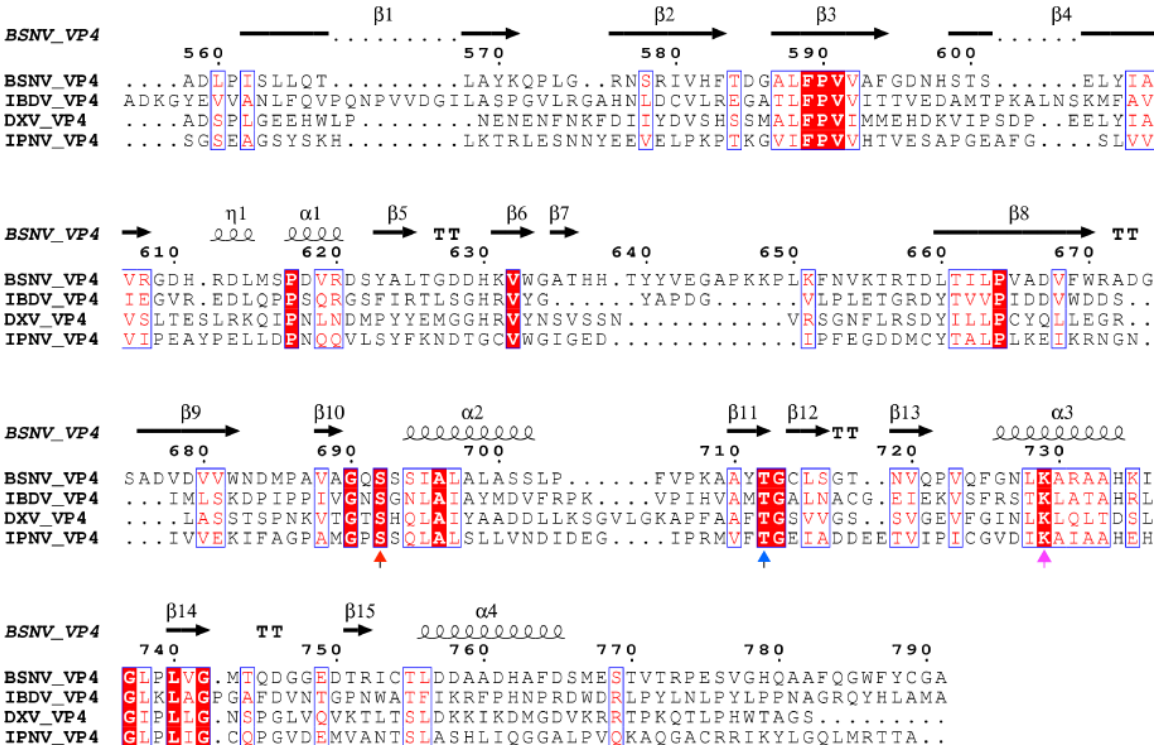

Figure 1.7. Sequence alignment of the S50 family of VP4s.
Includes the VP4 sequences for BSNV (Q8AZM0), IBDV (P61825), DXV (Q96724) and IPNV (P05844); the accession numbers, written parenthetically, were obtained from the UniProt database. The figure indicates the amino acids of BSNV VP4 that constitute the β-sheets (black, horizontal arrows), α-helices (squiggles) and β-turns (TT). Vertical arrows denote major active site residues including the nucleophile, serine (red arrow), the coordinator, threonine (blue arrow), and the lysine general base (violet arrow). The alignment was prepared using ClustalW (Larkin *et al.*, 2007) [86]. The figure was prepared using ESPript (http://espript.ibcp.fr) (Gouet *et al.*, 1999) [87].

Overlapping their peptide backbones demonstrates their structural conservation - they both have α/β structures that differ most significantly in that BSNV VP4 has a β-strand at its N-terminus, which is lacking in IPNV VP4 (Lee *et al.*, 2007) [51]. IPNV VP4 also has one more α-helix and 3_{10}-helix than BSNV VP4. Both BSNV and IPNV VP4 constructs have shown the ability to assume hexagonal crystal forms in crystallization experiments (Lee *et al.*, 2006a; Lee *et al.*, 2006b) [55, 88].

Unlike BSNV VP4, an acyl-enzyme structure is available for IPNV VP4. This structure confirms the active site's location and key residues. It also offers insights to the oxyanion hole (Kraut, 1977) [89] - a region that stabilizes the negative charge of the

transient, tetrahedral intermediate's carbonyl oxygen - and the substrate binding pockets.

Tellina virus 1 (TV-1) VP4

Unlike BSNV VP4, TV-1 VP4 has not been assigned to the S50 peptidase family. It is a member of a different serine peptidase family, the S69 family, because it lacks the glycine residue of the conserved 'Gly - X - Ser' active site motif; it has a phenylalanine (position 736) rather than a glycine (fig. 1.8.) (Nobiron *et al.*, 2008) [2]. TV-1 VP4 is part of the SJ clan and shares many properties with the S50 peptidases including the Ser-Lys catalytic dyad machinery; the catalytic residues are Ser738 and Lys777 (fig. 1.10.c). Site-directed mutagenesis studies by Nobiron *et al.* (2008) have shown that TV-1 VP4 is highly intolerant of mutations to either of the two dyad residues: polyprotein maturation is inhibited by an S738T mutation and also by K777R or K777H mutations[2]. A S738C mutant shows low activity levels, but only when cleaving the VP4-3 junction. Like BSNV VP4, TV-1 VP4 also has the conserved threonine and proline residues in the active site that position the general base, lysine (Chung and Paetzel, 2011a) [85]. TV-1 VP4 is α/β in structure, with three more β-strands, and one more α-helix and 3_{10}-helix than BSNV VP4. Hexagonal crystals of TV-1 VP4 have been reported (Chung and Paetzel, 2011b) [90].

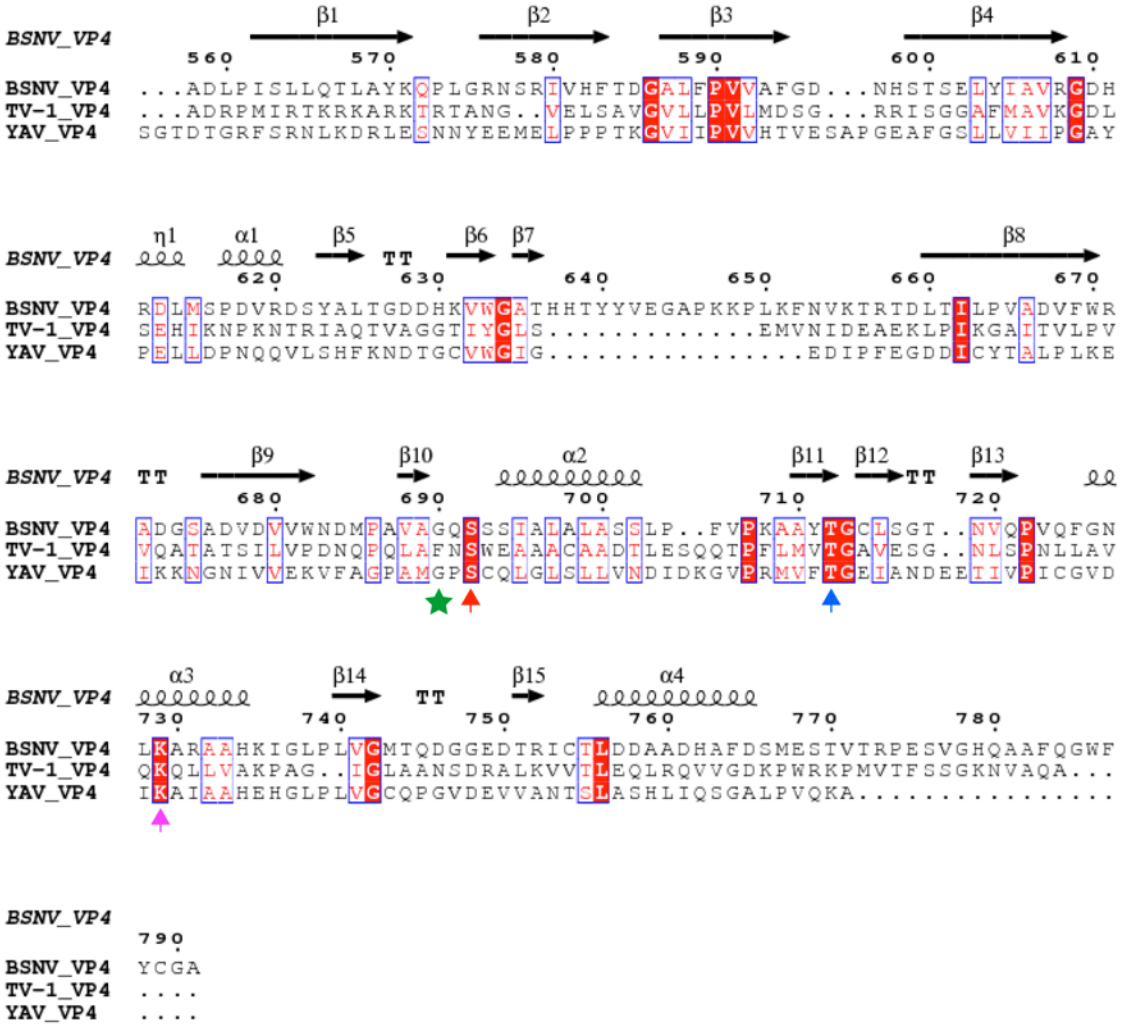

Figure 1.8. Sequence alignment of BSNV, TV-1 and YAV VP4.
Includes the VP4 sequences for BSNV (Q8AZM0), TV-1 (Q2PBR5), and YAV (P89521); the accession numbers, written parenthetically, were obtained from the UniProt database. The YAV VP4 sequence does not include the C-terminal residues after the internal cleavage site, 716/717. The amino acids of BSNV VP4 that constitute the β-sheets (black, horizontal arrows), α-helices (squiggles) and β-turns (TT) are indicated. The major active site residues are indicated with vertical arrows: they include the nucleophile, serine (red arrow), the coordinator, threonine (blue arrow), and the lysine general base (violet arrow). The green star highlights the position of TV-1 VP4's Phe736. The alignment was prepared using ClustalW (Larkin *et al.*, 2007) [86]. The figure was prepared using ESPript (http://espript.ibcp.fr) (Gouet *et al.*, 1999) [87].

TV-1 VP4 is the only birnaviral VP4 for which there is an intramolecular (*cis*) acyl-enzyme complex structure (Chung and Paetzel, 2011a) [85]. This structure shows two amino acids constituting the oxyanion hole: the main-chain amides of Ser738 and Asn737 are within hydrogen bonding distance of the tetrahedral intermediate's carbonyl

oxygen. By contrast, the solved BSNV VP4 apoenzyme structure shows two candidates - the main-chain amides of Ser692 and Gln691 - for the oxyanion hole (Feldman *et al.*, 2006) [56]. The structural data by Chung and Paetzel (2011a) also helps explain why TV-1 VP4 displays the narrowest substrate specificity (Ala-X-Ala ↓) of any VP4: the S1 and S3 pockets - using the Schechter and Berger (1967) nomenclature - are shallow and thereby able to accommodate alanine residues at P1 and P3, but presumably few larger amino acids[85, 91].

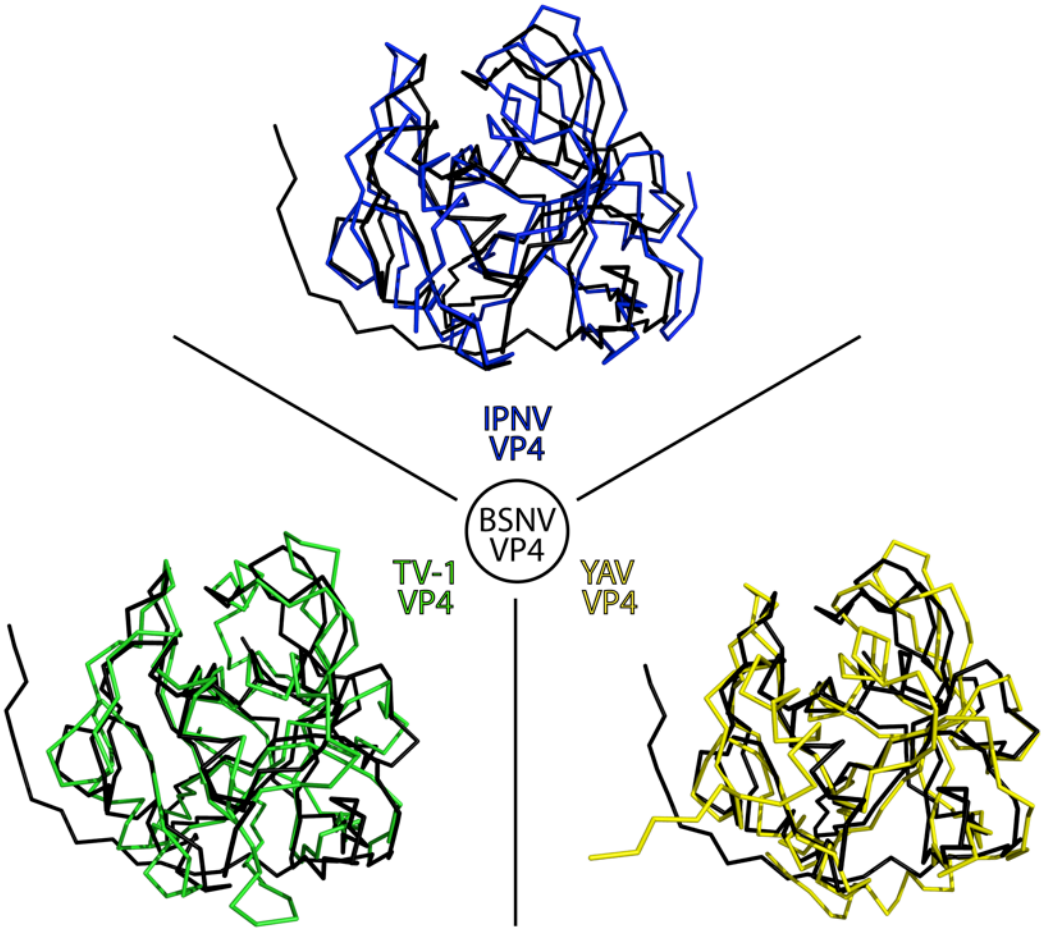

Fig. 1.9. (*Legend on the next page.*)

Figure 1.9. VP4s display conservation of tertiary structure.
The superpositions of the backbones from IPNV, TV-1 and YAV VP4 with the backbone of BSNV VP4 are shown. BSNV VP4 (PDB ID 2GEF) is shown in black in each superposition. IPNV VP4 (PDB ID 2PNM) is blue (top), TV-1 VP4 (PDB ID 3P06) is green (left) and YAV VP4 (PDB ID 4IZK) is yellow (right). The root mean square deviation for the superposition of BSNV VP4 with IPNV VP4 is 1.8 Å for 170 aligned residues (Lee *et al.*, 2007) [51]. The root mean square deviation for the superposition of BSNV VP4 with TV-1 VP4 is 2.0 Å for 160 aligned residues; this was determined with PDBeFold (Krissinel and Henrick, 2004) [92]. The root mean square deviation for the superposition of BSNV VP4 with YAV VP4 is 1.6 Å for 172 aligned residues; this was determined with PDBeFold (Krissinel and Henrick, 2004) [92]. Molecule A was taken from each of the PDB files to make this figure.

Yellowtail ascites virus (YAV) VP4

The MEROPS database includes YAV VP4 as an unassigned homologue of the S50 family of peptidases (Rawlings *et al.*, 2010) [93]. It is α/β in structure, but has one more α-helix and 3_{10}-helix than BSNV VP4 (Chung and Paetzel, 2013; Feldman *et al.*, 2006) [52, 56]. The tertiary structures of YAV and BSNV VP4 are conserved (fig. 1.9.).

YAV VP4 has an internal cleavage site, near its C-terminus, that is analogous to the internal cleavage site of IPNV VP4. All of the solved YAV VP4 structures are cleaved at this site (Chung and Paetzel, 2013) [52]. This protease's structure has been solved in a variety of conformations including, with an empty active site, in an intermolecular (*trans*) acyl-enzyme state, and in a product-bound state (Chung and Paetzel, 2013) [52].

The initial characterization of YAV VP4 did not confirm the identity of the nucleophile, serine (Imajoh *et al.*, 2007) [94]; however, structural data conclusively showed that Ser633 is the nucleophile. YAV VP4 is the first birnaviral VP4 to display an internal disulfide bond: Cys588 and Cys604 participate in this type of bond (Chung and Paetzel, 2013) [52]. It is also the first VP4 to display a channel lined with many hydrophilic contacts that may allow the deacylating water to gain access to the active site, or aid its positioning for nucleophilic attack (Chung and Paetzel, 2013) [52].

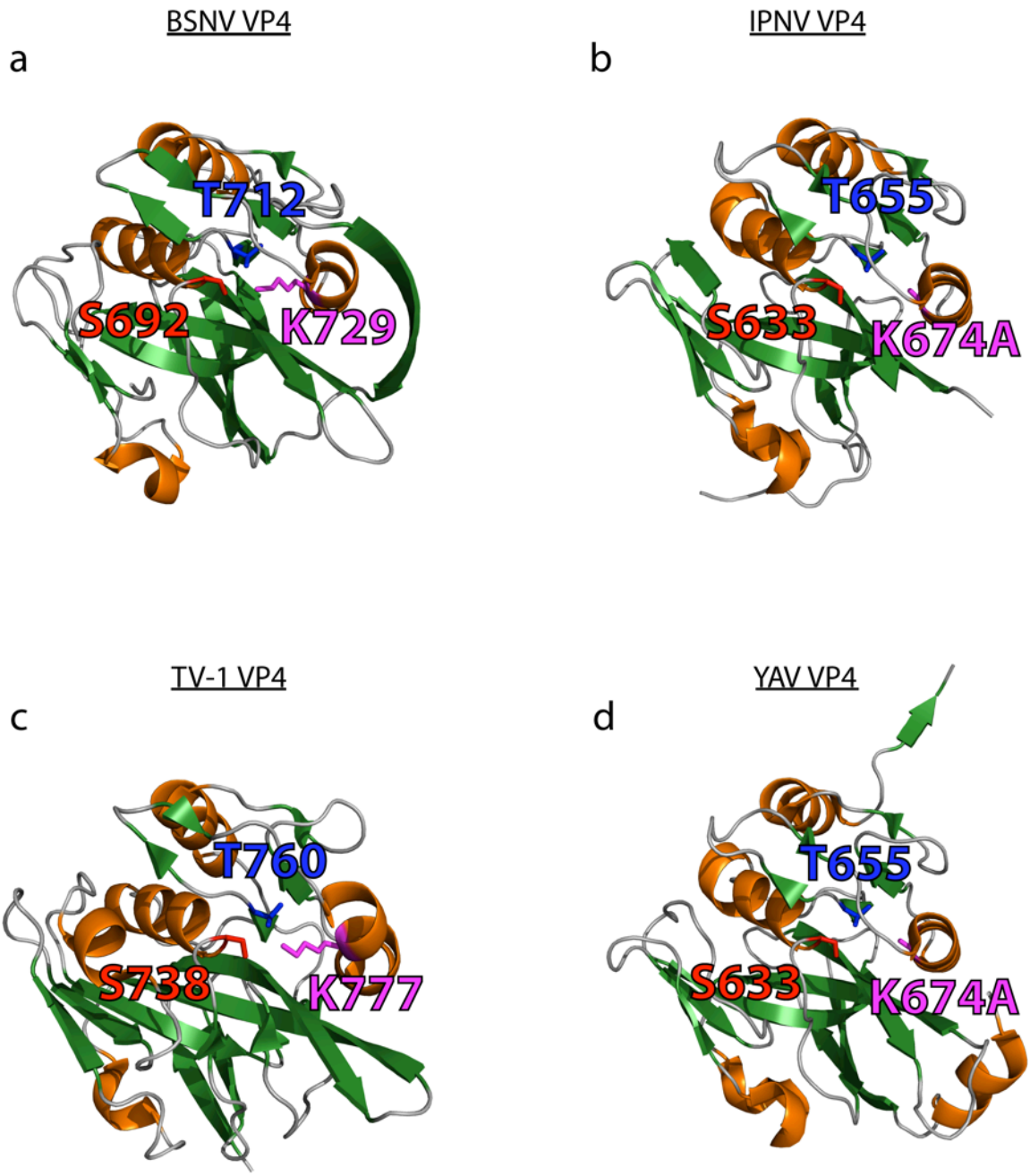

Figure 1.10. Crystal structures of four birnaviral VP4s.
(a) BSNV VP4 (PDB ID 2GEF). (b) IPNV VP4 (PDB ID 2PNM). (c) TV-1 VP4 (PDB ID 3P06). (d) YAV VP4 (PDB ID 4IZK). α-helices are coloured orange, β-strands are green, and random coils are grey. In each structure, the active site serine (red) and lysine (violet) of the Ser-Lys catalytic dyad are indicated. The conserved, active site threonine is indicated in blue. The IPNV (b) and YAV (d) VP4 structures display alanines in the place of the active site lysine residues.

1.4. Proposed significance of Thr712

It is noteworthy that *Birnaviridae* proteases - VP4s - have conserved tertiary structures despite their low, interspecies, sequence identities (fig. 1.7., 1.8., 1.9. and appendix A). It is of further note that certain amino acids in *Birnaviridae* VP4s are absolutely conserved, such as the active site serine and lysine residues, which have been the subject of mutagenesis experiments with several birnaviruses (table 1.2.). However, functional studies of other absolutely conserved residues, such as the active site threonine, have been lacking. The active site threonine is of particular interest to the Ser-Lys catalytic dyad mechanism, because either it, or alternatively, the structurally similar amino acid, serine, is found within the active sites of many of the best characterized bacterial and bacteriophage Ser-Lys proteases, including SPase I[95], SppA [96, 97], LexA[98], Lon[99], UmuD[100] and cIλ[101] (see table 1.3.). There is also a eukaryotic Ser-Lys protease, the *S. obliquus* D1 protease, whose structure confirms the presence of a functionally comparable, active site threonine (Liao *et al.*, 2000) [102]. Hence, the Ser-Lys catalytic dyad architecture, of which an active site threonine or second serine is often an integral part, is relevant to the molecular biology of bacteria and eukaryotes, as well as to the viruses that infect them.

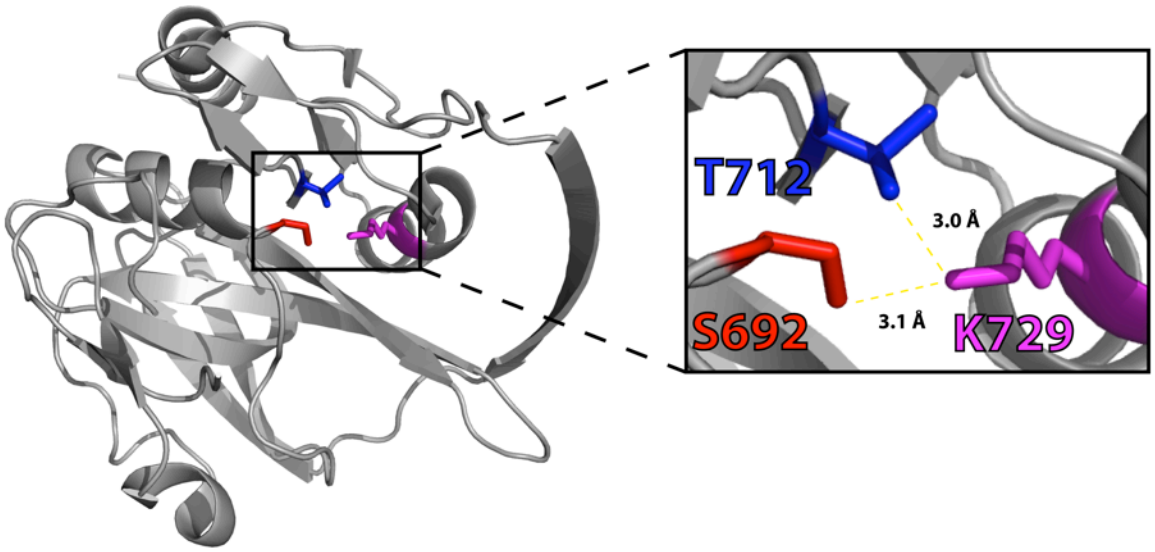

Figure 1.11. BSNV VP4 active site.
Monomeric VP4 (PDB ID 2GEF; molecule B) is depicted in gray, for clarity, on the left. No side-chains are displayed, except for those of Ser692, Thr712, and Lys729; these aa are coloured red, blue and violet, respectively. A close-up of the catalytic dyad residues, and Thr712, is shown on the right.

1.5. Project overview

1.5.1. Experimental objectives

To study the role of the conserved, active site threonine of birnaviral proteases, we have used BSNV VP4 as a model. Its active site threonine residue is Thr712, of which the O^{γ} has been shown, by X-ray crystallography, to be within hydrogen bonding distance of the general base, Lys729's N^{ζ} (fig. 1.11.). What effect, if any, does introducing a T712A mutation have on BSNV VP4's *trans*-cleavage activity? Does BSNV VP4 tolerate conservative mutations, such as T712C, T712S, or T712V? And if a VP4 with one of these mutations is active, does activity increase, decrease or remain unchanged? Herein, we address these questions and progress towards the structural solution of BSNV VP4 (K729A).

Table 1.2. Birnaviral VP4 active site residues

Protease	Species	Nucleophile	General Base	Coordinator	Reference
VP4	BSNV	Ser692	Lys729	Thr712	Feldman *et al.* (2006)
VP4	IBDV	Ser652	Lys692	Thr674	Lejal *et al.* (2000)
VP4	IPNV	Ser633	Lys674	Thr655	Lee *et al.* (2007)
VP4	TV-1	Ser738	Lys777	Thr760	Chung and Paetzel (2011)
VP4	YAV	Ser633	Lys674	Thr655	Chung and Paetzel (2013)

Active site residues of birnaviral VP4s. The DXV VP4 active site residues were excluded from this table due to the lack of experimental data supporting their identities.

Table 1.3. Active site residues of select Ser-Lys proteases

Protease	Species	Nucleophile	General Base	Coordinator	Reference
cI	*Bacteriophage λ*	Ser149	Lys192	Thr190	Bell *et al.* (2000)
LexA	*E. coli*	Ser119	Lys156	Thr154	Luo *et al.* (2001)
SPase I	*E. coli*	Ser91[a]	Lys146[a]	Ser279[a]	Paetzel *et al.* (1998)
SppA	*B. subtilis*	Ser147	Lys199	Ser169	Nam *et al.* (2012)
SppA	*E. coli*	Ser409	Lys209	Ser431	Kim *et al.* (2008)
UmuD'	*E. coli*	Ser60	Lys97	Thr95[b]	Peat *et al.* (1996)

(*a*) These residues are numbered according to the updated SPase I sequence available through the UniProt database with accession number P00803 (Paetzel, 2014) [84].

(*b*) Thr95 is located in close proximity to Lys97 in the crystal structure, but its side-chain's O^{γ} is directed away from the general base.

1.5.2. Experimental approach

The experimental objectives were addressed by *in vitro* methods in the Paetzel laboratory. Expression vectors encoding the BSNV VP4 constructs were prepared in advance of the experiments described herein. Expression vectors encoding polypeptide-substrates of BSNV VP4 were also employed - these substrates mimicked portions of the BSNV polyprotein that included only one, intact, VP4 cut site. Specific mutations of BSNV VP4's codon for Thr712 were made by site-directed mutagenesis and confirmed by sequencing. All constructs of BSNV VP4 and the substrates were purified from bacterial lysates and stored at -80˚C in multiple aliquots for later use. Only constructs used for crystallization trials were not immediately frozen after the completion of expression and purification experiments.

Time-course cleavage assays were performed to assess the effects of different mutations to Thr712. Each assay monitored the progress of cleavage of one substrate by one Thr712 mutant, across time. The extent of each cleavage-reaction was determined by collecting multiple time-points, which were assessed by SDS-PAGE. Wild type (wt) BSNV VP4 and BSNV VP4 (K729A) served as positive and negative control constructs, respectively. Cleavage experiments were replicated to ensure data-reproducibility.

Chapter 2. The effects of threonine 712 mutations on the *trans*-cleavage of VP4-3 by BSNV VP4

2.1. Introduction

Ser692 and Lys729 compose the Ser-Lys catalytic dyad of BSNV VP4's active site. BSNV VP4 features additional conserved residues in close proximity to the dyad residues. One of them is Thr712, whose O^{γ} appears to aid the positioning of Lys729's side chain to properly serve as a general base. Mutating Thr712 to alanine causes a significant decrease in BSNV VP4's rate of *trans*-cleavage. Position 712 appears to tolerate few conservative amino acid substitutions, as either a T712C or T712V substitution results in a decrease in the *trans*-cleavage rate. However, BSNV VP4 (T712S) displays a slight increase in its *trans*-cleavage abilities over wild type BSNV VP4. This result is intriguing: The T712S mutation renders BSNV VP4 a more efficient enzyme, and yet there is no known birnaviral VP4 with a second, active site serine, rather than a threonine, coordinating the general base.

2.2. Materials and methods

2.2.1. Expression and purification of BSNV VP4 constructs

Eight constructs of BSNV VP4 were generated for *in vitro* cleavage assays,

including six enzymes, whose cleavage efficiencies were assessed, and two substrates. The six BSNV VP4 constructs included a (1) wt, (2) K729A, (3) T712A, (4) T712C, (5) T712S, and (6) T712V construct. The two substrates for the cleavage assays included a VP4-VP3 (S692A, K729A; Δ894-1069) construct and an X-VP4 (K729A; Δ774-791) construct. Henceforth, these substrates are abbreviated VP4-3 and X-VP4, respectively. In the gel images presented in this thesis, these substrates are called VP4**-3 and X-VP4* to distinguish them from other VP4 constructs.

All BSNV VP4 constructs were purified according to the scheme in fig. 2.1.a. Lee *et al.* (2006a) demonstrated that, with the steps outlined in fig. 2.1.a, high purity BSNV VP4 could be obtained [55]. Anion exchange chromatography was consistently employed because each VP4-construct was predicted to have a net negative charge at pH 8.0; the surface electrostatics of the solved structure of wt BSNV VP4 supports this prediction (fig. 2.1.b).

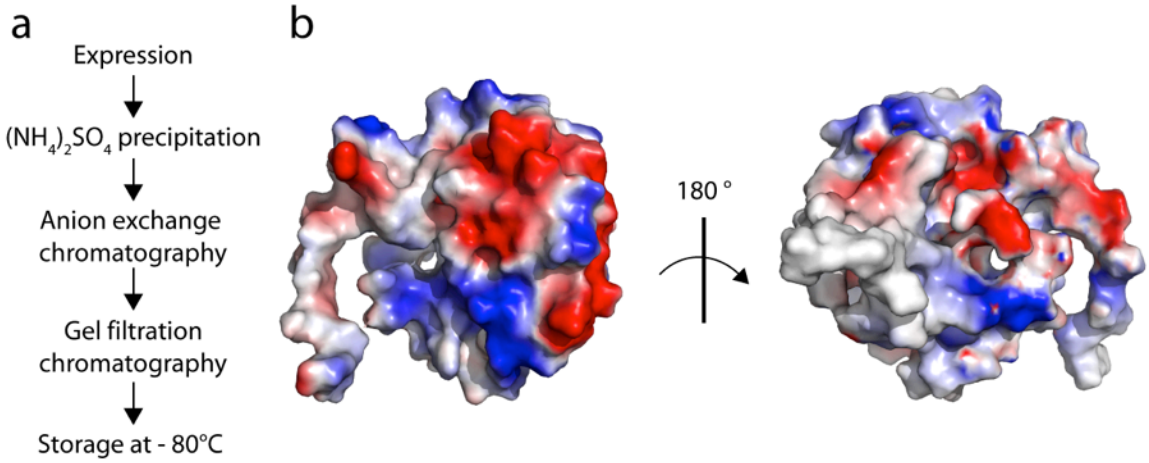

Figure 2.1. Purification of BSNV polypeptide constructs.
(a) Purification scheme. The purification of the X-VP4 construct included one deviation to this scheme: Ni^{2+}-column affinity chromatography was used between the expression and ammonium sulfate precipitation steps. (b) Surface electrostatics of BSNV VP4 (PDB ID 2GEF). Positive (blue), negative (red), and neutral charges (grey) are displayed.

The only exception to the purification scheme, summarized in fig. 2.1.a, applied to the purification of X-VP4: following the expression of X-VP4 and isolation of the soluble fraction of the bacterial lysate, X-VP4 was first purified by nickel (Ni^{2+})-column affinity chromatography. X-VP4 was thereafter purified by ammonium sulfate precipitation, anion exchange and gel-filtration chromatography. The X-VP4 construct had an N-terminal his-tag, which facilitated purification by Ni^{2+}-column affinity chromatography. As none of the other seven BSNV VP4 constructs, described in this chapter, had his-tags, Ni^{2+}-column affinity chromatography was not used at any stage of their purification.

In nature, BSNV VP4 lacks a start codon as it is expressed as part of the BSNV polyprotein where protein X is found at its N-terminus. A start codon, ATG, was present at the N-terminus of the full-length, BSNV VP4 constructs, described in this chapter, for expression. Full-length, wt BSNV VP4 (residues 558 - 791) was cloned into pET-28b(+) - by Dr. Bernard Delmas' group - with the restriction enzymes BamH I and Nco I, downstream of the T7 promoter. This construct, which lacks a tag, was given to the Paetzel lab as a gift. It was deposited into the Paetzel lab glycerol stock with the identifier MWP # 67. Dr. Chung generated the K729A (MWP # 347) and T712A (MWP # 997) mutant constructs of BSNV VP4 by site-directed mutagenesis with the wt BSNV VP4 construct (MWP # 67). For this thesis project, I generated three additional mutant constructs - T712C, T712S, and T712V - using wt BSNV VP4 (MWP # 67) as the template; the sequences of the primers used to make these three constructs are listed in appendix B. Irene Ng cloned the X-VP4 construct (residues 487 – 773) into pET-28a(+) with Nhe I and Sal I. The X-VP4 construct has an N-terminal his-tag and was deposited into the Paetzel lab glycerol stock with the identifier MWP # 267. The VP4-3 construct

(residues 558 – 893), which was cloned into pET-28a(+) with Nco I and EcoR I, was prepared by Dr. Lee and Dr. Chung. This construct lacks a tag and was deposited into the Paetzel lab glycerol stock with the identifier MWP # 991. BL21 (DE3), *E. coli* cells were consistently used to express these constructs to control for the co-purification of bacterial lysate impurities. Schematics of the protein constructs are shown in fig. 2.2.

Expression and purification of BSNV VP4 (K729A)

The pET-28b(+) vector encoding the untagged, full-length BSNV VP4 (K729A) construct was transformed into BL21 (DE3) cells. The cells were plated onto LB agar containing kanamycin at 50 µg/mL to select for transformants. A single colony of cells was used to inoculate 100 mL of LB media with kanamycin (50 µg/mL). The cells were grown overnight (O/N) at 37˚C, shaking at 250 RPM. This O/N culture was used to inoculate 2 L of LB media for large scale growth: to each litre of LB, 10 mL of O/N culture was added as well as kanamycin, with a final concentration of 50 µg/mL. The cells were grown for four hours, at 37˚C, while shaking at 250 RPM. 500 µL of 1 M IPTG was then added to each liter to induce expression of full-length BSNV VP4 (K729A) - expression proceeded O/N at 25˚C while shaking at 250 RPM. A Fiberlite™ F10-6 x 500y fixed-angle rotor (Thermo Scientific) was then used to harvest the cells at 6,000 RPM (6,371 x *g*) for five min. The supernatant was discarded and the harvested cells were resuspended in an extraction buffer (50 mM Tris-HCl (pH 8.0), 10% glycerol, 1 mM DTT, 7 mM magnesium acetate, 0.2 mg/mL lysozyme, 250 U/mL benzonase, 0.1% triton X-100) and lysed O/N at 4˚C.

The BL21 (DE3) lysate was centrifuged at 14,500 RPM (28,964 x *g*) and 4˚C, for 30 min using a JA-17 fixed-angle rotor (Beckman Coulter®) to pellet the cell debris. BSNV VP4 (K729A) was then purified from the supernatant by $(NH_4)_2SO_4$ precipitation

with 10%, 20%, and 30% (w/v) steps. Following each step, the supernatant was incubated on ice for 15 min and then centrifuged at 14,500 RPM (28,964 x *g*) for 15 min to isolate the precipitated protein, which was then resuspended in 2 mL of standard buffer (SB) (20 mM Tris-HCl (pH 8.0), 50 mM NaCl, 1 mM EDTA, 10% glycerol, 1 mM DTT). The 20% and 30% steps had the most BSNV VP4 (K729A) relative to impurities, as assessed by 15% SDS-PAGE, and were poured into dialysis tubing (Fisherbrand®) with a 6,000 – 8,000 Da cut-off. The samples were dialyzed O/N at 4˚C in 2 L of standard buffer. The dialyzed samples were poured over an anion exchange column with a 5 mL, Q-sepharose matrix - the matrix was equilibrated with SB and purification was conducted at 4˚C. The column was washed with 25 mL of SB to remove impurities, and VP4 (K729A) was eluted using a NaCl step-gradient approach (100 mM, 300 mM, 500 mM, and 1 M NaCl steps). Each step was 10 mL in volume and was assessed for purity and yield by 15% SDS-PAGE; the 500 mM NaCl fraction contained the most BSNV VP4 and was carried forward to gel filtration chromatography. The VP4 (K729A) sample was concentrated to approximately 3 mL and centrifuged at top speed on a 4˚C, tabletop centrifuge to pellet any precipitated sample. The supernatant was injected into a pre-packed gel-filtration chromatography column (HiPrep 16/60 Sephacryl S-100 HR) connected to an ÄKTA Prime system at 4˚C. The column had a flow rate of 1.0 mL/min with buffer B (20 mM Tris-HCl (pH 8.0), 100 mM NaCl, 10% glycerol, and 1% β-mercaptoethanol). 3 mL fractions were collected and a high peak, corresponding to fractions 45 to 52, was shown by 15% SDS-PAGE to contain BSNV VP4 (K729A). One 3 mL fraction - number 50 - was concentrated to 500 µL with a concentration of 2.48 mg/mL, as determined via NanoDrop, using the construct's molecular mass, 25.3 kDa, and extinction coefficient, 32,430 M^{-1} cm^{-1}, as inputs. Multiple aliquots of this sample were stored at -80˚C.

Expression and purification of wt BSNV VP4

Full-length, wt BSNV VP4 was expressed and purified using the same methods employed for BSNV VP4 (K729A), described in chapter 2, but with the following differences. After the large-scale expression of wt BSNV VP4, the harvested cells were resuspended in 40 mL of SB and lysis was performed by sonication (45 s) and treatment with a high-pressure homogenizer by AVESTIN®. The cell debris was isolated by centrifugation at 14,500 RPM (28,964 x *g*) for 45 min; the supernatant was carried forward for further purification. $(NH_4)_2SO_4$ precipitation was conducted in the same way as for BSNV VP4 (K729A), although 14,000 RPM (27,001 x *g*) was used to collect the precipitates. Following 15% SDS-PAGE diagnostics of the purified samples, the 20% (w/v) fraction had the highest concentration of wt VP4, and thus was carried forward to anion exchange purification. Following anion exchange purification, the 500 mM and 1 M NaCl fractions had the most wt VP4, and were pooled, concentrated to 2.5 mL, and subjected to gel-filtration chromatography with the same pre-packed column (HiPrep 16/60 Sephacryl S-100 HR) used to purify BSNV VP4 (K729A). A peak on the chromatogram, corresponding to fractions 39 to 46, was shown by 15% SDS-PAGE diagnostics to signify the elution wt BSNV VP4. Fractions 41 to 43 were pooled and concentrated to 6.77 mg/mL, as determined via NanoDrop, using the construct's molecular mass, 25.4 kDa, and extinction coefficient, 32,430 M^{-1} cm^{-1}, as inputs. The final sample was divided into multiple aliquots and frozen at -80˚C.

Expression and purification of BSNV VP4 (T712A)

Full-length, BSNV VP4 (T712A) was expressed and purified using the same methods employed for BSNV VP4 (K729A), described in chapter 2, but with the following differences. 4 L of LB were used for large-scale expression of the T712A construct.

Growth occurred for 4 h at 37˚C, while shaking at 250 RPM; following induction with 500 µL of 1 M IPTG per 1 L of LB, expression proceeded for 4 h at 25˚C, while shaking at 250 RPM. The cells were harvested and lysed using the same method employed for the cells expressing the full-length, BSNV VP4 (K729A) construct; the cell debris was collected by centrifugation at 14,000 RPM (27,001 x *g*) for 30 min. The supernatant was carried forward to $(NH_4)_2SO_4$ precipitation, which was conducted in the same way as for BSNV VP4 (K729A), with the exception that 14,000 RPM (27,001 x *g*) was used to collect the precipitate. Anion exchange chromatography was also performed in the same way as for the K729A construct, except that the 500 mM and 1 M step fractions were carried forward to gel filtration chromatography, as they contained the most VP4 (T712A). Following gel filtration chromatography, a peak revealed by the chromatogram, corresponding to fractions 44 to 50, was shown by 15% SDS-PAGE to indicate the elution of the T712A construct. Fraction 48 had a concentration of 1.00 mg/mL, as determined via NanoDrop, using the construct's molecular mass, 25.4 kDa, and extinction coefficient, 32,430 M^{-1} cm^{-1}, as inputs. The sample was divided into multiple aliquots and frozen at -80˚C.

Expression and purification of BSNV VP4 (T712C)

Full-length, BSNV VP4 (T712C) was expressed and purified using the same methods employed for BSNV VP4 (K729A), described in chapter 2, but with the following differences. 3 L of LB were used for large-scale expression of the T712C construct. Growth occurred for 4 h at 37˚C, while shaking at 250 RPM; the cells were induced with 500 µL of 1 M IPTG per 1 L of LB and expression proceeded for 3 h at 25˚C, while shaking at 250 RPM. The cells were harvested and lysed using the same method employed for the cells expressing the full-length, BSNV VP4 (K729A) construct; the cell

debris was collected by centrifugation at 13,500 RPM (25,107 x *g*) for 30 min. The supernatant was carried forward to $(NH_4)_2SO_4$ precipitation with 10%, 30%, 40% and 50% (w/v) steps. Following each step, the sample was centrifuged at 13,500 RPM (25,107 x *g*) to collect the precipitate. The 30% fraction had a high concentration of the T712C construct, as shown by 15% SDS-PAGE, and was carried forward to anion exchange chromatography. The 300 mM and 500 mM anion exchange steps had a high concentration of the T712C construct, as shown by 15% SDS-PAGE, and were carried forward to gel filtration chromatography. The chromatogram showed a peak corresponding to fractions 42 to 48, which were shown by 15% SDS-PAGE to contain the T712C construct. Fraction 48 was concentrated to 4.28 mg/mL, as determined via NanoDrop, using the construct's molecular mass, 25.4 kDa, and extinction coefficient, 32,430 M^{-1} cm^{-1}, as inputs. Multiple aliquots were stored at -80˚C.

Expression and purification of BSNV VP4 (T712S)

Full-length, BSNV VP4 (T712S) was expressed and purified using the same methods employed for BSNV VP4 (K729A), described in chapter 2, but with the following differences. 4 L of LB were used for large-scale expression of the T712S construct. Growth occurred for 4 h at 37˚C, while shaking at 250 RPM; the cells were induced with 500 µL of 1 M IPTG per 1 L of LB and expression proceeded for 3 h at 25˚C, while shaking at 250 RPM. After harvesting the cells, and lysis, the cell debris was collected by centrifugation at 13,500 RPM (25,107 x *g*) for 30 min. The supernatant was carried forward to $(NH_4)_2SO_4$ precipitation with 10%, 30% and 40% (w/v) steps. Following each step, the sample was centrifuged at 13,500 RPM (25,107 x *g*) to collect the precipitate. 15% SDS-PAGE diagnostics showed that the 30% step had the T712S construct, and thus was carried forward to further purification steps. Anion exchange chromatography

was performed in the same way as for full-length BSNV VP4 (K729A); the 300 mM and 500 mM NaCl steps had the most VP4 (T712S), as shown by 15% SDS-PAGE analysis, and were concentrated to 5 mL for gel filtration chromatography. The chromatogram showed a large peak, corresponding to fractions 39 to 47. 15% SDS-PAGE diagnostics confirmed that these fractions contained VP4 (T712S). Fraction 45 was concentrated to 7.10 mg/mL, as determined via NanoDrop, using the construct's molecular mass, 25.4 kDa, and extinction coefficient, 32,430 M^{-1} cm^{-1}, as inputs. Multiple aliquots were stored at -80˚C.

Expression and purification of BSNV VP4 (T712V)

Full-length, BSNV VP4 (T712V) was expressed and purified using the same approach employed for BSNV VP4 (K729A), described in chapter 2, but with the following differences. 4 L of LB were used for large-scale expression of the T712V construct. The cells were grown for 4 h at 37˚C, induced with 500 µL of 1 M IPTG per 1 L of LB, and expression proceeded for 4 h at 25˚C; the cells were shaken at 250 RPM during growth and expression. The cells were harvested and lysed using the same method employed for the cells expressing the VP4 (K729A). The cell debris was collected by centrifugation at 13,500 RPM (25,107 x *g*) for 45 min. The supernatant was carried forward to $(NH_4)_2SO_4$ precipitation with 10%, 30%, 40% and 50% (w/v) steps. Following each step, the sample was centrifuged at 13,500 RPM (25,107 x *g*) to collect the precipitate. The 30% (w/v) fraction had the most VP4 (T712V), as shown by 15% SDS-PAGE, and was carried forward to further purification steps. Anion exchange chromatography was performed in the same way as for BSNV VP4 (K729A). The 300 mM and 500 mM NaCl steps had the most VP4 (T712V), as shown by 15% SDS-PAGE diagnostics, and were concentrated to 5 mL for gel filtration chromatography. The

chromatogram showed a peak, corresponding to fractions 42 to 48, indicating the elution of VP4 (T712V). This was confirmed by 15% SDS-PAGE diagnostics. Fractions 45 to 47 were concentrated to 4.78 mg/mL, as shown by NanoDrop analysis, using the construct's molecular mass, 25.4 kDa, and extinction coefficient, 32,430 M^{-1} cm^{-1}, as inputs. Multiple aliquots were stored at -80˚C.

Expression and purification of BSNV VP4-3

The untagged, BSNV VP4-3 construct was expressed and purified using the same methods employed for full-length BSNV VP4 (K729A), described in chapter 2, but with the following differences. After the large-scale expression of BSNV VP4-3 by BL21 (DE3) cells, and resuspension of the cells in 40 mL of SB, lysis was performed by sonication (45 s) and treatment with a high-pressure homogenizer by AVESTIN®. The cell debris was isolated by centrifugation at 14,500 RPM (28,964 x *g*), for 30 min at 4˚C, and the supernatant was carried forward to the purification steps. BSNV VP4-3 was first purified by $(NH_4)_2SO_4$ precipitation, with 10%, 20% and 30% (w/v) steps. 15% SDS-PAGE showed that the 20% and 30% (w/v) steps included the VP4-3 construct and were selected for further purification. Anion exchange chromatography was performed in the same way as it was for BSNV VP4 (K729A); the 1 M NaCl fraction was carried forward to gel filtration chromatography. A peak on the chromatogram, corresponding to fractions 36 to 41, indicated the elution of BSNV VP4-3. Fractions 36 and 37 were concentrated to 2.75 mg/mL, as determined by NanoDrop, using the construct's molecular mass, 37.0 kDa, and extinction coefficient, 44,920 M^{-1} cm^{-1}, as inputs. Multiple aliquots were stored at -80˚C.

Expression and purification of BSNV X-VP4

BSNV X-VP4, with an N-terminal his-tag, was expressed and purified using the methods employed for full-length BSNV VP4 (K729A), described in chapter 2, but with the following differences. After the large-scale expression of BSNV X-VP4, the harvested cells were resuspended in SB without EDTA (20 mM Tris-HCl (pH 8.0), 50 mM NaCl, 10% glycerol, 1 mM DTT). Lysis was performed by sonication (45 s) and treatment with a high-pressure homogenizer by AVESTIN®; the cell debris was collected in the same way as described for the K729A construct and the supernatant was isolated. The first purification step employed was Ni^{2+}-column affinity chromatography: the supernatant was poured over a Ni^{2+}-column, which included 3 mL of Ni^{2+} beads under room temperature conditions that were equilibrated with SB without EDTA. The column was washed with 25 mL of buffer and X-VP4 was eluted by a step gradient approach with increasing concentrations of imidazole (150 mM, 250 mM, 500 mM, and 1 M); each of the steps was 10 mL in volume. All four steps were pooled and subjected to $(NH_4)_2SO_4$ precipitation, with 20%, 30%, and 40% (w/v) steps. 15% SDS-PAGE diagnostics showed that the 30% and 40% (w/v) steps included X-VP4, and these steps were carried forward for further purification. Anion exchange purification was conducted in the same way as for full-length BSNV VP4 (K729A); the 300 mM, 500 mM and 1 M NaCl steps had the most X-VP4, as shown by 15% SDS-PAGE, and were carried forward to gel filtration chromatography. A peak on the chromatogram, corresponding to fractions 41 to 47, indicated the elution of BSNV X-VP4. Fractions 41 and 42 were concentrated to 3.77 mg/mL, as determined via NanoDrop, using the construct's molecular mass, 33.3 kDa, and extinction coefficient, 32,430 M^{-1} cm^{-1}, as inputs. Multiple aliquots were frozen at -80˚C.

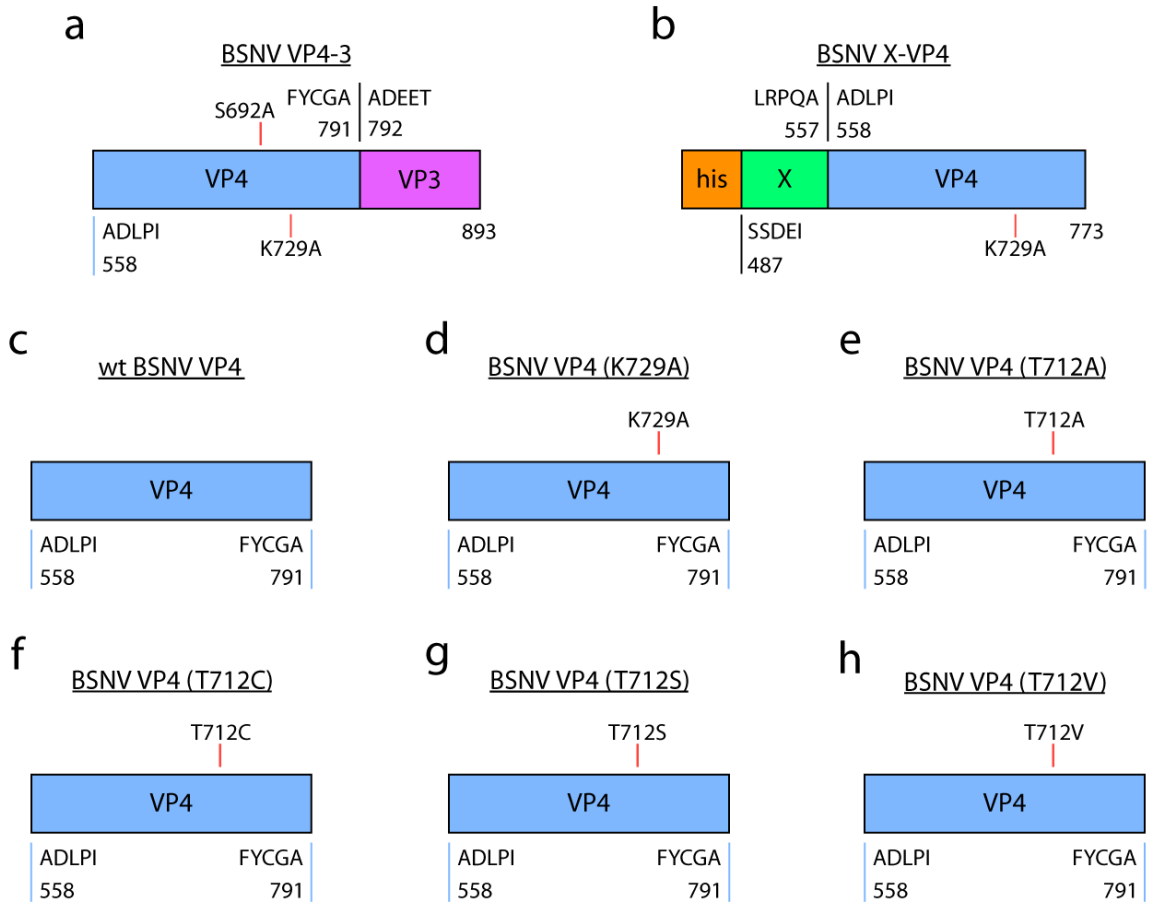

Figure 2.2. Cartoons of eight BSNV VP4 constructs.
The protein constructs include VP4 (a-h; blue), the N-terminus of VP3 (a; violet), protein X (b; pale green) and a his-tag (b; orange). The P5 - P5' amino acids present in each construct are included. Numbers also indicate the positions of the constructs' terminal amino acids based on their location in the BSNV polyprotein. Note that the N-terminal his-tag for X-VP4 includes the residues Met-Gly-Ser-Ser-His-His-His-His-His-His-Ser-Ser-Gly-Leu-Val-Pro-Arg-Gly-Ser-His-Met-Ala.

2.2.2. Construct stability tests

The stabilities of each of the six BSNV VP4 constructs, in buffer B, were assessed across one week at room temperature (fig. 2.3.). Differences between the stability experiments (such as VP4 concentrations, and the days on which time-points were collected) are accounted for by the fact the experiments were conducted at different times, often months apart.

All VP4s displayed integrity and stability during the one-week observation period. BSNV VP4 (T712S) displayed some minor degradation, particularly by day 7, but was otherwise stable during the first few days of observation. These tests demonstrated that the VP4 constructs would likely maintain their integrity during cleavage assays, which were performed during periods that lasted hours, rather than days, after being withdrawn from -80˚C storage. Cleavage assays were performed under the same temperature and buffer conditions as these stability assays.

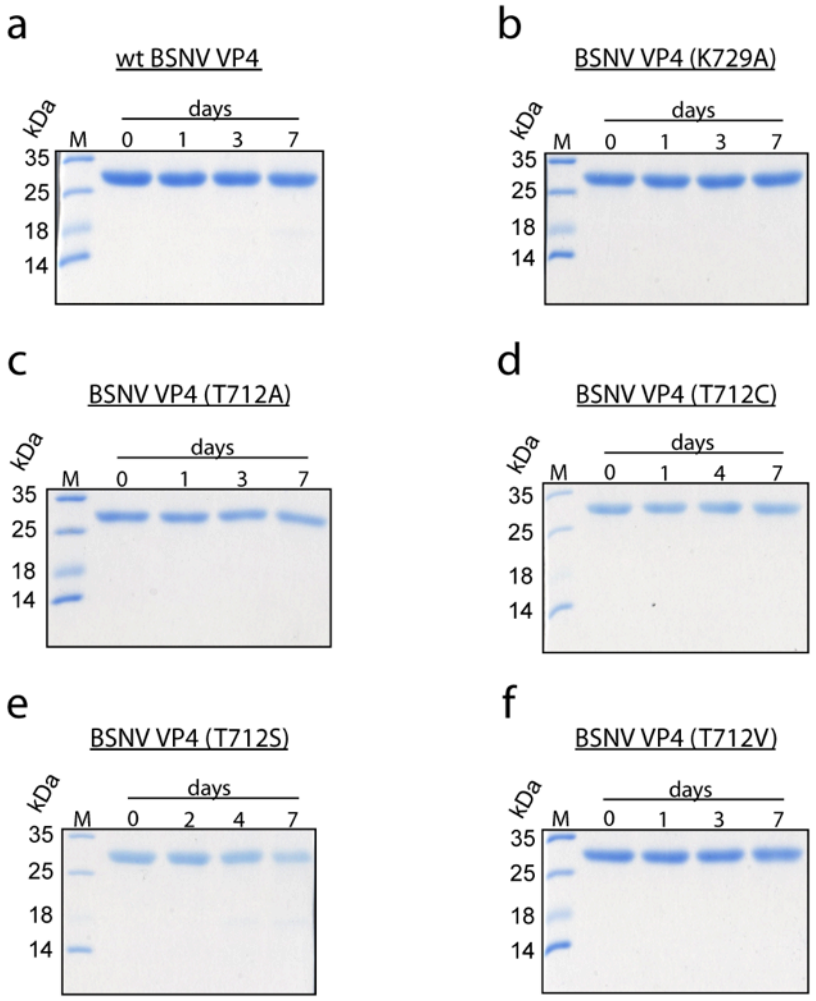

Figure 2.3. Stability assays of BSNV VP4 constructs.
The assays were conducted across seven days, at room temperature, and in the same buffer (20 mM Tris-HCl (pH 8.0), 100 mM NaCl, 10% glycerol, and 1% β-mercaptoethanol). M indicates marker lanes. (a) Stability of wt BSNV VP4 across 7 days. 10 µL of 0.5 µg/µL wt VP4 (5 µg) were loaded per time-point. (b) Stability of BSNV VP4 (K729A) across 7 days. 10 µL of 0.5 µg/µL VP4 (K729A) (5 µg) were loaded per time-point. (c) Stability of BSNV VP4 (T712A) across 7 days. 10 µL of 0.3 µg/µL VP4 (T712A) (3 µg) were loaded per time-point. (d) Stability of BSNV VP4 (T712C) across 7 days. 10 µL of 0.3 µg/µL VP4 (T712C) (3 µg) were loaded per time-point. (e) Stability of BSNV VP4 (T712S) across 7 days. 10 µL of 0.3 µg/µL VP4 (T712S) (3 µg) were loaded per time-point. (f) Stability of BSNV VP4 (T712V) across 7 days. 10 µL of 0.3 µg/µL VP4 (T712V) (3 µg) were loaded per time-point.

The substrates for the cleavage assays, X-VP4 and VP4-3, were also assessed for stability (fig. 2.4.). VP4-3 was found to be highly stable across seven days, and was therefore chosen as the substrate for more extensive cleavage assays with the VP4 constructs. X-VP4's degradation was apparent after one day of its stability experiment.

However, it did not completely degrade within one week, as can be seen by the day seven time point. The low stability of this batch of X-VP4 was given due consideration in all cleavage assays in which it served as a substrate for cleavage by a VP4 construct.

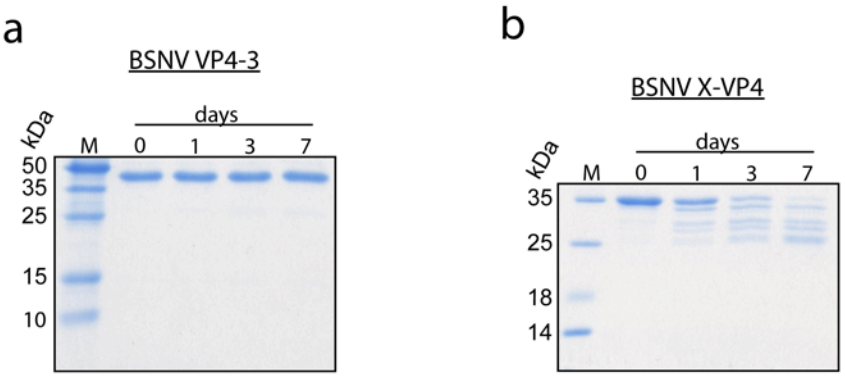

Figure 2.4. Stability assays of X-VP4 and VP4-3 constructs.
The assays were conducted across seven days, at room temperature, and in the same buffer (20 mM Tris-HCl (pH 8.0), 100 mM NaCl, 10% glycerol, and 1% β-mercaptoethanol). M indicates marker lanes. (a) Stability of BSNV VP4-3 across 7 days. 10 µL of 0.25 µg/µL VP4-3 (2.5 µg) were loaded per time-point. (b) Stability of BSNV X-VP4 across 7 days. 10 µL of 0.3 µg/µL X-VP4 (3 µg) were loaded per time-point.

2.2.3. Time-course cleavage assays and data analysis

Time-course cleavage assays were performed to assess the abilities of six BSNV VP4 constructs to cleave two substrate constructs: X-VP4 and VP4-3. All cleavage assays were performed at room temperature in buffer B (20 mM Tris-HCl (pH 8.0), 100 mM NaCl, 10% glycerol, and 1% β-mercaptoethanol). All eight VP4 constructs were in buffer B, and they were also diluted to final reaction concentrations with this buffer.

The VP4-3 and X-VP4 constructs were systematically subjected to digestion by the six VP4 constructs (K729A, T712A, T712C, T712S, T712V, and wt). The substrate-digestions with the VP4 (K729A) and wt VP4 constructs were performed as negative and positive control experiments, respectively. Performing cleavage assays with VP4

(K729A) ensured that no bacterial lysate impurities were responsible for substrate cleavage; they were also useful for confirming the observation by Da Costa *et al.* (2003) that the K729A mutation renders BSNV VP4 an extremely poor enzyme[80]. The positive control experiments were important for ensuring that the purification method described herein yielded active wt VP4.

Digestions of VP4-3 by each of the six VP4-constructs were assessed across two to three hours. Digestion of X-VP4 by each of the VP4-constructs was assessed across 25 hours. Multiple time-points were taken during each assay to assess reaction progress: for instance, all X-VP4 cleavage assays had 0, 1, 3, and 25 h time-points.

In the assays with VP4-3, the concentration of VP4-3 was 13.6 μM and the VP4 constructs' concentrations ranged from 19.7 x 10^{-2} μM to 19.7 μM, depending on the experiment. For assays with X-VP4, the concentration of X-VP4 was 15.0 μM and the VP4 constructs' concentrations were 19.7 μM. Reaction volumes ranged from 50 to 100 μL. 10 μL reaction-aliquots were collected for each time-point and mixed with 10 μL of loading dye and boiled for five min. The time-point aliquots were assessed by 15%-SDS-PAGE. The SDS-PAGE gels were stained with PageBlue, de-stained with dH_20, and scanned at 600 DPI. Densitometry was performed with ImageJ software (Schneider *et al.*, 2012) [103]. Images of the gels used for densitometry are in appendix C.

2.3. Results

2.3.1. trans-cleavage of X-VP4

We assessed the abilities of six BSNV VP4 constructs to cleave an X-VP4 polypeptide, which has an N-terminal his-tag. These experiments were performed by

the method of time-course cleavage assays with SDS-PAGE diagnostics. They were performed at room temperature, in buffer B, across 25 h. We found that BSNV VP4 (T712S) was the best construct at cleaving X-VP4, as per the nearly complete substrate-digestion at the 180 min time-point (fig. 2.5.a). wt VP4 completely digested X-VP4 by the 25 h time point (fig. 2.5.b), but at a lower rate than VP4 (T712S). The remaining four VP4 constructs - K729A, T712A, T712C, and T712V - were indistinguishable, based on SDS-PAGE diagnostics, in their abilities to cleave X-VP4: none of these constructs were able to bring the reaction to completion within 25 h (fig. 2.5.c-f).

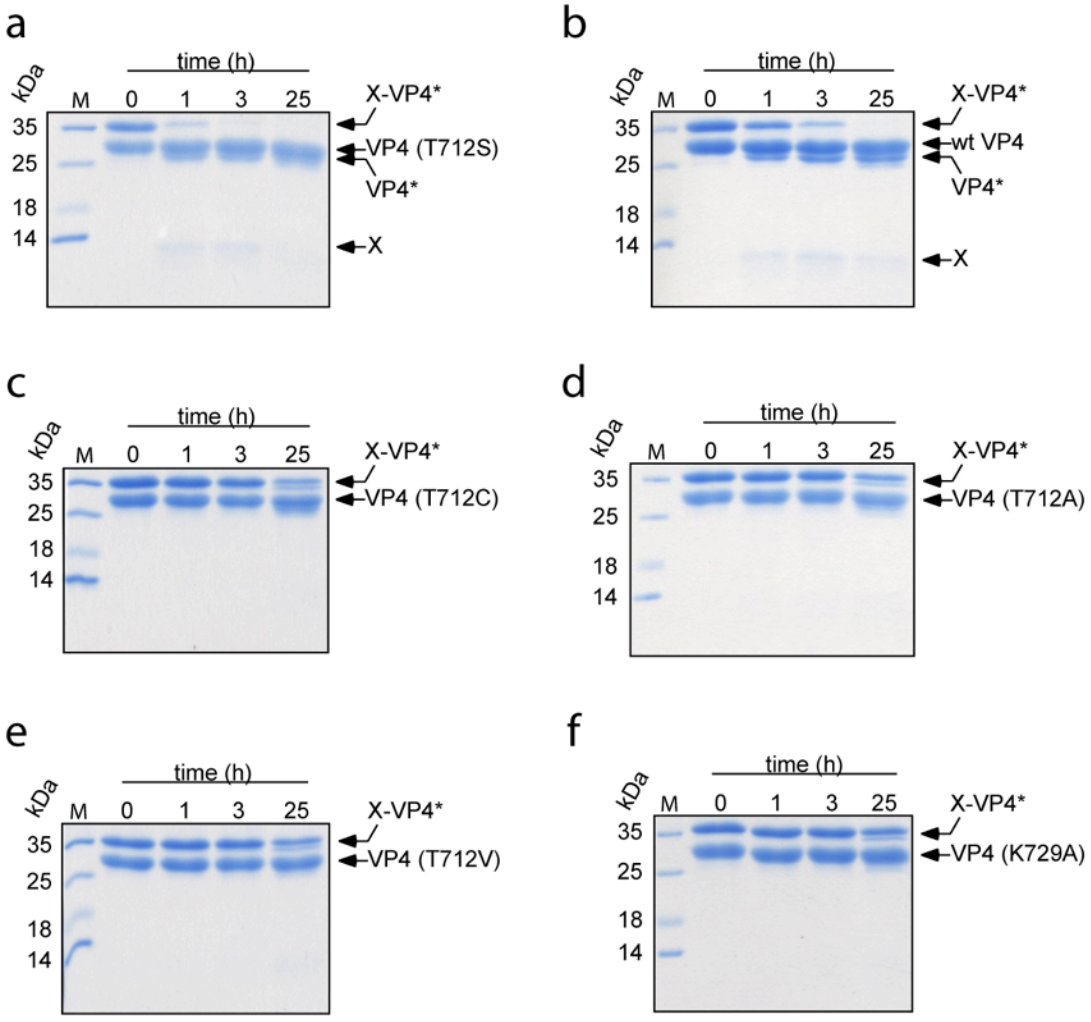

Figure 2.5. *trans*-cleavage of X-VP4.
15% SDS-PAGE gels summarizing the time-course cleavage assays of X-VP4 digested by (a) VP4 (T712S), (b) wt VP4, (c) VP4 (T712C), (d) VP4 (T712A), (e) VP4 (T712V), and (f) VP4 (K729A) at room temperature. The assays' buffer conditions were 20 mM Tris-HCl (pH 8.0), 100 mM NaCl, 10% glycerol, and 1% β-mercaptoethanol. The molar ratio of X-VP4 (K729A) to VP4 (T712S), wt, (T712C), (T712A), (T712V), or (K729A) was 0.8:1.0 in (a), (b), (c), (d), (e), and (f), respectively. The time-points taken for each of these assays were 0, 1, 3, and 25 h. M indicates marker lanes. The single star (*) denotes the K729A, active site mutation of the X-VP4 substrate.

2.3.2. trans-cleavage of VP4-3

Time-course cleavage assays, which assessed wt BSNV VP4's ability to cleave VP4-3, showed that wt VP4 cleaved this junction in *trans* with high efficiency. For these assays, the concentration of VP4-3 was 13.6 μM and the concentration of wt VP4 was

1.97×10^{-1} μM (the molar ratio of VP4-3 to wt VP4 was 69:1.0), such that the substrate was in excess. The reaction reached completion by the 60 min time-point (fig. 2.6.a). The VP4 (T712S) construct was more efficient than wt VP4 at cleaving VP4-3 under identical conditions: within 30 min, over 95% of VP4-3 was cleaved by VP4 (T712S) (fig. 2.6.b). None of the other VP4 constructs cleaved all of the VP4-3 within 120 min when the ratio of substrate to enzyme was 69:1.0 under the same reaction conditions. We observed that the average percentages of VP4-3 cleaved by VP4 (K729A), (T712A), (T712C), and (T712V) ranged from 3.4% ± 0.8% to 19% ± 11% (fig. 2.7.). This demonstrated that these four constructs were less efficient at cleaving the VP4-3 substrate than wt VP4 and VP4 (T712S). We next considered how increasing the concentrations of these four enzymes, relative to VP4-3's concentration, influenced their abilities to cleave this substrate.

The four VP4 constructs - K729A, T712A, T712C, and T712V - which displayed low rates of substrate cleavage when VP4-3 was in excess, were tested again but at higher concentrations relative to the substrate concentration. Cleavage assays in which the substrate to enzyme ratio was 0.7:1.0 were performed with each of these VP4 constructs; the concentration of VP4-3 was 13.6 μM and of each of the VP4 constructs was 19.7 μM.

VP4 (T712C) cleaved 95% ± 4.0% of the substrate by the 120 min time-point. VP4 (T712A) cleaved 73% ± 1.6% of the VP4-3 substrate by the 120 min time-point. VP4 (T712V) cleaved 49% ± 3.1% VP4-3 by the 120 min time-point. Also, in support of previous work, the BSNV VP4 (K729A) construct showed low levels of substrate cleavage (less than 10%) at 120 min (fig. 2.8.).

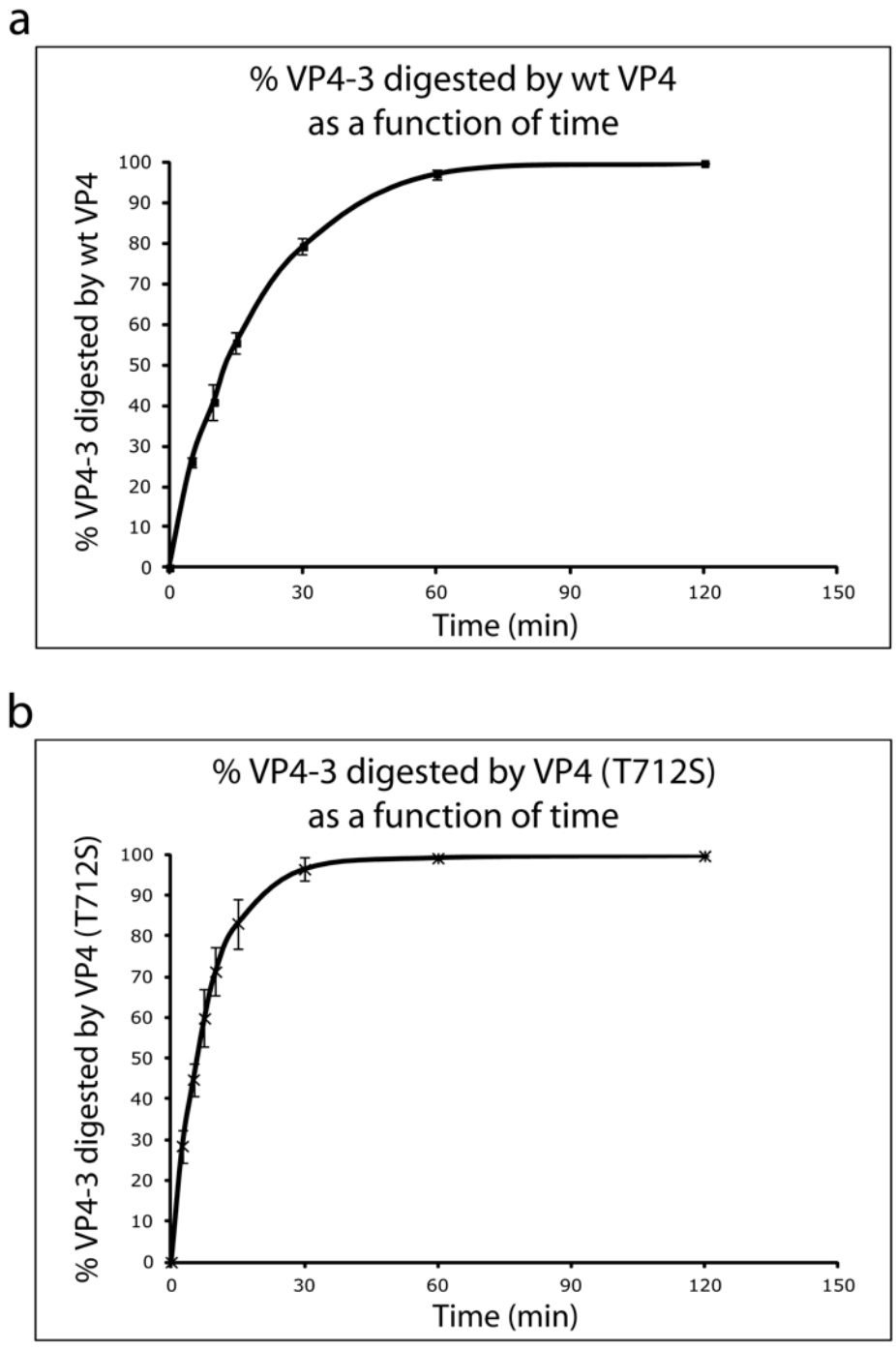

Fig. 2.6. (*Legend on the next page.*)

Figure 2.6. VP4-3 digestion by wt VP4 and VP4 (T712S).
Graphs summarizing the time-course cleavage assays of VP4-3 digested by (a) wt VP4 (n = 3) and (b) VP4 (T712S) (n = 3) at room temperature. The assays' buffer conditions were 20 mM Tris-HCl (pH 8.0), 100 mM NaCl, 10% glycerol, and 1% β-mercaptoethanol. The molar ratio of VP4-3 to VP4 (wt or T712S) was 69:1.0 in both (a) and (b). (a) The time-points for the cleavage assays with wt VP4 were 0, 5, 10, 15, 30, 60 and 120 min. (b) The cleavage assays with VP4 (T712S) had the time points 0, 2.5, 5, 7.5, 10, 15, 30, 60 and 120 min. The cleavage assay samples were boiled for 5 min and resolved via 15% SDS-PAGE. Densitometry was performed with ImageJ software. Data points represent the mean %-cleaved ± SEM.

Does a T712A mutation change the substrate specificity of BSNV VP4? A sample of VP4-3, digested by BSNV VP4 (T712A), was subjected to 15% SDS-PAGE diagnostics and then western blotted onto a PVDF membrane. After staining the membrane with Coomassie Brilliant Blue, the VP3 digestion-product was identified; the membrane was sent to the Iowa State University Protein Facility and the VP3 band was subjected to N-terminal sequencing by Edman degradation. The first six, N-terminal residues were identified as ADEETI, which are the correct P1' - P6' residues of VP3's N-terminus. This indicated that the T712A mutation did not alter BSNV VP4's ability to recognize and cleave the VP4-3 junction at the correct location.

a

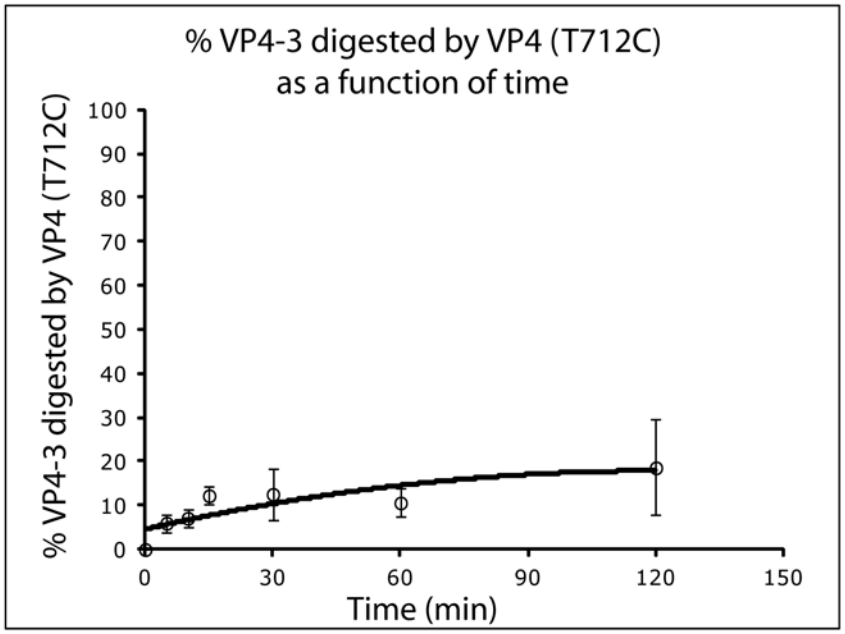

b

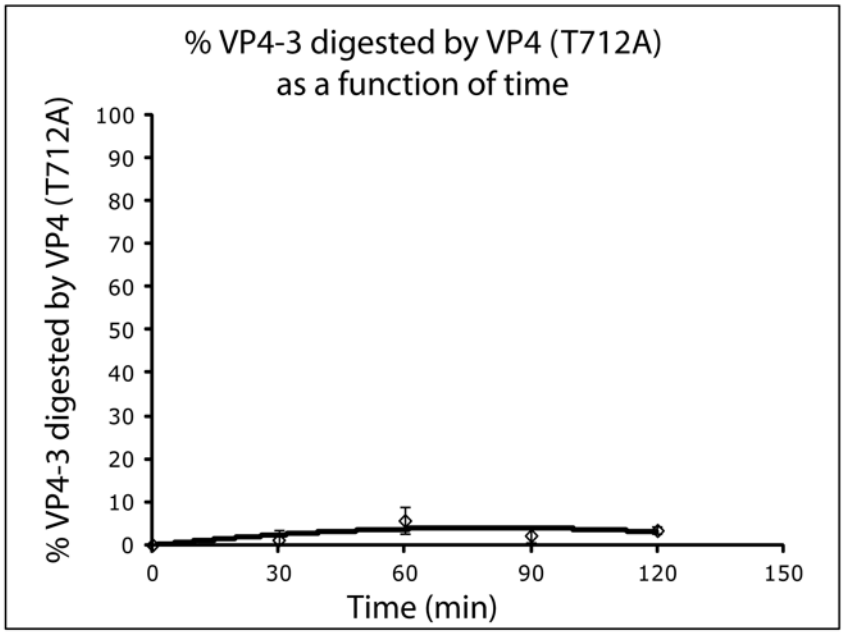

Fig. 2.7. (*Continued on the next page.*)

c

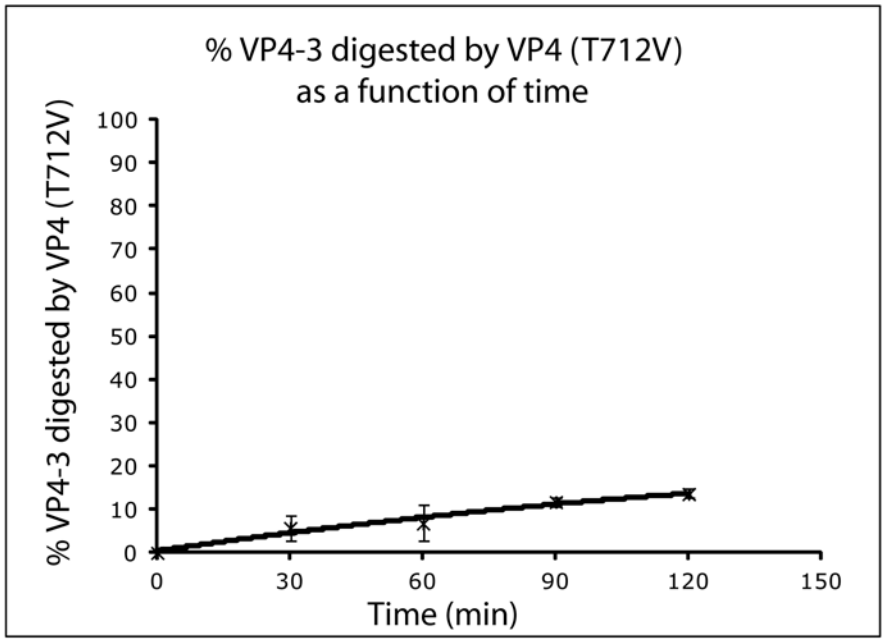

d

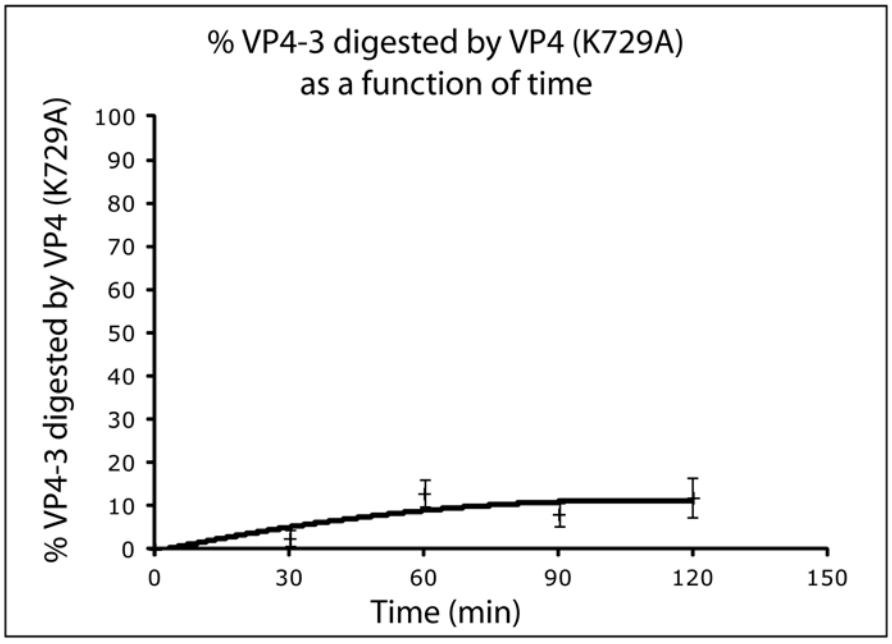

Fig. 2.7. (*Legend on the next page.*)

Figure 2.7. VP4-3 is poorly digested by four different mutant VP4s.
The graphs summarize the time-course cleavage assays of VP4-3 digested by (a) VP4 (T712C) (n = 3), (b) VP4 (T712A) (n = 3), (c) VP4 (T712V) (n = 3), and (d) VP4 (K729A) (n = 3) at room temperature. The assays' buffer conditions were 20 mM Tris-HCl (pH 8.0), 100 mM NaCl, 10% glycerol, and 1% β-mercaptoethanol. The molar ratio of VP4-3 to VP4 (T712C), (T712A), (T712V), or (K729A) was 69:1.0 in (a), (b), (c), and (d), respectively. (a) The time-points taken for the cleavage assays with VP4 (T712C) were 0, 5, 10, 15, 30, 60 and 120 min. (b) The cleavage assays with VP4 (T712A) had the time points 0, 30, 60, 90, and 120 min. (c) The cleavage assays with VP4 (T712V) had the time points 0, 30, 60, 90, and 120 min. (d) The cleavage assays with VP4 (K729A) had the time points 0, 30, 60, 90, and 120 min. The cleavage assay samples were boiled for 5 min and resolved via 15% SDS-PAGE. Densitometry was performed with ImageJ software. Data points represent the mean %-cleaved ± SEM.

2.4. Discussion

When analyzing the band density of VP4-3 at the different time-points, the assumption was made that all decreases in VP4-3 concentration were caused by VP4-mediated cleavage at the recognition site between VP4 and VP3 (whose P5 to P5' residues are FYCGA ↓ ADEET). However, there is an alternative explanation, besides substrate cleavage, for decreases in the band intensity of VP4-3: a small population of acyl-enzyme complexes - including a VP4-3 substrate and a VP4 construct, which would have a combined molecular mass of approximately 62 kDa - may account for band shifts of the substrate that we were unable to detect with PageBlue staining of the polyacrylamide gels. As no band shifts to a molecular mass of approximately 62 kDa were observed in the cleavage assay gels, it was presumed that the formation of stable acyl-enzyme intermediates was rare. If any long-lasting acyl-enzyme intermediates did form, they were deemed to be negligible by-products of the reactions.

a

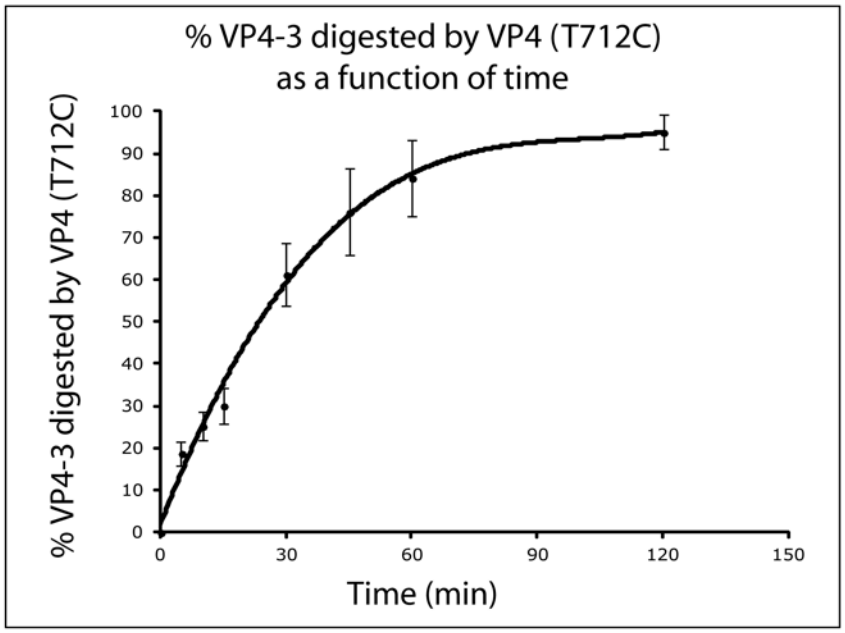

b

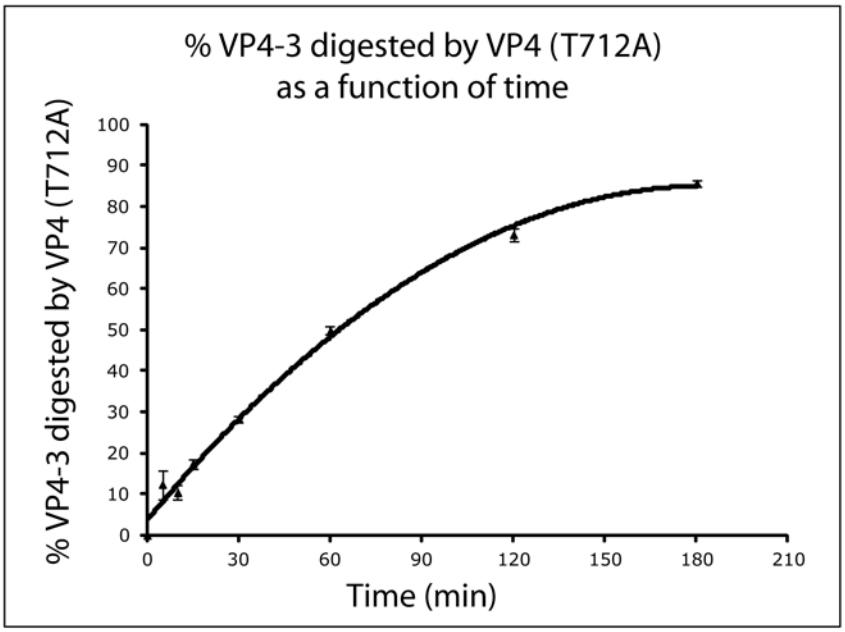

Fig. 2.8. (*Continued on the next page.*)

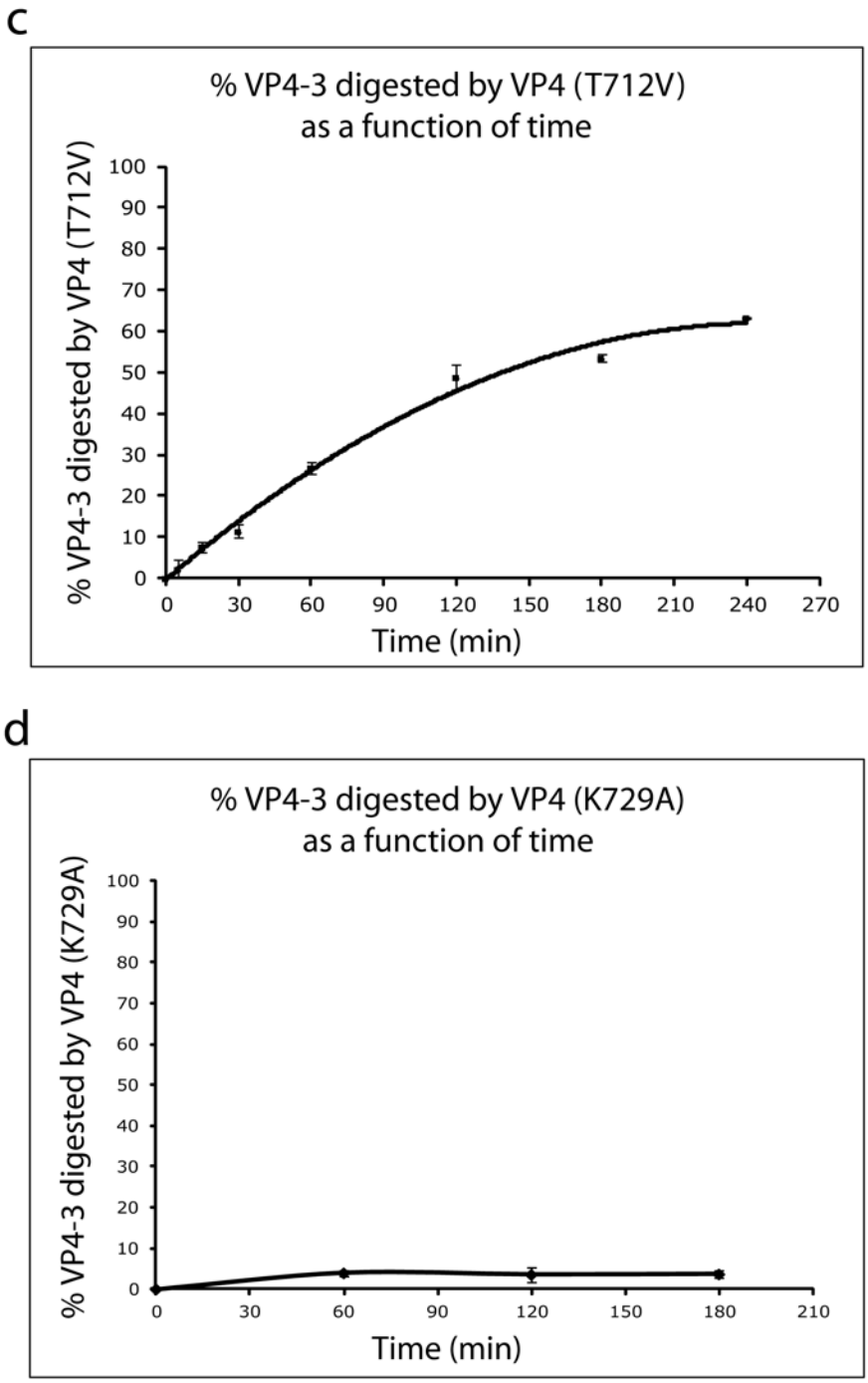

Fig. 2.8. (*Legend on the next page.*)

Figure 2.8. VP4-3 digestion by four different VP4s.
Graphs summarizing the time-course cleavage assays of VP4-3 digested by (a) VP4 (T712C) (n = 3), (b) VP4 (T712A) (n = 3), (c) VP4 (T712V) (n = 3), and (d) VP4 (K729A) (n = 3) at room temperature. The assays' buffer conditions were 20 mM Tris-HCl (pH 8.0), 100 mM NaCl, 10% glycerol, and 1% β-mercaptoethanol. The molar ratio of VP4-3 to VP4 (T712C), (T712A), (T712V), or (K729A) was 0.7:1.0 in (a), (b), (c), and (d), respectively. The time-points taken for the cleavage assays with VP4 (T712C) were 0, 5, 10, 15, 30, 45, 60 and 120 min. The cleavage assays with VP4 (T712A) had the time points 0, 5, 10, 15, 30, 60, 120, and 180 min. The cleavage assays with VP4 (T712V) had the time points 0, 5, 15, 30, 60, 120, 180, and 240 min. The cleavage assays with VP4 (K729A) had the time points 0, 60, 120, and 180 min. The cleavage assay samples were boiled for 5 min and resolved via 15% SDS-PAGE. Densitometry was performed with ImageJ software. Data points represent the mean %-cleaved ± SEM.

The X-VP4 cleavage assays, described in this chapter, were less extensive experiments than the VP4-3 cleavage assays in two respects: (1) each cleavage assay with X-VP4 was duplicated whereas each assay with VP4-3 was performed in triplicate and (2) densitometry was performed with the VP4-3 cleavage assay polyacrylamide gels, but not with the gels for the X-VP4 cleavage experiments. The VP4-3 construct was chosen for densitometric analysis because it proved to be a highly stable substrate when incubated in buffer B, at a concentration of 0.25 μg/μL (6.8 μM), at room temperature (fig. 2.4.a). It was also of interest as an analog of the native BSNV VP4-3 junction. In contrast, X-VP4 was cleaved less efficiently than VP4-3 by wt BSNV VP4. Even when the molar concentration of X-VP4 relative to wt VP4 was approximately 1:1, substrate-cleavage did not go to completion within 180 min. Also, the X-VP4 construct proved to be less stable when incubated in buffer at 0.3 μg/μL (9.0 μM) and room temperature (fig. 2.4.b). The 25 h time points for the X-VP4 cleavage assays, shown in fig. 2.5.c-f, display the X-VP4 band as a doublet.

In the first ten to 15 min of the assays shown in fig. 2.6., there was an approximately linear rate of VP4-3 digestion, suggesting that the substrate's concentration was high enough to facilitate the achievement of the maximum velocity, V_{max}. V_{max} was determined with the Michaelis-Menten equation, $V = V_{max}[S]/(K_m+[S])$:

under conditions where the substrate concentration was significantly greater than K_m, such that K_m could be disregarded, $V = V_{max}$. From applying this logic to the first five min of the assays summarized in fig. 2.6., V_{max} for the wt and T712S VP4 constructs was determined to be 1.2 x 10^{-2} μM s^{-1} and 2.0 x 10^{-2} μM s^{-1}, respectively. The turnover number, k_{cat}, was determined through its relationship with V_{max} by the formula, $V_{max} = k_{cat}[E_t]$. $[E_t]$ represents the total enzyme concentration. The wt and T712S VP4 constructs displayed k_{cat} values of 6.0 x 10^{-2} s^{-1} and 1.0 x 10^{-1} s^{-1}, respectively. With regard to the cleavage of the VP4-3 substrate, the k_{cat} and V_{max} values for wt VP4 and VP4 (T712S) have been estimated to be between one and three orders of magnitude higher than those of the four, slower constructs - T712A, T712C, T712V, and K729A (fig. 2.6. and 2.7.). Future studies should be directed towards probing the activities of the four, slower constructs to determine their rate constants.

Future studies are also needed to accurately determine the Michaelis constant (K_m) values for the cleavage of the VP4-3 substrate by the VP4 constructs. Ekici *et al.* (2009) determined the K_m values of wt BSNV VP4 for the cleavage of three peptide substrates that did not mimic any recognition sites of the BSNV polyprotein: 30 to 71 μM [83]. These K_m values could not be applied to the six VP4 constructs assessed in the context of the VP4-3 substrate: although the VP4-3 substrate had active site mutations that rendered it an extremely poor enzyme, it could bind its own recognition sites, potentially in *cis* or *trans*, blocking binding and cleavage in *trans* by the VP4 constructs. The poor accessibility of the VP4-3 cleavage sites presumably contributes to apparent increases in the K_m values of the VP4 constructs and, in turn, decreases in the specificity constant (k_{cat}/K_m) values.

The X-VP4 and VP4-3 cleavage assay results demonstrate that BSNV VP4 (T712S) is the most efficient protease of the six tested. It is noteworthy that VP4 (T712S) is more efficient than wt VP4: during the initial five min of the cleavage reactions shown in fig. 2.6., VP4 (T712S) shows an approximately 72% higher rate of cleaving VP4-3 than wt VP4. The only structural difference between serine and threonine is, of course, the presence of a methyl group on the side-chain of threonine that is absent from serine's side-chain. The crystal structure of wt BSNV VP4 shows that Thr712 is within hydrogen bonding distance of Lys729. It is likely that when a serine residue occupies position 712 in BSNV VP4, it hydrogen bonds with Lys729 and thereby functions as threonine does - albeit with the effect of producing a more efficient enzyme.

It is intriguing that the T712C mutation resulted in reduced activity relative to wt VP4. Cysteine is of course different from threonine in three respects: (1) it has a thiol group (S^{γ}) rather than a hydroxyl group (O^{γ}), (2) lacks a methyl group, and (3) is capable of forming disulfide bonds. Is the lower electronegativity of Cys712's S^{γ}, relative to Thr712's O^{γ}, a factor in the decreased activity of BSNV VP4 (T712C)? An alternative explanation for the decreased activity of BSNV VP4 (T712C) involves Cys714, which is two residues away from Cys712. Perhaps Cys712 and Cys714 form a destabilizing disulfide bond, due to the fact that they are buried within VP4 and cannot physically contact the reducing agent, β-mercaptoethanol, in buffer B. This construct is an interesting candidate for structural studies to investigate the source of its catalytic perturbation.

By introducing a T712A mutation to BSNV VP4, one hydrogen bond involving the general base, lysine, was eliminated. This mutation decreased the ability of BSNV VP4 (T712A) to cleave the VP4-3 and X-VP4 junctions, indicating that the presence of the

conserved Thr712 in the active site is crucial for VP4's catalytic activity. This finding agrees with studies of *E. coli* SPase I's Ser279 (using the revised SPase I aa numbering): Ser279 performs a function that appears to be analogous to that of BSNV VP4's Thr712; it hydrogen bonds with the active site's general base, Lys146 (Klenotic *et al.*, 2000) [104]. When an S279A mutation is introduced to SPase I, activity is significantly reduced (Klenotic *et al.*, 2000) [104]. The significance of Ser279 led Paetzel (2014) to propose that SPase I may be more accurately classified as a Ser-Lys-Ser triad protease[84]. Similarly, perhaps birnavirus VP4s should be classified as Ser-Lys-Thr triad proteases.

Is the shape of Thr712's side-chain significant to catalysis? To address this question, we made the BSNV VP4 (T712V) construct, whose active site valine is not able to hydrogen bond with Lys729; but, as valine is isosteric with threonine, it is not expected to disrupt the active site geometry. Cleavage assay data indicated that valine, although analogous to threonine in size and shape, was not capable of replacing threonine at position 712 without decreasing activity. Experiments with the T712V construct indicated that Thr712's hydroxyl group is a critical feature of BSNV VP4's active site for the alignment of the general base with the nucleophile, Ser692.

Based on the cleavage data for the substrates X-VP4 and VP4-3, it seems that we are observing a trend: the T712S construct has a higher rate of substrate cleavage over wt VP4 whereas the other three constructs - T712A, T712C, and T712V - have lower rates of substrate cleavage than wt VP4. Is this observation true as well for the junctions that we have not experimentally evaluated, including all five cuts sites within the pVP2-X region of the BSNV polyprotein? Future experiments could address this question.

Why didn't BSNV VP4 evolve a serine at position 712 rather than threonine? The data presented herein is the first to show that a birnavirus protease can be engineered by site-directed mutagenesis to display higher catalytic efficiency. But would BSNV virions encoding VP4 (T712S) display improved infectivity and virulence? Babé and Craik (1997) acknowledged that RNA viruses are capable of introducing many mutations to their genomes, and thereby rapidly evolving under new selection pressures[105]. Perhaps BSNV virions encoding a VP4 (T712S) would display reduced infectivity due to altered spatial and temporal coordination of morphogenesis. *In vivo* experiments should be performed to compare the virulence of wt BSNV virions to BSNV virions with the VP4 (T712S) mutation.

Is it surprising, given previous research of the Ser-Lys catalytic dyad, that the wt and T712S constructs of VP4 are more efficient proteases than the other constructs with conservative mutations - T712C and T712V? No, it agrees with the previous structural studies of Ser-Lys peptidases, which demonstrated that either a second serine or a threonine, in addition to the nucleophile, serine, is often within hydrogen bonding distance of the general base. This observation led Paetzel *et al.* (2002) to propose that Ser-Lys proteases may be more appropriately named Ser - Lys - Ser/Thr proteases[106].

Chapter 3. Crystallization of BSNV VP4 (K729A; Δ774-791)

3.1. Introduction

To date, one structure of the protease, BSNV VP4, has been solved: it displays the wt protease in a homodimer conformation. This structure helped confirm that Ser692 and Lys729 are the protease's nucleophile and general base, respectively. It also revealed that the conserved, active site residue, Thr712, could be within hydrogen bonding distance of the general base. Here, we present data for the crystallization of a mutant construct of BSNV VP4, in which Lys729 has been mutated to alanine (K729A). Da Costa *et al.* (2003) showed that this mutation rendered VP4 into an extremely poor enzyme[80]. Solving a high-resolution crystal structure of BSNV VP4 (K729A) will allow us to study the configurations of the active site's Ser692 and Thr712, as well as the active site geometry, in the absence of the general base.

3.2. Materials and methods

3.2.1. The construct

A mutant (K729A) construct of BSNV VP4 was crystallized, for structure solution by X-ray crystallography, to study the conformation of Thr712 in the absence of its hydrogen-bonding partner, Lys729. The untagged, BSNV VP4 (K729A; Δ774-791) construct's gene was cloned into pET-28b(+), with the restriction enzymes BamH I and

Nco I, downstream of the T7 promoter. The gene construct has a stop codon, introduced by site-directed mutagenesis at the codon corresponding to residue 774, which truncates the C-terminus by 18 residues. Lee *et al.* (2006a) reported that attempts to crystallize full length, wt BSNV VP4 were unsuccessful, but that removing the 18 residues of the C-terminus facilitated crystallization efforts [55]. Dr. Chung and Dr. Feldman prepared this construct and deposited it into the Paetzel lab glycerol stocks, under the identifier MWP # 199. The plasmid was sequenced and transformed into BL21 (DE3) cells for expression. Henceforth, this construct will be referred to as VP4 (K729A).

3.2.2. Expression

100 mL of LB media were inoculated with cells from a single colony of an LB agar plate. Both the LB media and agar had kanamycin at 50 µg/mL. The cells were grown overnight (O/N) at 37˚C, shaking at 250 RPM. To each liter of LB (6 L for large-scale expression), kanamycin was added to a final concentration of 50 µg/mL and 10 mL of O/N culture was added. Growth occurred at 37˚C, while shaking at 250 RPM for four hours. 500 µL of 1 M IPTG was then added, per liter of LB, to induce expression of VP4 (K729A) and the cells were grown for four hours in a temperature controlled shaker at 25˚C. The cells were harvested by centrifugation using a Fiberlite™ F10-6 x 500y fixed-angle rotor (Thermo Scientific) at 5,000 RPM (4,424 x *g*) for five min. The supernatant was discarded and the cells were resuspended in an extraction buffer (50 mM Tris-HCl (pH 8.0), 10% glycerol, 1 mM DTT, 7 mM magnesium acetate, 0.2 mg/mL lysozyme, 250 U/mL benzonase, 0.1% triton X-100) and lysed O/N at 4˚C.

3.2.3. Purification

The BL21 (DE3) lysate was subjected to 4˚C centrifugation at 15,241 RPM (32,000 x *g*), for 45 min, using a JA-17 fixed-angle rotor (Beckman Coulter®); this step was performed to pellet the cell debris. The supernatant was carried forward to $(NH_4)_2SO_4$ precipitation with 15%, 45%, 55% and 65% steps (w/v) (fig. 3.1.a). Following each step, the supernatant was incubated on ice for 15 min and then centrifuged at 14,500 RPM (28,964 x *g*). The 45% and 55% steps that had the most VP4, relative to impurities, were poured into dialysis tubing (Fisherbrand®) with a 6,000 – 8,000 Da cut-off. The samples were dialyzed O/N at 4˚C in 2 L of standard buffer (SB) (20 mM Tris-HCl (pH 8.0), 50 mM NaCl, 1 mM EDTA, 10% glycerol, 1 mM DTT). Dialyzed VP4 (K729A) samples were poured over a Q-sepharose anion exchange column with 5 mL of matrix, at 4˚C, that was equilibrated with SB. The column was washed with 25 mL of SB to remove impurities, and VP4 (K729A) was eluted using a NaCl step-gradient approach (100 mM, 300 mM, 500 mM, and 1 M NaCl steps). Each step was 10 mL in volume. All of the 10 mL steps (100 mM NaCl through to the 1 M NaCl step) were pooled for further purification (fig. 3.1.b). The VP4 (K729A) sample was concentrated to approximately 3 mL, centrifuged at top speed on a 4˚C, tabletop centrifuge and purified using a pre-packed gel-filtration chromatography column (HiPrep 16/60 Sephacryl S-100 HR) connected to a ÄKTA prime system at 4˚C. The column had a flow rate of 1.2 mL/min with buffer B (20 mM Tris-HCl (pH 8.0), 100 mM NaCl, 10% glycerol, and 1% β-mercaptoethanol). 3 mL fractions were collected, and the chromatogram showed two peaks. The early peak corresponded to impurities that either formed oligomers or had a high molecular mass, represented by fraction # 33 (fig. 3.1.c). The late peak, corresponding to fractions 46 - 52, was shown by 15% SDS-PAGE diagnostics to correspond to purified VP4 (K729A). Fractions 46 - 52 were pooled and concentrated to

a final volume of approximately 60 µL using a spin column with a 10,000 Da cut-off. The concentration of VP4 (K729A) was found to be 22.97 mg/mL, as determined via NanoDrop using the construct's molecular mass, 23.38 kDa, and extinction coefficient (25,440 M^{-1} cm^{-1}), as inputs. The molecular mass and extinction coefficient of VP4 (K729A) were determined with the ExPASy ProtParam tool.

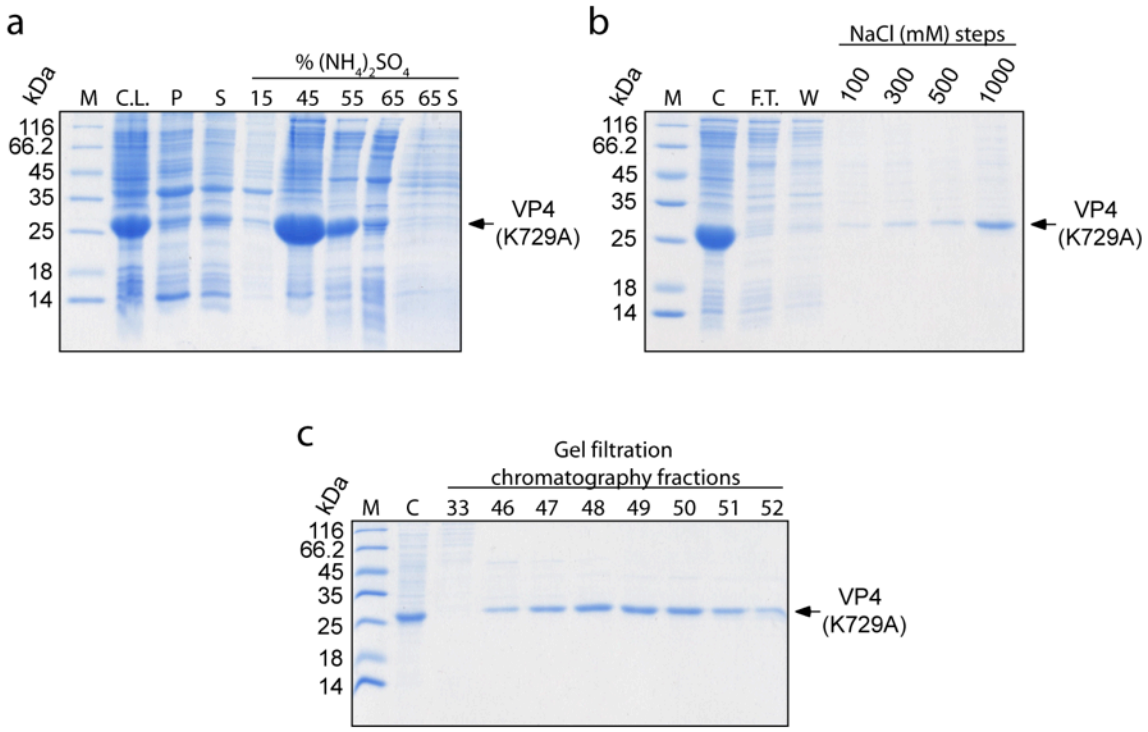

Figure 3.1. Stages of VP4 (K729A) purification.
M stands for the marker lane in all SDS-PAGE gels. (a) 15% SDS-PAGE summarizing cell lysis and $(NH_4)_2SO_4$ precipitation. From left to right, C.L. is the cell lysate. P is the pellet. S is the supernatant. The remaining lanes mark the 15%, 45%, 55%, 65% (w/v) $(NH_4)_2SO_4$ precipitation steps. 65 S is the 65% $(NH_4)_2SO_4$ precipitation step's supernatant. (b) 15% SDS-PAGE summarizing anion exchange purification conducted at 4˚C. C is the positive control sample of the input for anion exchange, which included the pooled and dialyzed 45% and 55% (w/v) $(NH_4)_2SO_4$ precipitation fractions. F.T. is flow-through. W is wash. Samples of the step-gradient fractions - 100, 300, 500 mM and 1 M NaCl - were also included. (c) 15% SDS-PAGE of the most significant gel filtration chromatography (GFC) fractions. C is the positive control sample of the GFC input: the pooled 100 mM - 1 M steps from anion exchange. The remaining lanes were loaded with GFC fractions (33, 46 - 52) corresponding to chromatogram peaks.

3.2.4. Crystallization

24 µL of purified VP4 (K729A) was diluted to 21 mg/mL and crystal-plated, by the sitting-drop method, with a 24-well, custom plate. To prepare each drop, 1 µL of the protein sample was combined with 1 µL of a 1 mL reservoir solution. The reservoir conditions were similar to those that yielded hexagonal crystals for Lee *et al.* (2006a) [55]. A 1/10 dilution of the VP4 (K729A) sample was assessed for purity by 15% SDS-PAGE (fig. 3.2.a). The remainder of this batch was stored at -80˚C.

The single crystal plate was set up at room temperature on Nov 4, 2013. After one day, small, chunky crystals were noticeable in many of the drops, but no significant crystals were observed to be growing. On Dec 3, 2013, a small crystal was observed near the edge of one of the drops in this crystal plate; a picture of this drop, shown in figure 3.2.b, was taken that day. Five days later, the crystal had grown in size (fig. 3.2.c). The reservoir condition that yielded the crystal was 1.4 M ammonium sulfate, 20% glycerol, and 100 mM Tris-HCl (pH 8.5). A new custom plate with a narrower range of conditions was prepared based on this condition. Nearly the entire remaining VP4 (K729A) sample was used to prepare drops in this custom crystallization trial. Many crystals grew, that were either ideal or non-ideal in shape, within days (data not shown).

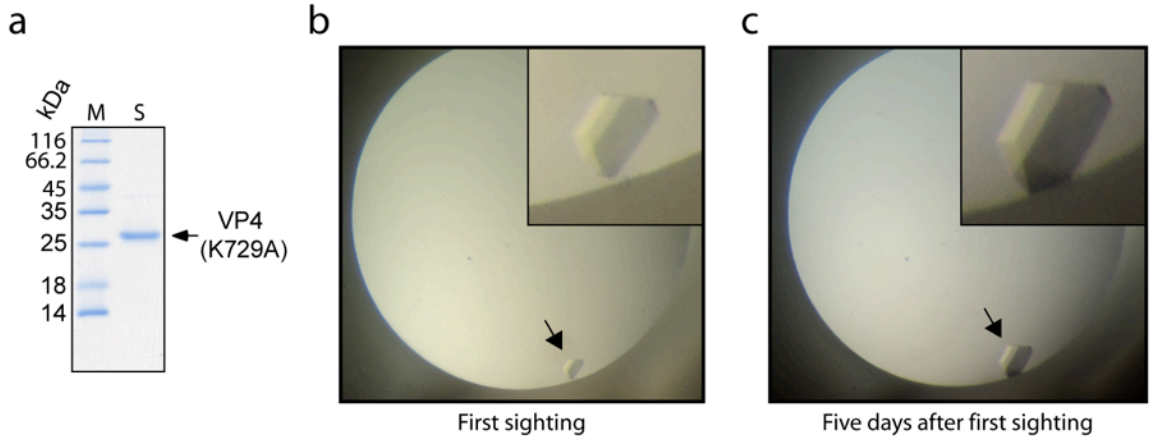

Figure 3.2. Crystallization of BSNV VP4 (K729A).
(a) 15% SDS-PAGE of a 1/10 dilution (2.1 mg/mL) of VP4 (K729A) used for crystallization. M is the marker and S is the sample lane loaded with VP4 (K729A). (b) This image shows a VP4 (K729A) crystal (indicated by a black arrow) that formed during optimization trials. The inset image is an enlargement of the crystal. (c) This image shows the same drop as in fig. 3.2.b, but five days later.

3.3. Results and discussion

3.3.1. Crystals of BSNV VP4 (K729A) can assume a hexagonal morphology

One crystal form of VP4 (K729A) - hexagonal - has been obtained. The crystals are reproducible and appropriate in size for X-ray diffraction analysis. Like the crystals generated by Lee *et al.* (2006a) [55], the crystals formed, under optimized conditions, within one week. Interestingly, we observed that, with each freeze thaw cycle experienced by the soluble, concentrated VP4 (K729A) sample, there appeared to be a decrease in the number of nucleation events per crystal drop. This appeared to promote the growth of fewer but larger crystals; future crystallization trials should be performed to verify this observation.

VP4 (K729A) is not the first construct of BSNV VP4 to form hexagonal crystals: wt BSNV VP4 can also assume this crystal form (Lee *et al.*, 2006a) [55]. Additionally,

BSNV VP4 is not the only birnaviral protease that forms hexagonal crystals – it has been reported that IPNV and TV-1 VP4 form this crystal morphology as well (Lee *et al.*, 2006b; Chung and Paetzel, 2011b) [88, 90].

Interestingly, Feldman *et al.* (2006) solved the structure of wt VP4 from the polyhedral (cubic) crystal form obtained under conditions of 0.1 M Tris-HCl (pH 8.5), 25% (w/v) PEG2000 MME, and 60 mM $Mg(OAc)_2$ [56]. A structure of a BSNV VP4 construct solved from the hexagonal crystal form has not been deposited in the PDB. Perhaps new features of VP4 will be observed from this crystal form. For instance, electron density for residues 637 - 648 of wt BSNV VP4 was not generated from the polyhedral crystals (Feldman *et al.*, 2006) [56]. The diffraction data from the hexagonal crystals of BSNV VP4 (K729A) may provide electron density for these residues, which are presumed to constitute a mobile loop at the protease's surface.

3.3.2. Future work

In future structural studies of BSNV VP4, efforts could be made to solve a substrate-bound structure: either peptide or polypeptide substrates, which mimic BSNV polyprotein cleavage sites, could be subjected to crystallization trials with BSNV VP4. Also, as VP4s are known to form type II tubules, it would be remarkable if BSNV VP4 could be shown to form them as well; electron microscopy and crystallography are proven methods for accomplishing this. At present, only two VP4s have been captured in tubular form via X-ray crystallography - the VP4s from the *aquabirnaviruses*, IPNV and YAV (Lee *et al.*, 2007; Chung and Paetzel, 2013) [51, 52].

In birnaviruses, polyprotein maturation is an essential event during viral morphogenesis and is absolutely dependent upon self-cleavage by the internal protease,

VP4. Thus, VP4s are potential targets for antiviral therapeutics specific for birnaviruses. The birnaviral proteases that are of the greatest economic significance, including those of IBDV and IPNV, are excellent candidates for drug-based inhibition. In addition to the design and efficacy assessment of VP4 inhibitors, structural studies will play a key part in understanding their mode of action.

Chapter 4. Discussion and conclusions

4.1. *Birnaviridae* VP4 kinetic constants

Kinetic constants for the VP4s from the birnaviruses BSNV and IBDV have been published. Chang *et al.* (2012) showed that wt IBDV VP4 (with an N-terminal his-tag) cleaved the fluorogenic peptide (K(Dabcyl)GKARAASE(Edans)G) at 37˚C, pH 8.8, and had a k_{cat} of 0.04 ± 0.01 min^{-1}, a K_M of 43 ± 2 μM, and a k_{cat}/K_M of 15.4 ± 2.5 M^{-1} s^{-1} [107]. The IBDV VP4 construct was optimally active at pH 8.8 between temperatures of 40˚C and 60˚C. Chang *et al.* (2012) also presented the intriguing result that mutating IBDV VP4's nucleophile, serine, or general base, lysine, to alanine significantly decreased the rate of catalysis rather than absolutely inactivated the protease[107]. The notion that mutating either of the *Birnaviridae* VP4 catalytic dyad residues to alanine causes inactivation should be clarified and, if need be, corrected by future research.

BSNV VP4 was shown to have a higher specificity constant than IBDV VP4 (Ekici *et al.*, 2009) [83]. Based on kinetic assays with three fluorogenic peptides - none of which shared sequence identity with native BSNV polyprotein cleavage sites - BSNV VP4 was characterized as having a k_{cat} of 0.075 - 0.35 min^{-1}, a K_M of 30 - 71 μM, and a k_{cat}/K_M of 41 - 166 M^{-1} s^{-1}. As the cleavage assays were performed at room temperature and pH 8.0, the optimal temperature and pH conditions for BSNV VP4 kinetics have yet to be defined. In future experiments, the reaction buffer constituents could also be optimized and fluorogenic peptides, which mimic native cleavage sites, could be employed.

4.2. The search for a triad-constituting residue in the Ser-Lys proteases, *E. coli* LexA and IPNV VP4

In 1991, Slilaty and Vu described their efforts to identify a glutamate or aspartate residue that coordinated the general base, lysine, of the Ser-Lys enzyme, *E. coli* LexA[108]. They used site-directed mutagenesis and kinetic measurements to assess two of LexA's conserved, negatively charged residues: Asp127 and Glu152. Neither of these residues proved to be essential to catalysis, which led them to conclude that the residues of the Ser-Lys dyad were sufficient for catalysis and that an acidic coordinator might raise the pK_a of the general base, lysine, to the detriment of catalysis. Not only did they apply this conclusion to the Ser-Lys dyad of LexA, but also to Ser-Lys dyad enzymes in general. However, more recent research has led to a reappraisal of this conclusion: the work of Slilaty and Vu (1991) was performed prior to the solution of the LexA structure, which revealed a threonine-coordinator for the general base (Luo *et al.*, 2001) [98, 108]. This result suggested that the Ser-Lys dyad residues were not sufficient for catalysis.

Just as Slilaty and Vu (1991) attempted to identify a glutamate or aspartate triad residue of LexA, Bernard Delmas' group performed experiments to address the possibility that IPNV VP4 might have an aspartate or glutamate catalytic residue (Petit *et al.*, 2000) [7, 108]. They mutated every negatively charged, IPNV VP4 residue, individually, to assess if any of them were significant to catalysis; none of the mutations affected polyprotein maturation and thus neither an aspartate nor a glutamate was deemed a potential triad residue. Seven years after Petit *et al.* (2000) published these findings, Lee *et al.* (2007) published the structure of IPNV VP4, which confirmed that the active site lacked a glutamate or aspartate as a catalytic triad residue[7, 51]. Their structure did,

however, reveal a threonine within hydrogen bonding distance of the general base; indeed, the presence of a threonine or second serine in close proximity to the general base, lysine, is regarded as a theme of Ser-Lys proteases (Ekici *et al.*, 2008) [109].

4.3. Clarifying the contributions of BSNV VP4's active site Ser692, Lys729 and Thr712 residues to catalysis

To what extent do the three active site residues of BSNV VP4 - Ser692, Thr712, and Lys729 - contribute to catalytic activity? Carter and Wells (1988) addressed a similar question in the context of the 'classical' catalytic triad - Ser/His/Asp - of the peptidase, *B. amyloliquefaciens* subtilisin[110]. They found that subtilisin increases the rate of peptide bond hydrolysis by a factor of approximately 10^9 to 10^{10} relative to non-enzymatic peptide bond hydrolysis. By mutating subtilisin's catalytic triad residues to alanine, and testing the mutant enzyme's catalytic properties, they found that the triad residues contribute to the total rate enhancement by a factor of 2×10^6. This not only signified that the triad residues contribute immensely to subtilisin's peptidase activity, but also that the enzyme retained a low level of catalytic activity even when the crucial triad residues were absent. Can these findings by Carter and Wells (1988) [110] be extended to BSNV VP4? Presumably, BSNV VP4 would retain a very low level of activity if its dyad residues, and Thr712, were mutated to alanine; kinetic experiments are needed to address this.

Carter and Wells's research, published in 1988[110], was also notable for identifying the contribution of each triad residue to rate enhancement: mutating the nucleophile, serine, or the general base, histidine, to alanine, decreased the activity of *B. amyloliquefaciens* subtilisin by a factor of 2×10^6. Mutating the coordinator, aspartate, to

alanine decreased activity by a factor of 3 x 10^4. This was an intriguing result because it indicated that, of the three, triad residues, the nucleophile and the general base contributed more to substrate turnover than the coordinator, aspartate. Similarly, in the BSNV VP4 catalytic dyad, the nucleophile, serine, and the general base, lysine, appear to contribute the most to catalytic activity: no *cis*-cleavage or *trans*-cleavage activity has been reported for BSNV VP4 when either of these residues are mutated to alanine. Our data shows that VP4 (T712A) is more active than VP4 (K729A). In a more comprehensive study of the contributions of BSNV VP4's active site residues to enzyme kinetics, perhaps Ser692 and Lys729 will be shown to be the most important contributors to activity, followed by Thr712.

4.4. Is BSNV VP4 an immunosuppressive agent?

Li *et al.* (2013) demonstrated that IBDV VP4 contributes to the immunosuppression of host cells and thereby promotes virus survival and propagation[111]. They showed that VP4 interacts with the host's glucocorticoid-induced leucine zipper protein (GILZ), which is implicated as an endogenous regulator of signalling pathways of the immune system (Beaulieu and Morand, 2011) [112]. Multiple methodologies were used to confirm the genuineness of this interaction: yeast two-hybrid and co-immunoprecipitation assays provided evidence for VP4's ability to bind GILZ. Confocal microscopy experiments showed that VP4 co-localizes with GILZ in tissue culture cells, which provided further support for their interaction. That VP4 necessarily used GILZ to mediate the down-regulation of the innate immune system was a corollary from this discovery; during IBDV infection experiments, the RNAi-mediated knockdown of GILZ resulted in improved immunity and decreased viral growth. Also,

cells transfected with a plasmid for IBDV VP4 expression showed decreased expression levels of innate immune system genes; this effect could be attenuated via GILZ knockdown. Future research should address the full spectrum of IBDV VP4's immunological impacts, as well as the extent of the conservation of VP4-mediated immunosuppression among birnaviruses.

4.5. Is threonine at position 712 the product of evolutionary "fine-tuning" of BSNV VP4?

The data presented herein shows that mutations to BSNV VP4's Thr712 can either improve cleavage activity, as in the case of the T712S construct, or, more commonly, decrease it (as with the T712A, T712C, and T712V mutants). The observation that the evolution of BSNV produced a threonine at VP4's position 712, rather than serine, suggests that the former amino acid confers an advantage to the virus, whether to the stability of VP4, the rate of polyprotein maturation, viral morphogenesis, or another facet of viral activity.

Why does BSNV VP4 have a threonine at position 712 rather than a serine? By extension, why is a threonine, whose side chain's O^{γ} is within hydrogen bonding distance of the general base, Lysine's N^{ζ}, conserved in the VP4s of the *Birnaviridae* family as per the structural and sequence data available? These questions are underscored by the high mutation rates of RNA viruses, which facilitate the selection of beneficial mutations (Babé and Craik, 1997) [105]. It seems that the presence of an alternative residue to threonine at position 712 in BSNV VP4, and at the corresponding threonines of other birnaviral VP4s, was disfavoured by natural selection. Perhaps the occurrence of Thr712 in BSNV VP4 was the result of evolutionary "fine-tuning" of the

enzyme for optimal viral functionality rather than to yield the highest possible rate of catalysis. Future work should address how the T712S mutation in the VP4 gene of an engineered BSNV strain influences polyprotein maturation, as well as BSNV infectivity and pathogenicity.

References

1. Delmas, B., Mundt, E., Vakharia, V. N. & Wu, J. L. in *Virus Taxonomy* (eds King, A. M. Q., Adams, M. J., Carstens, E. B. & Lefkowitz, E. J.) 499-507 (Elsevier, San Diego, 2012).

2. Nobiron, I. *et al*. Genome and polypeptides characterization of Tellina virus 1 reveals a fifth genetic cluster in the Birnaviridae family. *Virology* **371**, 350-361 (2008).

3. Guy, J. S., West, M. A. & Fuller, F. J. Physical and genomic characteristics identify chicken proventricular necrosis virus (R11/3 virus) as a novel birnavirus. *Avian Dis.* **55**, 2-7 (2011).

4. Bernard, J. Drosophila X virus RNA polymerase: tentative model for in vitro replication of the double-stranded virion RNA. *J. Virol.* **33**, 717-723 (1980).

5. Mertens, P. P., Jamieson, P. B. & Dobos, P. In vitro RNA synthesis by infectious pancreatic necrosis virus-associated RNA polymerase. *J. Gen. Virol.* **59**, 47-56 (1982).

6. Macdonald, R. D. & Dobos, P. Identification of the proteins encoded by each genome segment of infectious pancreatic necrosis virus. *Virology* **114**, 414-422 (1981).

7. Petit, S., Lejal, N., Huet, J. C. & Delmas, B. Active residues and viral substrate cleavage sites of the protease of the birnavirus infectious pancreatic necrosis virus. *J. Virol.* **74**, 2057-2066 (2000).

8. Macdonald, R. D., Roy, K. L., Yamamoto, T. & Chang, N. Oligonucleotide fingerprints of the RNAs from infectious pancreatic necrosis virus. *Arch. Virol.* **54**, 373-377 (1977).

9. Nagy, E. & Dobos, P. Synthesis of drosophila X virus proteins in cultured Drosophila cells. *Virology* **134**, 358-367 (1984).

10. Lange, H., Müller, H., Käufer, I. & Becht, H. Pathogenic and structural properties of wild type infectious bursal disease virus (IBDV) and virus grown in vitro. *Arch. Virol.* **92**, 187-196 (1987).

11. von Einem, U. I. *et al*. VP1 of infectious bursal disease virus is an RNA-dependent RNA polymerase. *J. Gen. Virol.* **85**, 2221-2229 (2004).

12. Persson, R. H. & Macdonald, R. D. Evidence that infectious pancreatic necrosis virus has a genome-linked protein. *J. Virol.* **44**, 437-443 (1982).

13. Calvert, J. G., Nagy, E., Soler, M. & Dobos, P. Characterization of the VPg-dsRNA linkage of infectious pancreatic necrosis virus. *J. Gen. Virol.* **72**, 2563-2567 (1991).

14. Xu, H., Si, W. & Dobos, P. Mapping the site of guanylylation on VP1, the protein primer for infectious pancreatic necrosis virus RNA synthesis. *Virology* **322**, 199-210 (2004).

15. Salas, M. Protein-priming of DNA replication. *Annu. Rev. Biochem.* **60**, 39-71 (1991).

16. Dobos, P. In vitro guanylylation of infectious pancreatic necrosis virus polypeptide VP1. *Virology* **193**, 403-413 (1993).

17. Poch, O., Sauvaget, I., Delarue, M. & Tordo, N. Identification of four conserved motifs among the RNA-dependent polymerase encoding elements. *EMBO J.* **8**, 3867-3874 (1989).

18. Duncan, R., Mason, C. L., Nagy, E., Leong, J. & Dobos, P. Sequence analysis of infectious pancreatic necrosis virus genome segment B and its encoded VP1 protein: A putative RNA-dependent RNA polymerase lacking the Gly-Asp-Asp motif. *Virology* **181**, 541-552 (1991).

19. Shwed, P. S., Dobos, P., Cameron, L. A., Vakharia, V. N. & Duncan, R. birnavirus VP1 proteins form a distinct subgroup of RNA-dependent RNA polymerases lacking a GDD motif. *Virology* **296**, 241-250 (2002).

20. Pan, J., Vakharia, V. N. & Tao, Y. J. The structure of a birnavirus polymerase reveals a distinct active site topology. *Proc. Natl. Acad. Sci. U.S.A.* **104**, 7385-7390 (2007).

21. Gorbalenya, A. E. *et al*. The palm subdomain-based active site is internally permuted in viral RNA-dependent RNA polymerases of an ancient lineage. *J. Mol. Biol.* **324**, 47-62 (2002).

22. Coulibaly, F. *et al*. The birnavirus crystal structure reveals structural relationships among icosahedral viruses. *Cell* **120**, 761-772 (2005).

23. Kibenge, F. S., Qian, B., Nagy, E., Cleghorn, J. R. & Wadowska, D. Formation of virus-like particles when the polyprotein gene (segment A) of infectious bursal disease virus is expressed in insect cells. *Can. J. Vet. Res.* **63**, 49-55 (1999).

24. Böttcher, B. *et al*. Three-dimensional structure of infectious bursal disease virus determined by electron cryomicroscopy. *J. Virol.* **71**, 325-330 (1997).

25. Martinez-Torrecuadrada, J. L. *et al*. Different architectures in the assembly of infectious bursal disease virus capsid proteins expressed in insect cells. *Virology* **278**, 322-331 (2000).

26. Delgui, L. *et al*. The capsid protein of infectious bursal disease virus contains a functional α4β1 integrin ligand motif. *Virology* **386**, 360-372 (2009).

27. Azad, A. A., Jagadish, M. N., Brown, M. A. & Hudson, P. J. Deletion mapping and expression in *Escherichia coli* of the large genomic segment of a birnavirus. *Virology* **161**, 145-152 (1987).

28. Letzel, T. *et al*. Molecular and structural bases for the antigenicity of VP2 of infectious bursal disease virus. *J. Virol.* **81**, 12827-12835 (2007).

29. Bayliss, C. D. *et al*. A comparison of the sequences of segment A of four infectious bursal disease virus strains and identification of a variable region in VP2. *J. Gen. Virol.* **71**, 1303-1312 (1990).

30. Fernández-Arias, A., Martínez, S. & Rodríguez, J. F. The major antigenic protein of infectious bursal disease virus, VP2, is an apoptotic inducer. *J. Virol.* **71**, 8014-8018 (1997).

31. Busnadiego, I., Maestre, A. M., Rodríguez, D. & Rodríguez, J. F. The infectious bursal disease virus RNA-binding VP3 polypeptide inhibits PKR-mediated apoptosis. *PLoS One* **7**, e46768 (2012).

32. Chung, H. K., Kordyban, S., Cameron, L. & Dobos, P. Sequence analysis of the bicistronic drosophila X virus genome segment A and its encoded polypeptides. *Virology* **225**, 359-368 (1996).

33. Galloux, M. *et al*. Peptides resulting from the pVP2 C-terminal processing are present in infectious pancreatic necrosis virus particles. *J. Gen. Virol.* **85**, 2231-2236 (2004).

34. Da Costa, B. *et al*. The capsid of infectious bursal disease virus contains several small peptides arising from the maturation process of pVP2. *J. Virol.* **76**, 2393-2402 (2002).

35. Chevalier, C. *et al*. Structural peptides of a nonenveloped virus are involved in assembly and membrane translocation. *J. Virol.* **79**, 12253-12263 (2005).

36. Galloux, M. *et al*. Infectious bursal disease virus, a non-enveloped virus, possesses a capsid-associated peptide that deforms and perforates biological membranes. *J. Biol. Chem.* **282**, 20774-20784 (2007).

37. Dobos, P. *et al*. Biophysical and biochemical characterization of five animal viruses with bisegmented double-stranded RNA genomes. *J. Virol.* **32**, 593-605 (1979).

38. Casañas, A. *et al*. Structural insights into the multifunctional protein VP3 of birnaviruses. *Structure* **16**, 29-37 (2008).

39. Tacken, M. G. J., Peeters, B. P. H., Thomas, A. A. M., Rottier, P. J. M. & Boot, H. J. Infectious bursal disease virus capsid protein VP3 interacts both with VP1, the RNA-dependent RNA polymerase, and with viral double-stranded RNA. *J. Virol.* **76**, 11301-11311 (2002).

40. Lombardo, E. *et al*. VP1, the putative RNA-dependent RNA polymerase of infectious bursal disease virus, forms complexes with the capsid protein VP3, leading to efficient encapsidation into virus-like particles. *J. Virol.* **73**, 6973-6983 (1999).

41. Bahar, M. W. *et al*. Structure of a VP1-VP3 complex suggests how birnaviruses package the VP1 polymerase. *J. Virol.* **87**, 3229-3236 (2013).

42. Chevalier, C., Lepault, J., Da Costa, B. & Delmas, B. The last C-terminal residue of VP3, glutamic acid 257, controls capsid assembly of infectious bursal disease virus. *J. Virol.* **78**, 3296-3303 (2004).

43. Luque, D. *et al*. Infectious bursal disease virus: ribonucleoprotein complexes of a double-stranded RNA virus. *J. Mol. Biol.* **386**, 891-901 (2009).

44. Jeffery, C. J. Molecular mechanisms for multitasking: recent crystal structures of moonlighting proteins. *Curr. Opin. Struct. Biol.* **14**, 663-668 (2004).

45. Hudson, P. J., McKern, N. M., Power, B. E. & Azad, A. A. Genomic structure of the large RNA segment of infectious bursal disease virus. *Nucleic Acids Res.* **14**, 5001-5012 (1986).

46. Nagy, E., Duncan, R., Krell, P. & Dobos, P. Mapping of the large RNA genome segment of infectious pancreatic necrosis virus by hybrid arrested translation. *Virology* **158**, 211-217 (1987).

47. Duncan, R., Nagy, E., Krell, P. J. & Dobos, P. Synthesis of the infectious pancreatic necrosis virus polyprotein, detection of a virus-encoded protease, and fine structure mapping of genome segment A coding regions. *J. Virol.* **61**, 3655-3664 (1987).

48. Manning, D. S., Mason, C. L. & Leong, J. C. Cell-free translational analysis of the processing of infectious pancreatic necrosis virus polyprotein. *Virology* **179**, 9-15 (1990).

49. Magyar, G. & Dobos, P. Evidence for the detection of the infectious pancreatic necrosis virus polyprotein and the 17-kDa polypeptide in infected cells and of the NS protease in purified virus. *Virology* **204**, 580-589 (1994).

50. Granzow, H. *et al*. A second form of infectious bursal disease virus-associated tubule contains VP4. *J. Virol.* **71**, 8879-8885 (1997).

51. Lee, J., Feldman, A. R., Delmas, B. & Paetzel, M. Crystal structure of the VP4 protease from infectious pancreatic necrosis virus reveals the acyl-enzyme complex for an intermolecular self-cleavage reaction. *J. Biol. Chem.* **282**, 24928-24937 (2007).

52. Chung, I. Y. & Paetzel, M. Crystal structures of yellowtail ascites virus VP4 protease: trapping an internal cleavage site trans acyl-enzyme complex in a native Ser/Lys dyad active site. *J. Biol. Chem.* **288**, 13068-13081 (2013).

53. Birghan, C., Mundt, E. & Gorbalenya, A. E. A non-canonical Lon proteinase lacking the ATPase domain employs the Ser-Lys catalytic dyad to exercise broad control over the life cycle of a double-stranded RNA virus. *EMBO J.* **19**, 114-123 (2000).

54. Lejal, N., Da Costa, B., Huet, J. C. & Delmas, B. Role of Ser-652 and Lys-692 in the protease activity of infectious bursal disease virus VP4 and identification of its substrate cleavage sites. *J. Gen. Virol.* **81**, 983-992 (2000).

55. Lee, J., Feldman, A. R., Delmas, B. & Paetzel, M. Expression, purification and crystallization of a birnavirus-encoded protease, VP4, from blotched snakehead virus (BSNV). *Acta Crystallogr. Sect. F Struct. Biol. Cryst. Commun.* **62**, 353-356 (2006a).

56. Feldman, A. R., Lee, J., Delmas, B. & Paetzel, M. Crystal structure of a novel viral protease with a serine/lysine catalytic dyad mechanism. *J. Mol. Biol.* **358**, 1378-1389 (2006).

57. Mundt, E., Beyer, J. & Müller, H. Identification of a novel viral protein in infectious bursal disease virus-infected cells. *J. Gen. Virol.* **76**, 437-443 (1995).

58. Mundt, E., Köllner, B. & Kretzschmar, D. VP5 of infectious bursal disease virus is not essential for viral replication in cell culture. *J. Virol.* **71**, 5647-5651 (1997).

59. Wei, L. *et al*. Infectious bursal disease virus activates the phosphatidylinositol 3-kinase (PI3K)/Akt signaling pathway by interaction of VP5 protein with the p85α subunit of PI3K. *Virology* **417**, 211-220 (2011).

60. Müller, H., Islam, M. R. & Raue, R. Research on infectious bursal disease—the past, the present and the future. *Vet. Microbiol.* **97**, 153-165 (2003).

61. Roberts, R. J. & Pearson, M. D. Infectious pancreatic necrosis in Atlantic salmon, *Salmo salar* L. *J. Fish Dis.* **28**, 383-390 (2005).

62. Cosgrove, A. S. An apparently new disease of chickens: avian nephrosis. *Avian Dis.* **6**, 385-389 (1962).

63. Barnes, H. J., Wheeler, J. & Reed, D. Serologic evidence of infectious bursal disease virus infection in Iowa turkeys. *Avian Dis.* **26**, 560-565 (1982).

64. Wood, E. M., Snieszko, S. F. & Yasutake, W. T. Infectious pancreatic necrosis in brook trout. *Am. Med. Assoc. Arch. Pathol.* **60**, 26-28 (1955).

65. Knott, R. M. & Munro, A. L. The persistence of infectious pancreatic necrosis virus in Atlantic salmon. *Vet. Immunol. Immunopathol.* **12**, 359-364 (1986).

66. Winterfield, R. W., Fadly, A. M. & Bickford, A. Infectivity and distribution of infectious bursal disease virus in the chicken. Persistence of the virus and lesions. *Avian Dis.* **16**, 622-632 (1972).

67. Cheville, N. F. Studies on the pathogenesis of gumboro disease in the bursa of fabricius, spleen, and thymus of the chicken. *Am. J. Pathol.* **51**, 527-551 (1967).

68. Käufer, I. & Weiss, E. Significance of bursa of fabricius as target organ in infectious bursal disease of chickens. *Infect. Immun.* **27**, 364-367 (1980).

69. Rodríguez-Lecompte, J. C., Niño-Fong, R., Lopez, A., Frederick Markham, R. J. & Kibenge, F. S. B. Infectious bursal disease virus (IBDV) induces apoptosis in chicken B cells. *Comp. Immunol. Microbiol. Infect. Dis.* **28**, 321-337 (2005).

70. Rosenberger, J. K. & Gelb, J. J. Response to several avian respiratory viruses as affected by infectious bursal disease virus. *Avian Dis.* **22**, 95-105 (1978).

71. Chettle, N., Stuart, J. C. & Wyeth, P. J. Outbreak of virulent infectious bursal disease in East Anglia. *Vet. Rec.* **125**, 271-272 (1989).

72. van den Berg, T. P., Gonze, M. & Meulemans, G. Acute infectious bursal disease in poultry: Isolation and characterisation of a highly virulent strain. *Avian. Pathol.* **20**, 133-143 (1991).

73. Ismail, N. M., Saif, Y. M. & Moorhead, P. D. Lack of pathogenicity of five serotype 2 infectious bursal disease viruses in chickens. *Avian Dis.* **32**, 757-759 (1988).

74. Kibenge, F. S. B., McKenna, P. K. & Dybing, J. K. Genome cloning and analysis of the large RNA segment (segment A) of a naturally avirulent serotype 2 infectious bursal disease virus. *Virology* **184**, 437-440 (1991).

75. Wolf, K., Snieszko, S. F., Dunbar, C. E. & Pyle, E. Virus nature of infectious pancreatic necrosis in trout. *Proc. Soc. Exp. Biol. Med.* **104**, 105-108 (1960).

76. Wolf, K. Fish viruses and fish viral diseases. Ithaca, NY: Canstock Publishing Associates/Cornell University Press (1988).

77. Frantsi, C. & Savan, M. Infectious pancreatic necrosis virus-temperature and age factors in mortality. *J. Wildl. Dis.* **7**, 249-255 (1971).

78. Swanson, R. N. & Gillespie, J. H. An indirect fluorescent antibody test for the rapid detection of infectious pancreatic necrosis virus in tissues. *J. Fish Dis.* **4**, 309-315 (1981).

79. John, K. R. & Richards, R. H. Characteristics of a new birnavirus associated with a warm-water fish cell line. *J. Gen. Virol.* **80**, 2061-2065 (1999).

80. Da Costa, B. *et al*. Blotched snakehead virus is a new aquatic birnavirus that is slightly more related to avibirnavirus than to aquabirnavirus. *J. Virol.* **77**, 719–725 (2003).

81. Gasteiger, E. *et al*. ExPASy: The proteomics server for in-depth protein knowledge and analysis. *Nucleic Acids Res.* **31**, 3784-3788 (2003).

82. Bürgi, H. B., Dunitz, J. D. & Shefter, E. Geometrical reaction coordinates. II. Nucleophilic addition to a carbonyl group. *J. Am. Chem. Soc.* **95**, 5065-5067 (1973).

83. Ekici, O. D. *et al*. Profiling the substrate specificity of viral protease VP4 by a FRET-based peptide library approach. *Biochemistry* **48**, 5753-5759 (2009).

84. Paetzel, M. Structure and mechanism of Escherichia coli type I signal peptidase. *Biochim. Biophys. Acta* **1843**, 1497-1508 (2014).

85. Chung, I. Y. & Paetzel, M. Crystal structure of a viral protease intramolecular acyl-enzyme complex: insights into cis-cleavage at the VP4/VP3 junction of Tellina birnavirus. *J. Biol. Chem.* **286**, 12475-12482 (2011a).

86. Larkin, M. A. *et al*. Clustal W and Clustal X version 2.0. *Bioinformatics* **23**, 2947-2948 (2007).

87. Gouet, P., Courcelle, E., Stuart, D. I. & Métoz, F. ESPript: analysis of multiple sequence alignments in PostScript. *Bioinformatics* **15**, 305-308 (1999).

88. Lee, J. *et al*. Purification, crystallization and preliminary X-ray analysis of truncated and mutant forms of VP4 protease from infectious pancreatic necrosis virus. *Acta Crystallogr. Sect. F Struct. Biol. Cryst. Commun.* **62**, 1235-1238 (2006b).

89. Kraut, J. Serine proteases: structure and mechanism of catalysis. *Annu. Rev. Biochem.* **46**, 331-358 (1977).

90. Chung, I. Y. & Paetzel, M. Expression, purification and crystallization of VP4 protease from Tellina virus 1. *Acta Crystallogr. Sect. F Struct. Biol. Cryst. Commun.* **67**, 157-160 (2011b).

91. Schechter, I. & Berger, A. On the size of the active site in proteases. I. Papain. *Biochem. Biophys. Res. Commun.* **27**, 157-162 (1967).

92. Krissinel, E. & Henrick, K. Secondary-structure matching (SSM), a new tool for fast protein structure alignment in three dimensions. *Acta Crystallogr. D Biol. Crystallogr.* **60**, 2256-2268 (2004).

93. Rawlings, N. D., Barrett, A. J. & Bateman, A. MEROPS: the peptidase database. *Nucleic Acids Res.* **38**, D227-D233 (2010).

94. Imajoh, M., Goto, T. & Oshima, S. Characterization of cleavage sites and protease activity in the polyprotein precursor of Japanese marine aquabirnavirus and expression analysis of generated proteins by a VP4 protease activity in four distinct cell lines. *Arch. Virol.* **152**, 1103-1114 (2007).

95. Paetzel, M., Dalbey, R. E. & Strynadka, N. C. Crystal structure of a bacterial signal peptidase in complex with a beta-lactam inhibitor. *Nature* **396**, 186-190 (1998).

96. Kim, A. C., Oliver, D. C. & Paetzel, M. Crystal structure of a bacterial signal peptide peptidase. *J. Mol. Biol.* **376**, 352-366 (2008).

97. Nam, S., Kim, A. C. & Paetzel, M. Crystal structure of Bacillus subtilis signal peptide peptidase A. *J. Mol. Biol.* **419**, 347-358 (2012).

98. Luo, Y. *et al*. Crystal structure of LexA: a conformational switch for regulation of self-cleavage. *Cell* **106**, 585-594 (2001).

99. Botos, I. *et al*. The catalytic domain of Escherichia coli Lon protease has a unique fold and a Ser-Lys dyad in the active site. *J. Biol. Chem.* **279**, 8140-8148 (2004).

100. Peat, T. S. *et al*. Structure of the UmuD' protein and its regulation in response to DNA damage. *Nature* **380**, 727-730 (1996).

101. Bell, C. E., Frescura, P., Hochschild, A. & Lewis, M. Crystal structure of the λ repressor C-terminal domain provides a model for cooperative operator binding. *Cell* **101**, 801-811 (2000).

102. Liao, D. I., Qian, J., Chisholm, D. A., Jordan, D. B. & Diner, B. A. Crystal structures of the photosystem II D1 C-terminal processing protease. *Nat. Struc. Biol.* **7**, 749-753 (2000).

103. Schneider, C. A., Rasband, W. S. & Eliceiri, K. W. NIH Image to ImageJ: 25 years of image analysis. *Nat. Methods.* **9**, 671-675 (2012).

104. Klenotic, P. A. *et al*. The role of the conserved box E residues in the active site of the Escherichia coli type I signal peptidase. *J. Biol. Chem.* **275**, 6490-6498 (2000).

105. Babé, L. M. & Craik, C. S. Viral proteases: evolution of diverse structural motifs to optimize function. *Cell* **91**, 427-430 (1997).

106. Paetzel, M., Dalbey, R. E. & Strynadka, N. C. Crystal structure of a bacterial signal peptidase apoenzyme: implications for signal peptide binding and the Ser-Lys dyad mechanism. *J. Biol. Chem.* **277**, 9512-9519 (2002).

107. Chang, G. R., Wang, M. Y., Liao, J. H., Hsiao, Y. P. & Lai, S. Y. Endopeptidase activity characterization of E. coli-derived infectious bursal disease virus protein 4 tubules. *Protein Eng. Des. Sel.* **25**, 789-795 (2012).

108. Slilaty, S. N. & Vu, H. K. The role of electrostatic interactions in the mechanism of peptide bond hydrolysis by a Ser-Lys catalytic dyad. *Protein Eng.* **4**, 919-922 (1991).

109. Ekici, O. D., Paetzel, M. & Dalbey, R. E. Unconventional serine proteases: variations on the catalytic Ser/His/Asp triad configuration. *Protein Sci.* **17**, 2023-2037 (2008).

110. Carter, P. & Wells, J. A. Dissecting the catalytic triad of a serine protease. *Nature* **332**, 564-568 (1988).

111. Li, Z. *et al*. Critical roles of glucocorticoid-induced leucine zipper in infectious bursal disease virus (IBDV)-induced suppression of type I Interferon expression and enhancement of IBDV growth in host cells via interaction with VP4. *J. Virol.* **87**, 1221-1231 (2013).

112. Beaulieu, E. & Morand, E. F. Role of GILZ in immune regulation, glucocorticoid actions and rheumatoid arthritis. *Nat. Rev. Rheumatol.* **7**, 340-348 (2011).

Appendices

Appendix A. Alignment of six birnaviral VP4 sequences

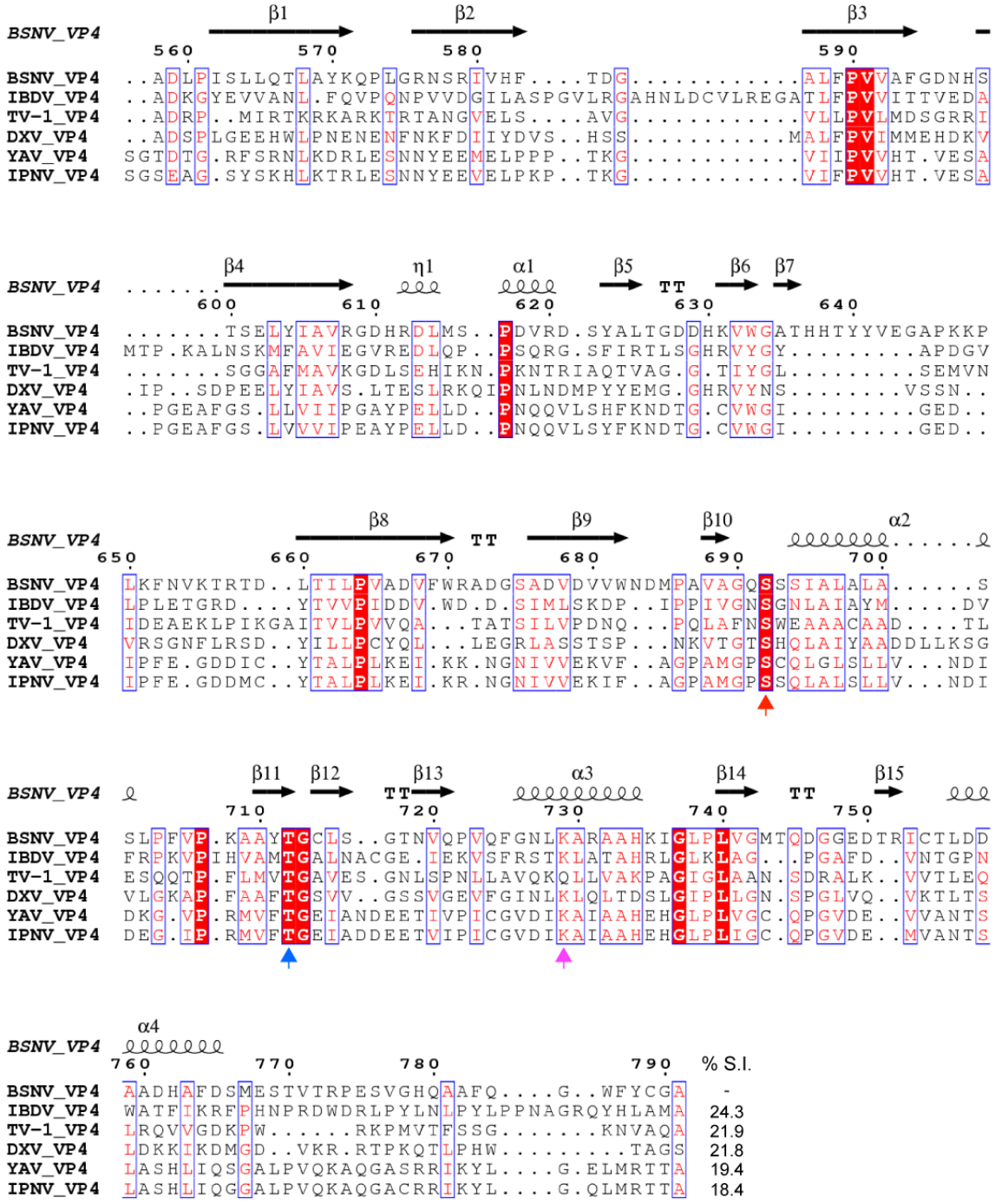

Fig. A. (*Legend on the next page.*)

Figure A. This alignment includes the VP4 sequences for BSNV (Q8AZM0), IBDV (P61825), TV-1 (Q2PBR5), DXV (Q96724), YAV (P89521) and IPNV (P05844); the accession numbers, written parenthetically, were obtained from the UniProt database. The figure indicates the amino acids of BSNV VP4 that constitute the β-sheets (black, horizontal arrows), α-helices (squiggles) and β-turns (TT). Vertical arrows denote major active site residues including the nucleophile, serine (red arrow), the coordinator, threonine (blue arrow), and the lysine general base (violet arrow). The catalytic lysine of TV-1 VP4 is located one amino acid to the left of the other aligned catalytic lysine residues that are indicated by the vertical, violet arrow. % S.I. indicates the percent sequence identity of the VP4s relative to BSNV VP4. The alignment was prepared using ClustalW (Larkin *et al.*, 2007)[86]. The figure was prepared using ESPript (http://espript.ibcp.fr) (Gouet *et al.*, 1999)[87].

Appendix B. Site-directed mutagenesis primers

Construct	Primer	Primer Sequence
BSNV VP4 (T712C)	Forward Primer	5' - CCA AAG GCA GCA TAC TGC GGC TGC CTA TCG GGG - 3'
	Reverse Primer	5’ - CCC CGA TAG GCA GCC GCA GTA TGC TGC CTT TGG - 3'
BSNV VP4 (T712S)	Forward Primer	5' - CA AAG GCA GCA TAC TCC GGC TGC CTA TCG - 3'
	Reverse Primer	5' - CGA TAG GCA GCC GGA GTA TGC TGC CTT TG - 3'
BSNV VP4 (T712V)	Forward Primer	5' - CCA AAG GCA GCA TAC GTC GGC TGC CTA TCG GGG - 3'
	Reverse Primer	5' - CCC CGA TAG GCA GCC GAC GTA TGC TGC CTT TGG - 3'

These primers were used to prepare the BSNV VP4 constructs with the T712C, T712S, and T712V mutations described in chapter 2.

Appendix C. 15% SDS-PAGE diagnostics of time-course cleavage assays

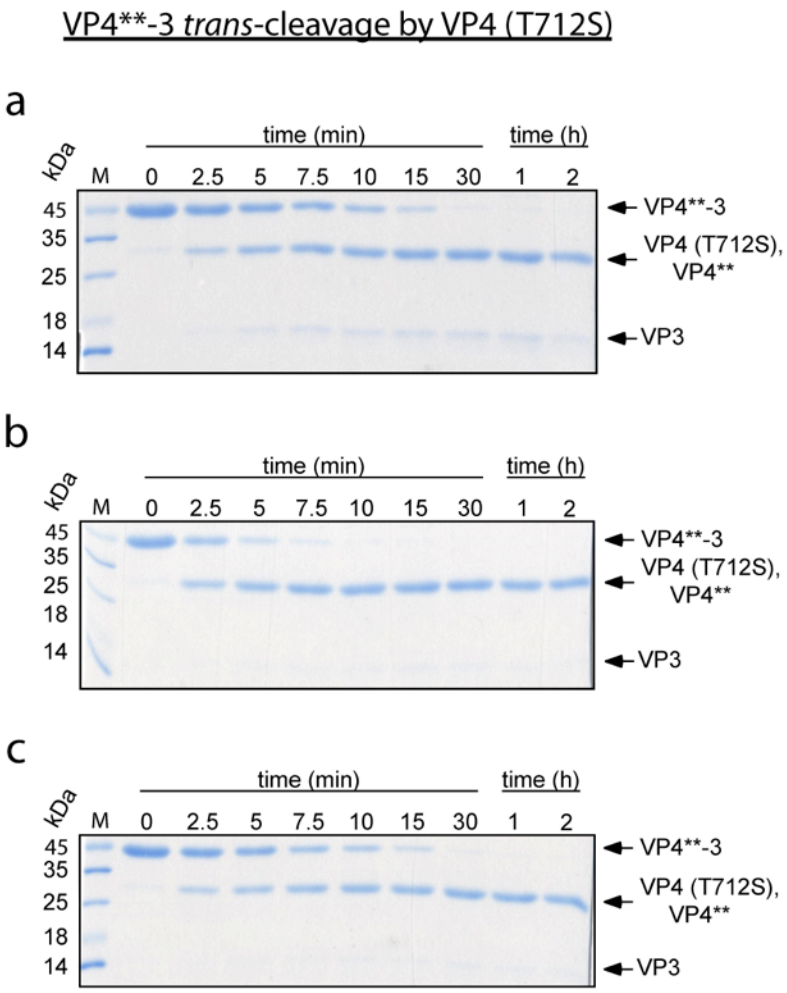

Figure C1. 15% SDS-PAGE summary of the *trans*-cleavage of VP4**-3 by VP4 (T712S). The time-course cleavage assays were performed in triplicate; the results from the assays are shown in (a), (b) and (c). The buffer conditions were 20 mM Tris-HCl (pH 8.0), 100 mM NaCl, 10% glycerol, and 1% β-mercaptoethanol and the molar ratio of VP4**-3 to VP4 (T712S) was 69:1.0. M indicates the marker lane. The two stars (**) of VP4**-3 denote the two active site mutations, S692A and K729A, of this substrate-construct. The cleavage product, VP4**, co-migrates with VP4 (T712S).

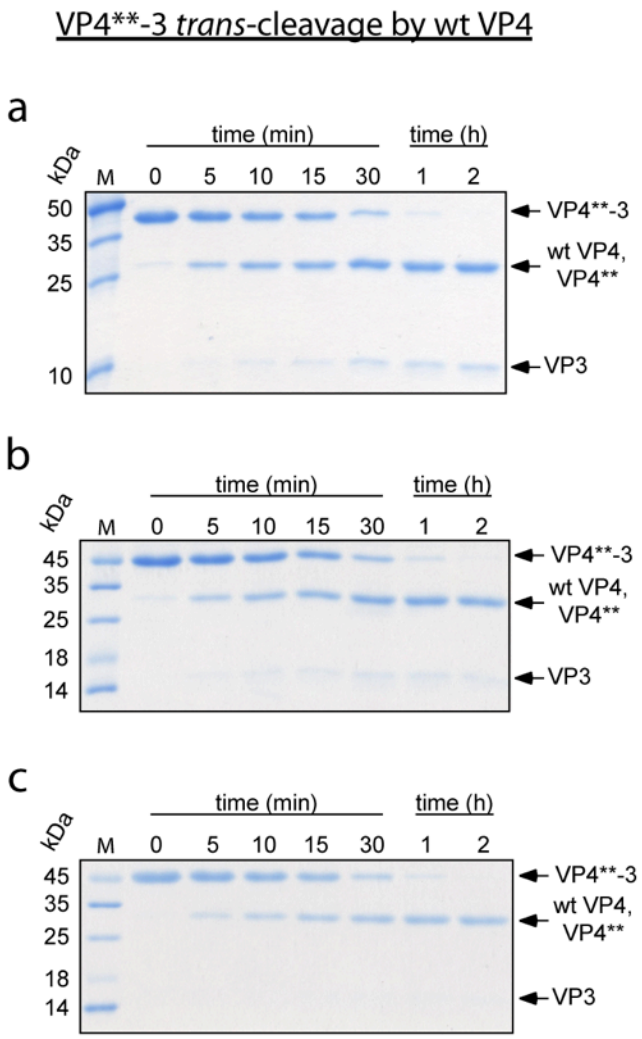

Figure C2. 15% SDS-PAGE summary of the *trans*-cleavage of VP4**-3 by wt VP4. The time-course cleavage assays were performed in triplicate; the results from the assays are shown in (a), (b) and (c). The buffer conditions were 20 mM Tris-HCl (pH 8.0), 100 mM NaCl, 10% glycerol, and 1% β-mercaptoethanol and the molar ratio of VP4**-3 to wt VP4 was 69:1.0. M indicates the marker lane. The two stars (**) of VP4**-3 denote the two active site mutations, S692A and K729A, of this substrate-construct. The cleavage product, VP4**, co-migrates with wt VP4.

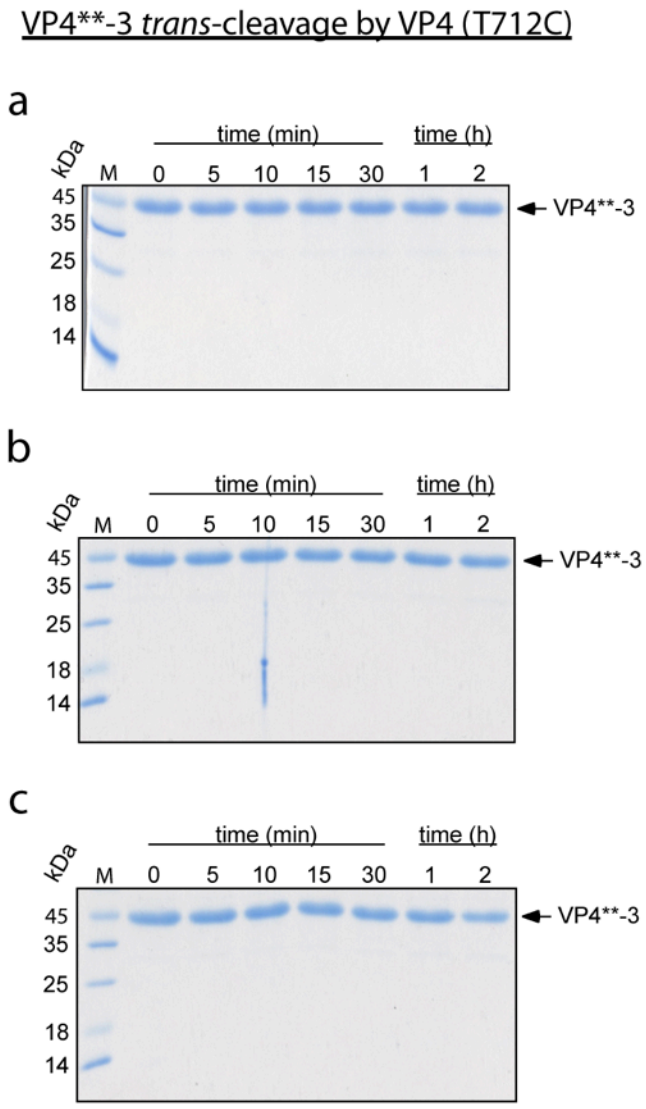

Figure C3. 15% SDS-PAGE summary of the *trans*-cleavage of VP4**-3 by VP4 (T712C). The time-course cleavage assays were performed in triplicate; the results from the assays are shown in (a), (b) and (c). The buffer conditions were 20 mM Tris-HCl (pH 8.0), 100 mM NaCl, 10% glycerol, and 1% β-mercaptoethanol. The molar ratio of VP4**-3 to VP4 (T712C) was 69:1.0. M indicates the marker lane. The two stars (**) of VP4**-3 denote the two active site mutations, S692A and K729A, of this substrate-construct.

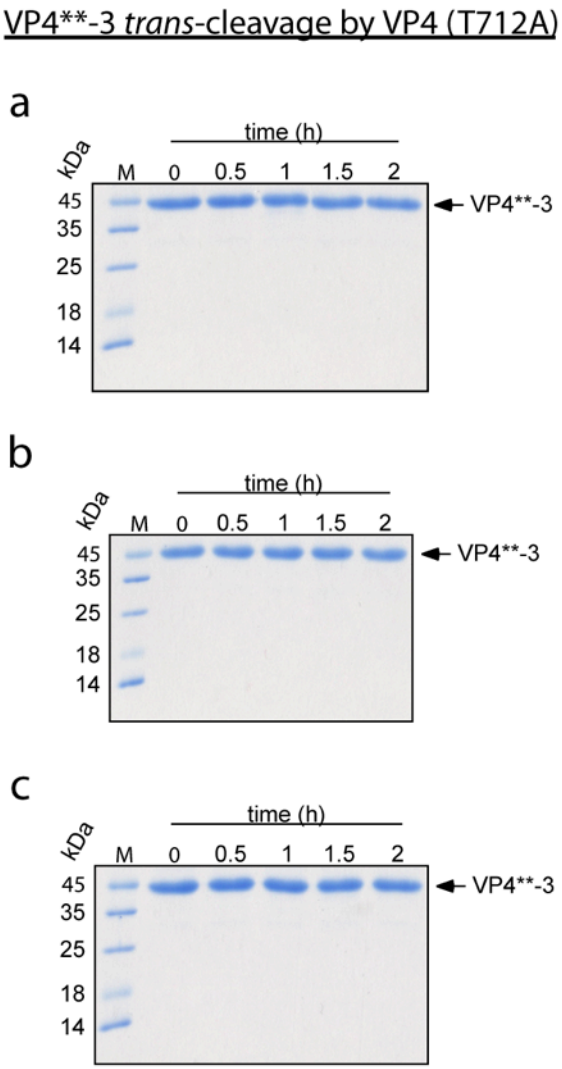

Figure C4. 15% SDS-PAGE summary of the *trans*-cleavage of VP4**-3 by VP4 (T712A). The time-course cleavage assays were performed in triplicate; the results from the assays are shown in (a), (b) and (c). The buffer conditions were 20 mM Tris-HCl (pH 8.0), 100 mM NaCl, 10% glycerol, and 1% β-mercaptoethanol. The molar ratio of VP4**-3 to VP4 (T712A) was 69:1.0. M indicates the marker lane. The two stars (**) of VP4**-3 denote the two active site mutations, S692A and K729A, of this substrate-construct.

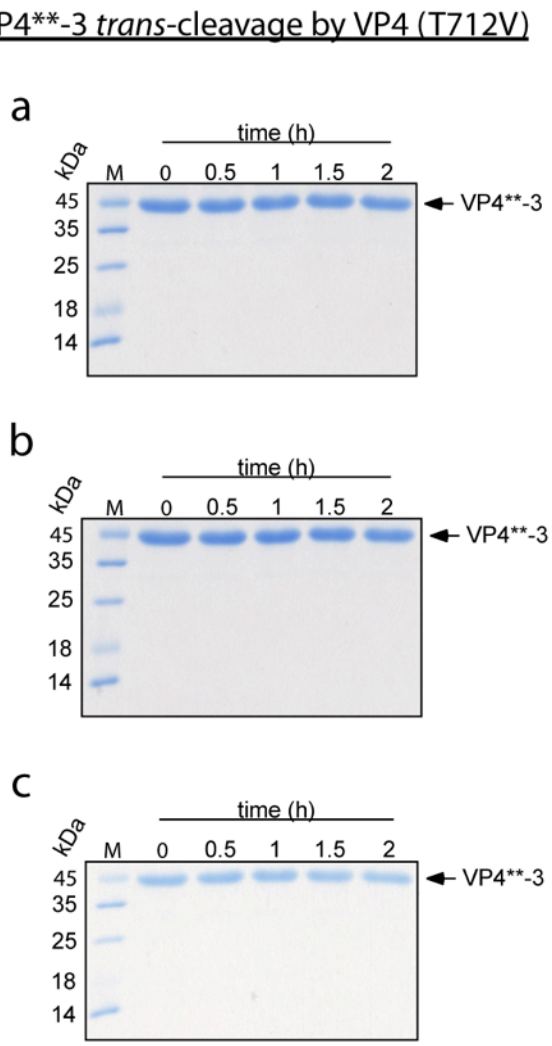

Figure C5. 15% SDS-PAGE summary of the *trans*-cleavage of VP4**-3 by VP4 (T712V). The time-course cleavage assays were performed in triplicate; the results from the assays are shown in (a), (b) and (c). The buffer conditions were 20 mM Tris-HCl (pH 8.0), 100 mM NaCl, 10% glycerol, and 1% β-mercaptoethanol. The molar ratio of VP4**-3 to VP4 (T712V) was 69:1.0. M indicates the marker lane. The two stars (**) of VP4**-3 denote the two active site mutations, S692A and K729A, of this substrate-construct.

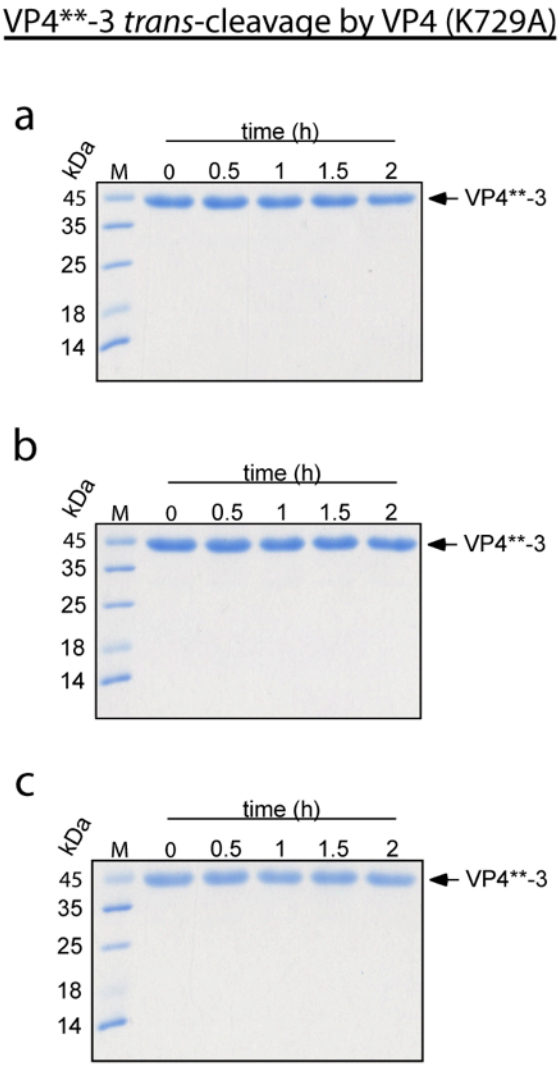

Figure C6. 15% SDS-PAGE summary of the *trans*-cleavage of VP4**-3 by VP4 (K729A). The time-course cleavage assays were performed in triplicate; the results from the assays are shown in (a), (b) and (c). The buffer conditions were 20 mM Tris-HCl (pH 8.0), 100 mM NaCl, 10% glycerol, and 1% β-mercaptoethanol. The molar ratio of VP4**-3 to VP4 (K729A) was 69:1.0. M indicates the marker lane. The two stars (**) of VP4**-3 denote the two active site mutations, S692A and K729A, of this substrate-construct.

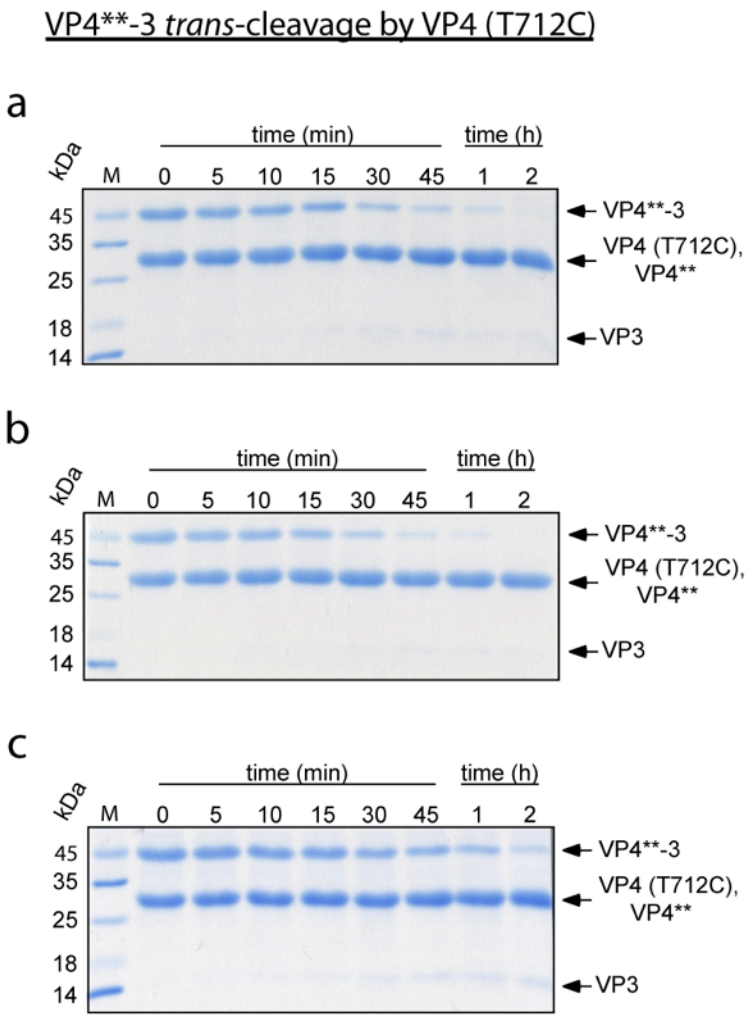

Figure C7. 15% SDS-PAGE summary of the *trans*-cleavage of VP4**-3 by VP4 (T712C). The time-course cleavage assays were performed in triplicate; the results from the assays are shown in (a), (b) and (c). The buffer conditions were 20 mM Tris-HCl (pH 8.0), 100 mM NaCl, 10% glycerol, and 1% β-mercaptoethanol and the molar ratio of VP4**-3 to VP4 (T712C) was 0.7:1.0. M indicates the marker lane. The two stars (**) of VP4**-3 denote the two active site mutations, S692A and K729A, of this substrate-construct. The cleavage product, VP4**, co-migrates with VP4 (T712C).

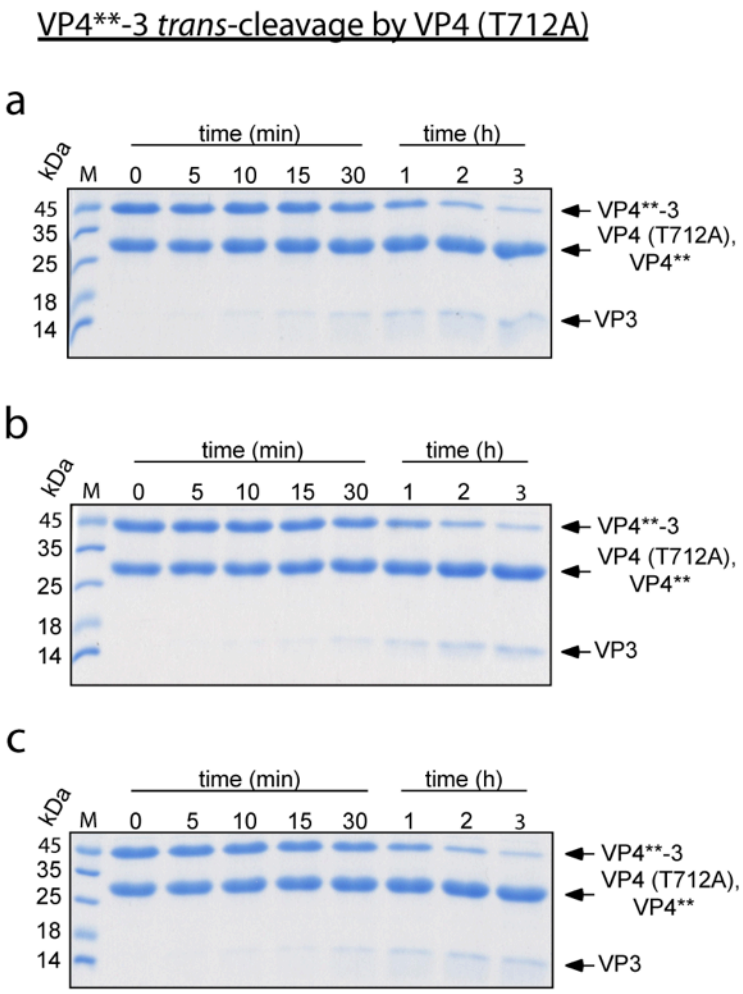

Figure C8. 15% SDS-PAGE summary of the *trans*-cleavage of VP4**-3 by VP4 (T712A). The time-course cleavage assays were performed in triplicate; the results from the assays are shown in (a), (b) and (c). The buffer conditions were 20 mM Tris-HCl (pH 8.0), 100 mM NaCl, 10% glycerol, and 1% β-mercaptoethanol. The molar ratio of VP4**-3 to VP4 (T712A) was 0.7:1.0. M indicates the marker lane. The two stars (**) of VP4**-3 denote the two active site mutations, S692A and K729A, of this substrate-construct. The cleavage product, VP4**, co-migrates with VP4 (T712A).

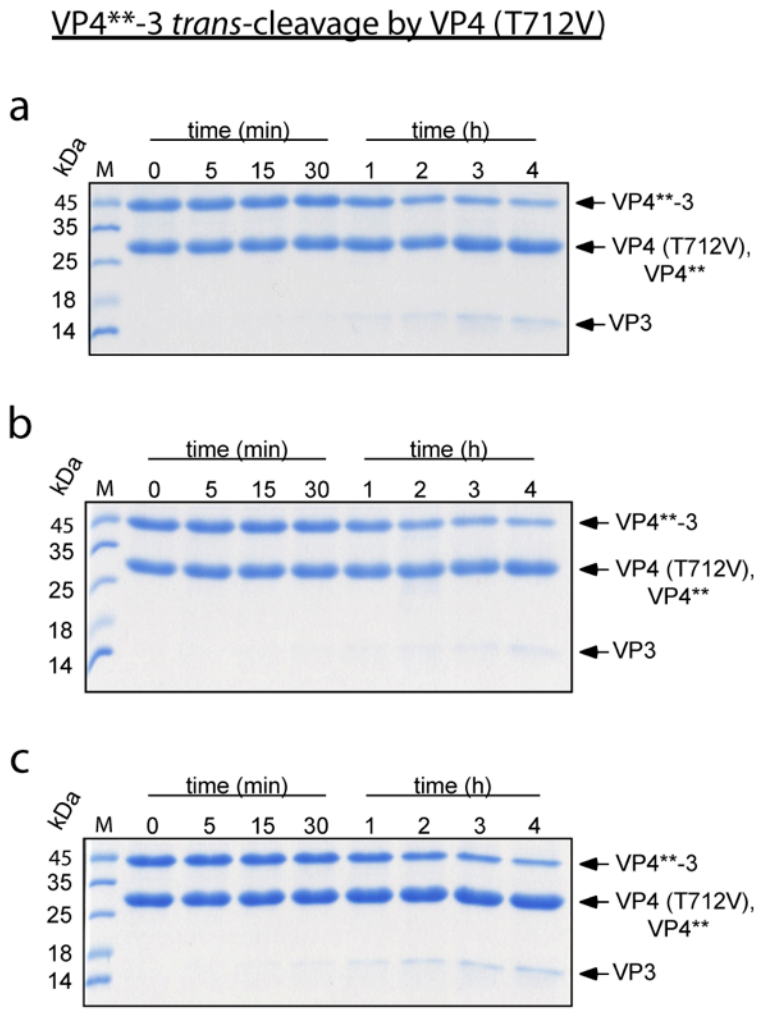

Figure C9. 15% SDS-PAGE summary of the *trans*-cleavage of VP4**-3 by VP4 (T712V). The time-course cleavage assays were performed in triplicate; the results from the assays are shown in (a), (b) and (c). The buffer conditions were 20 mM Tris-HCl (pH 8.0), 100 mM NaCl, 10% glycerol, and 1% β-mercaptoethanol and the molar ratio of VP4**-3 to VP4 (T712V) was 0.7:1.0. M indicates the marker lane. The two stars (**) of VP4**-3 denote the two active site mutations, S692A and K729A, of this substrate-construct. The cleavage product, VP4**, co-migrates with VP4 (T712V).

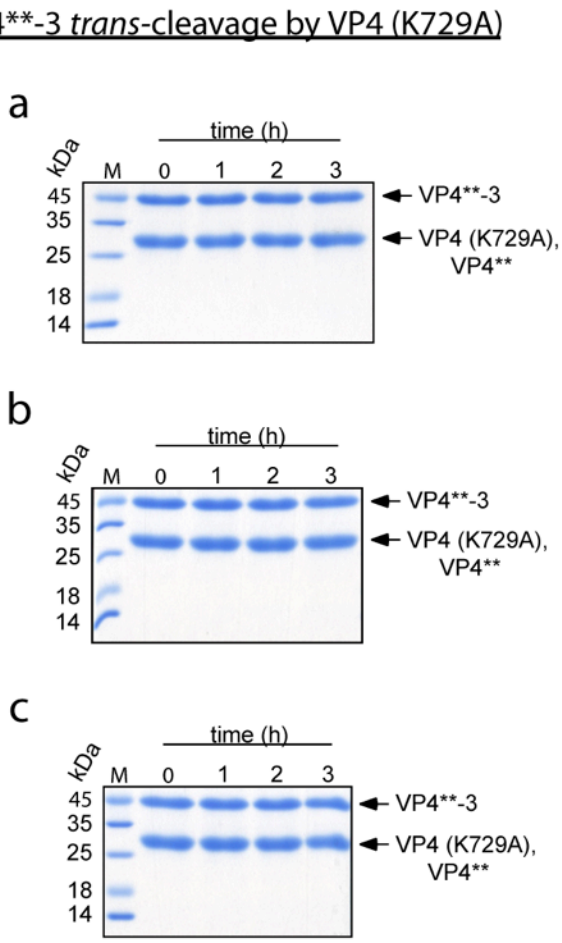

Figure C10. 15% SDS-PAGE summary of the *trans*-cleavage of VP4**-3 by VP4 (K729A). The time-course cleavage assays were performed in triplicate; the results from the assays are shown in (a), (b) and (c). The buffer conditions were 20 mM Tris-HCl (pH 8.0), 100 mM NaCl, 10% glycerol, and 1% β-mercaptoethanol. The molar ratio of VP4**-3 to VP4 (K729A) was 0.7:1.0. M indicates the marker lane. The two stars (**) of VP4**-3 denote the two active site mutations, S692A and K729A, of this substrate-construct. The cleavage product, VP4**, co-migrates with VP4 (K729A).